THEORY OF MOLECULAR PHOTOIONIZATION: FROM VIBRATIONAL DEPENDENT PROCESSES TO THE EFFECTS OF ROTATIONAL MOTION IN IONIZING NON-LINEAR MOLECULES ON MFPADs AND RFPADs

A Dissertation

by

JESÚS ALBERTO LÓPEZ DOMÍNGUEZ

Submitted to the Office of Graduate and Professional Studies of
Texas A&M University
in partial fulfillment of the requirements for the degree of

DOCTOR OF PHILOSOPHY

Chair of Committee,   Robert R. Lucchese
Committee members,   A. Lewis Ford
                        Simon W. North
                        Danny L. Yeager
Head of Department,   François Gabbaï

May 2015

Major Subject: Chemistry

ABSTRACT

In this work, I present a series of studies in the field of molecular photionization and in a more general way, in the electron-molecule scattering processes area. It takes as a starting point the study of well known molecular features in the photionization of small molecules and reviews the usual approach to compare experimental and theoretical cross sections and branching ratios. I then suggest a different theoretical model which enables a better frame of reference for the comparison. This method is based on the logarithmic derivative of the cross section. Also, a theoretical approach has been taken to study the effect that rotational motion has on the dynamics of photoionization between ionization and fragmentation, a series of equations are derived to compute the 3D recoil frame photoelectron angular distributions for non-linear molecules in the case where the axial-recoil approximation breaks down.

The main concepts and ideas relevant to most of the work presented are introduced at the beginning of this work, even those that are part of the standard literature in textbooks on the subject of scattering and collision theory, but being of fundamental importance to the later developments of this thesis, are treated in a way pertaining to the approaches taken in the analysis of results and in the elaboration of the new theoretical findings presented in the rest of this work.

I introduced what I call the *electronic factor*, which is a Franck-Condon factor that provides a common ground to compare experimental and theoretical branching ratios. For that purpose, two approaches are taken, one considering first an expansion of the matrix element of the dipole operator $\vec{\mu}$ up to first order terms and second, an extension where we also assume harmonic oscillator functions and the same frequencies in the initial and final vibrational states. Later on this methodology has been applied and analyzed for highly symmetric linear molecules and for a less symmetric polyatomic molecule with encouraging results.

I also present photoionization studies on different target molecules, where the different symmetries, number and type of atoms, and other properties derived from these, of the chosen targets, allowed for a theoretical elaboration on a diverse number of specific and more general ideas relative to molecular photoionization. Some of the ideas explored are the effects that Cooper minima play on the deviation of Franck-Condon behavior and how the contribution of individual partial waves are expressed

in the total experimental (or theoretical) cross section. As a mean of comparison between theory and experiment in this context, the electronic factor, F, derived previously is used. Effects of symmetry and complexity of the molecules in these studies are discussed.

Finally, I present studies of the effects of rotational motion on non-linear molecules undergoing an ionization and later fragmentation. For this purpose, the previously developed ideas for linear and diatomic molecules are extended into the general case which allows one to treat a wider range of molecular targets incorporating any symmetry type and limited only by the computational resources available to treat big systems. To demonstrate its usefulness we compute MFPADs for core C $1s$ photoionization of CH_4. I include the rotational motion by letting the pre-ionizing meta stable state to have lifetimes from $\tau = 0$ ps to ∞ ps, evidencing a better agreement with experimental results than previous theoretical predictions where the axial-recoil approximation was assumed.

DEDICATION

To my *loving* parents Guillermo and Pilar,
and my *caring* brother Guillermo.

❧

To my *Dearest* and *beloved* Sheila.

❧

ACKNOWLEDGMENTS

I would like to thank my advisor, Dr. Robert R. Lucchese, for his mentorship and patience, particularly considering the time required to learn the working essentials it takes to do research in this field. I deeply admire his extraordinaire academic leadership as a scientist and appreciate his human dimension.

I would also like to thank the people that has worked in the Lucchese group, for their friendship and support. In the early time of my arrival Raffaele showed me some of the rudiments of the work to be done, although at that point I was, perhaps, not ready to understand most of it. I also thank Luis and Jobin for their friendship and support, specially during this last years and moths prior to my defense, for being open to discuss the science and doubts in a friendly environment has proved always of great value in gaining the confidence needed, and for making the time at the office and out of it a better one. I have also to give special thanks for the very good memories from my early years at the department to Dongxia and Kousik who always made me feel welcomed into this new group of "theory people" I was starting to belong to and who remain good friends to these days. My sincere thanks and appreciation to many good friends that shared time, concerns and memories during my prolonged stay at this Department and that I really don't want to miss mentioning.

I am also very thankful for the family I have, for my parents set with their example and living the highest human standards I can think of. I appreciate the love and dedication that my parents put on their two children, and that they still do to these days, giving me and my brother the values and elements to grow as persons everyday. They also succeeded in making us look for our goals with persistence and dedication, something that took me here one day, and has me now celebrating its conclusion. For all their love and support I am very thankful.

I can not be thankful enough to Sheila Juárez, who has been instrumental in bearing the time, distance and sacrifices that it took to complete my Ph.D. during all these years. Her love, friendship and constant dedication to myself are qualities I treasure and greatly appreciate, as well as her support to all my endeavors, plans and interests, making them of her own. She has been a driving force in my life and has provided constant encouragement throughout these years.

CONTENTS

LIST OF TABLES

CHAPTER I

INTRODUCTION

Many, if not all of the studies at the molecular level of structure and dynamics have a common ancestor in the pioneering works of Faraday and Maxwell [1, 2] [1], back in the mid eighteen hundreds, that brought together the then independent fields of electromagnetism and optics, setting the ground for a plethora of future work to come in understanding the interaction of electromagnetic radiation with matter in general. Maxwell's equations set the foundation for a quantitative explanation of common light-matter phenomena such as dispersion and refraction, and its use extends to the semiclassical limit (assuming the interaction of classical radiation with a quantum system). Maxwell's relations in the international system of units (SI) are given by,

$$\nabla \times \boldsymbol{E} + \frac{\partial \boldsymbol{B}}{\partial t} = 0 \tag{I.1a}$$

$$\nabla \times \boldsymbol{H} - \frac{\partial \boldsymbol{D}}{\partial t} = \boldsymbol{J} \tag{I.1b}$$

$$\nabla \cdot \boldsymbol{D} = \bar{\rho} \tag{I.1c}$$

$$\nabla \cdot \boldsymbol{B} = 0 \tag{I.1d}$$

$$\boldsymbol{D} = \varepsilon_0 \varepsilon \boldsymbol{E}, \quad \boldsymbol{B} = \mu_0 \mu_p \boldsymbol{H} \tag{I.2}$$

where $\boldsymbol{E}$ and $\boldsymbol{D}$ are the electric field vector and induction respectively, related by the dielectric constant $\boldsymbol{\varepsilon}$, and the permitivity of a vacuum ε_0; $\boldsymbol{H}$ and $\boldsymbol{B}$ are the magnetic field vector and induction respectively, related by the relative magnetic permeability μ_p and the permeability of free space μ_0; and finally, $\boldsymbol{J}$ is the electric current density and the scalar $\bar{\rho}$ represents the electric charge density. Once the relation between this quantities is stablished and the theory of how electromagnetic waves propagate into a medium derived (see for example [4]), the road is settled to move forward into one of the most interesting applications from the wave theory of light involving its

---

[1]Many other scientists contributed to the fields of optics and electromagnetism whose work should not be overlooked. For a more complete review on the historic development of these fields and the minds behind it see reference [3]

Table I.1: Photon and electron induced processes in atomic and molecular collisions.

Process	Description
$AB + h\nu \rightarrow AB^*$	Photoabsorption
$AB + h\nu \rightarrow AB^+ + e^-$	Photoionization
$AB + h\nu \rightarrow A + B$	Photodissociation
$AB + h\nu \rightarrow A + B^+ + e^-$	Dissociative photoionization
$AB + e^- \rightarrow e^- + AB$	Elastic scattering
$AB + e^- \rightarrow 2e^- + AB^+$	Electron impact ionization
$AB + e^- \rightarrow AB^-$	Electron attachment

interaction with matter, the photoelectric effect.

I.1   Scattering theory

Scattering is a process which in a broad sense refers to the interaction of two types of objects or particles. The diversity and variety of phenomena that it encompasses is such that it includes how different types of radiation can interact at the nuclear level (*e.g.*, the bombardment of α particles to gold foil, experiment that lead Rutherford to the discovery of the nucleus in atoms), or at an electronic level to mention a few [5]. Scattering may involve redistribution or rearrangement of the constituents of the initial particles. The simplest experiment of scattering is the *potential scattering*, where a single particle interacts with a finite-range fixed force. If the two interacting particles come with an unchanged structure the process is said to be *elastic*; in more complicated and even realistic scenarios, where the incoming particles are somehow changed after the collision, are called *inelastic scattering* [6]. Although many different outcomes can be expected from the interaction of light (photons) or electrons with matter, we mention here the most likely to be used or mentioned throughout this work. *Photoabsorption* occurs when light of a certain frequency ν is absorbed by an atom or molecule M bringing it into an excited state M^*. When the absorption of light occurs into a repulsive state of a molecule and it dissociates into neutral fragments the process is called *photodissociation*. If the photon absorbed, $h\nu$, by the target excites an electron beyond the ionization limit, we have a *photoionization* process [7]. A summary of these processes and other light and electron interactions with matter is presented in Table I.1.

Scattering in general can be classified in several ways and some have already been mentioned. It is an inherently time dependent process, however through the use of appropriate approximations and choosing the right boundary conditions a time independent treatment can be formulated. The time dependent Schrödinger's equation that governs scattering has the form

$$i\hbar\frac{\partial}{\partial t}\left|\psi(t)\right\rangle = H\left|\psi(t)\right\rangle \tag{I.3}$$

where the total Hamiltonian of the system, H, is the sum of the kinetic energy, H_0, and the interaction potential H' [6],

$$H = H_0 + H'. \tag{I.4}$$

For a conservative system the Hamiltonian H is independent of t, and the time dependence of the evolution of the system is given by the phase factor e^{-iHt}. The scattering experiment can be divided in three steps: first is the approach of the electron (or other particle) along a trajectory $\boldsymbol{x}(t)$; second, the interaction region, where the description of the 'trajectory' might be very complicated; and third, the electron leaving the scattering site through an almost straight outgoing trajectory. While this orbit picture is adequate for the classical scattering, the quantum description is closely parallel but instead of a trajectory $\boldsymbol{x}(t)$ following Newton's equation of motion, there is a state vector $|\psi\rangle$ satisfying the time-dependent Schrödinger equation (I.3). To better address the quantum scattering that concerns the work presented here, let's start by introducing the classical picture, that will lead into a more clear explanation of the quantum case.

I.1.1 Classical scattering

As it was mentioned above, the scattering of classical particles by a central potential or by each other is better described by the particle's trajectory. The Hamiltonian for that system is [8]

$$H = \frac{p^2}{2m} + V(r) \tag{I.5}$$

where p is the momentum and m represents either the mass of the particle being scattered by a central potential or the reduced mass of a two particle system in the center of mass frame of reference. $V(r)$ is the potential acting on the system

and r represents the distance in the corresponding coordinate system between the components of the scattering experiment. Assuming that the scattering event occurs at an arbitrary time $t = 0$, the behavior of the orbit $\boldsymbol{x}(t)$ in the far past $t \to -\infty$ as it moves towards to the target approaches asymptotically a free trajectory $\boldsymbol{x}_{\text{in}}(t)$ and for the outgoing particle as $t \to +\infty$ similarly approaches the asymptotic trajectory $\boldsymbol{x}_{\text{out}}(t)$ so that [5],

$$\boldsymbol{x}(t) \xrightarrow[t \to -\infty]{} \boldsymbol{x}_{\text{in}}(t) \tag{I.6}$$

$$\boldsymbol{x}(t) \xrightarrow[t \to +\infty]{} \boldsymbol{x}_{\text{out}}(t) \tag{I.7}$$

A scattering trajectory is said to be completely characterized when both *in* and *out* asymptotes are known. It is important to note that just as for any pair of *in* and *out* asymptotes there is a trajectory $\boldsymbol{x}(t)$, the opposite is not necessarily always true, since there are potentials that can support a bounded orbit, not letting the particle out, and will not become a free asymptotic trajectory. In a scattering experiment, one cannot think of a single particle approaching a central potential or another particle, and a more realistic picture is that of a beam of particles being sent towards a target. The impact parameter b, defined as the distance of closest approach of the asymptotic trajectory to the target, is not unique in such an experiment, neither thus the azymuthal angle ϕ, and these quantities become a distribution rather than a specific number. All the particles in the incoming "tube" with element of area $b\,db\,d\phi$ go after the collision into a distribution cone of solid angle $d\phi\,d\theta\,\sin\theta$. Following these ideas is that the familiar scattering concept of *cross section* arises as a practical way of reporting experimental results. A cross section is an area normal to the incident direction containing all impact parameters that lead to scattering. It is important to distinguish between two different but related quantities, the total cross section, $\sigma(E)$, which contains all elastic scattering events and a differential cross section, $d\sigma/d\Omega$, referring to scattering at a specific solid angle Ω, or in an inelastic process the corresponding total, $\sigma_{ij}(E)$, and differential, $d\sigma_{ij}/d\Omega$, cross sections for scattering from the ith to the jth internal states [9]. We have mentioned the angle θ above, which is the magnitude of the deflection angle Θ modulo π, since experimentally it is not possible to differentiate between positive or negative values of Θ, thus

$$\theta = |\Theta|, \quad 0 < \theta < \pi \tag{I.8}$$

It is clear then, that the trajectories with an impact parameter in the range from b to $b+db$ have an area $2\pi b db$ and are deflected into the solid angle $d\Omega = 2\pi \sin\theta d\theta$. From this very intuitive definitions, the previously mentioned differential cross section in terms of the intensity of scattering per unit solid angle, can be expressed as,

$$\frac{d\sigma}{d\Omega} = I(\theta, E) = \left| \frac{2\pi b db}{2\pi \sin\theta d\theta} \right| = \left| \frac{b}{\sin\theta d\theta / db} \right| \tag{I.9}$$

and consequently the total elastic cross section is then defined as the integral of equation (I.9),

$$\sigma(E) = \int \frac{d\sigma}{d\Omega} d\Omega = 2\pi \int_0^\pi I(\theta, E) \sin\theta d\theta. \tag{I.10}$$

It is noteworthy to observe that in the previous definition of the classical differential cross section given in Equation (I.9) there are two different possible sources of singularities, that give rise to very well known effects. The first one happens when there is backward scattering (meaning $\theta = \pi$) or forward scattering ($\theta = 0$) meaning that $\sin\theta$ vanishes, and is called the *glory effect*. The second one will happen when there is a turning point in the θ vs. b curve, at which $d\theta/db = 0$, which will physically correspond to a point where the density of classical trajectories goes to infinity, this is known as the *rainbow effect* (and is indeed related to the rainbow we may see after a rainy day, see for example [9] or [10] and references therein). Also, for particular types of potentials and forces acting on the system, there might be defined or closed forms of the integral (I.10), for those cases one can refer to [8] for additional information.

I.1.2   Quantum scattering

The quantum picture of scattering theory [8] can be formulated in close connection to the classical one in some aspects, and although more elaborate, is also richer in the possibilities of describing natural phenomena. We can move to the quantum description of the scattering phenomena by identifying the state vector $|\psi(t)\rangle$ which, just as the trajectories from Equations (I.6) and (I.7) follow Newton's equation, follows Schrödinger's Equation (I.3). It is noteworthy that Schrödinger's equation contains complex valued functions and operators, and thus to remember the origin of the convention of the imaginary unit, $+i$, in Equation (I.3) to come from the accepted notion that e^{+ikr} describes an outgoing spherical wave and e^{-ikr} an incoming one [8].

The main objective now is to solve Equation (I.3), for which we will use a form of Green's function method. First, we write four Green's functions in the form of propagators,

$$\left(i\frac{\partial}{\partial t} - H_0\right) G^{\pm}(t) = \mathbb{1}\delta(t) \tag{I.11a}$$

$$\left(i\frac{\partial}{\partial t} - H\right) \mathscr{G}^{\pm}(t) = \mathbb{1}\delta(t) \tag{I.11b}$$

and establish the initial conditions,

$$G^{+}(t) = \mathscr{G}^{+}(t) = 0 \qquad \text{for } t < 0 \tag{I.12a}$$

$$G^{-}(t) = \mathscr{G}^{-}(t) = 0 \qquad \text{for } t > 0 \tag{I.12b}$$

With these equations and initial conditions in mind and considering that $\mathbb{1}$ stands for the unit operator and $\delta(t)$ is the Dirac's delta function, solutions for the Green's functions in Equations (I.11) can be written as,

$$G^{+}(t) = \begin{cases} -ie^{-iH_0 t} & t > 0 \\ 0 & t < 0 \end{cases} \tag{I.13a}$$

$$G^{-}(t) = \begin{cases} 0 & t > 0 \\ ie^{-iH_0 t} & t < 0 \end{cases} \tag{I.13b}$$

$$\mathscr{G}^{+}(t) = \begin{cases} -ie^{-iHt} & t > 0 \\ 0 & t < 0 \end{cases} \tag{I.13c}$$

$$\mathscr{G}^{-}(t) = \begin{cases} 0 & t > 0 \\ ie^{-iHt} & t < 0 \end{cases} \tag{I.13d}$$

Naming G and $\mathscr{G}$ as propagators results from the fact that they describe the propagation of state vectors in time. If again we take Equation (I.3) as model, but using the state vector $|\psi_0(t)\rangle$ and non-interaction Hamiltonian H_0, instead, then the operator G^{+} allows us to express the state vector $|\psi_0(t')\rangle$ for any time t' later than t, in terms of its value at $t' = t$,

$$|\psi_0(t')\rangle = iG^{+}(t' - t) |\psi_0(t)\rangle \tag{I.14}$$

6

By evaluating the limits

$$\lim_{t\to 0^+} G^+(t) = \lim_{t\to 0^+} \mathscr{G}^+(t) = -i\mathbb{1} \tag{I.15a}$$

$$\lim_{t\to 0^-} G^-(t) = \lim_{t\to 0^-} \mathscr{G}^-(t) = i\mathbb{1} \tag{I.15b}$$

it is easy to verify that in Equation (I.14) the state vector $|\psi_0(t')\rangle$ approaches $|\psi_0(t)\rangle$ when $t' \to 0^+$. In a similar way, we can see what happens in the past before the collision, or in the future, after the interaction. We can view the whole scattering process as the sum of three events, first there is an incoming state, approaching the scattering center which can be described by some type of potential, second there is an interaction, and finally there is an outgoing state. By taking advantage of the Green's function formulation presented above, we can define a state vector $|\psi_{\text{in}}(t)\rangle$ whose time development at $t > t'$ is governed by the free hamiltonian H_0 but, that at time t_0, as seen in Equation (I.14), is equal to $|\psi(t_0)\rangle$. This state is thus defined by the limit

$$|\psi_{\text{in}}(t)\rangle = \lim_{t'\to-\infty} iG^+(t - t') |\psi(t')\rangle \tag{I.16}$$

in a similar way, the definition for an outgoing state vector $|\psi_{\text{out}}(t)\rangle$ governed by H_0 and equal to the exact complete state vector $|\psi(t)\rangle$ in the infinite future, can be defined by the limit

$$|\psi_{\text{out}}(t)\rangle = \lim_{t'\to\infty} -iG^-(t - t') |\psi(t')\rangle. \tag{I.17}$$

The consequences of these two limits are known as the asymptotic conditions, and guarantees that any $|\psi_{\text{in}}(t)\rangle$ in a Hilbert space is the asymptote of some actual trajectory, and similarly, it guarantees that the actual complete state $|\psi(t)\rangle$ will evolve into the out asymptote $|\psi_{\text{out}}(t)\rangle$.

Møller operators

It is convenient to introduce the operators Ω_+ and Ω_- which are called wave operators or Møller operators. These operators convert the free state $|\psi_{\text{in}}(t)\rangle$ and $|\psi_{\text{out}}(t)\rangle$,

respectively, into the complete state $|\psi(t)\rangle$,

$$|\psi(t)\rangle = \Omega_+ |\psi_{\text{in}}(t)\rangle \tag{I.18a}$$

$$|\psi(t)\rangle = \Omega_- |\psi_{\text{out}}(t)\rangle \tag{I.18b}$$

A combination of (I.16), (I.17) with (I.14) leads to the accepted definitions for the Møller operators,

$$\Omega_+ = \mathbb{1} - i \int_{-\infty}^{\infty} dt \mathscr{G}^+(-t) H' G^-(t) \tag{I.19a}$$

$$\Omega_- = \mathbb{1} + i \int_{-\infty}^{\infty} dt \mathscr{G}^-(-t) H' G^+(t) \tag{I.19b}$$

Some relevant properties of this wave operators that will lead to an important result are listed below in Equations (I.20) (for a more complete explanation look at [8]), and take advantage of the previously stated definitions of $\Omega_\pm$ and the Hermiticity of H':

$$|\psi_{\text{in}}(t)\rangle = \Omega_+^\dagger |\psi(t)\rangle \tag{I.20a}$$

$$|\psi_{\text{out}}(t)\rangle = \Omega_-^\dagger |\psi(t)\rangle \tag{I.20b}$$

Equations (I.20) together with (I.18) show that

$$|\psi_{\text{in}}(t)\rangle = \Omega_+^\dagger \Omega_+ |\psi_{\text{in}}(t)\rangle \tag{I.21a}$$

$$|\psi_{\text{out}}(t)\rangle = \Omega_-^\dagger \Omega_- |\psi_{\text{out}}(t)\rangle \tag{I.21b}$$

The S-matrix: scattering operator

At this point we can introduce an operator that will allow us to express the *out* asymptotic state in terms of the *in* asymptotic state. By means of (I.18a) and (I.20b) we get the relation we were ultimately looking for,

$$|\psi_{\text{out}}(t)\rangle = \Omega_-^\dagger \Omega_+ |\psi_{\text{in}}(t)\rangle = S |\psi_{\text{in}}(t)\rangle \tag{I.22}$$

where $S = \Omega_-^\dagger \Omega_+$. One of the most important properties of the S operator, is that it conserves energy. As far as the asymptotic states are concerned, the actual energy is simply the kinetic energy and we should expect that S commutes with the kinetic

energy operator H_0, rather than H, so that $[S, H_0] = 0$. This has the implication that the mean final energy for the corresponding out state $|\psi_{\text{out}}\rangle = S|\psi_{\text{in}}\rangle$ is

$$\langle\psi_{\text{out}}|H_0|\psi_{\text{out}}\rangle = \langle\psi_{\text{in}}|S^\dagger H_0 S|\psi_{\text{in}}\rangle \tag{I.23}$$

This equality holds since the commutator of S with H_0 has the implication that $H_0 = S^\dagger H_0 S$. The free Hamiltonian H_0 has no proper eigenvectors, although the choice of expanding in the "improper" momentum eigenvectors set $|\boldsymbol{p}\rangle$ has proven to be useful. In this context, the energy of a free particle of momentum p is $E_p = \frac{p^2}{2m}$. In this manner, using the momentum representation as the basis, we can write for the S operator the matrix elements as $\langle\boldsymbol{p}'|S|\boldsymbol{p}\rangle$ which is what we refer as the "S matrix". Although the above mentioned S matrix does not represent the amplitude of a physical realizable process, the importance of this "improper" matrix elements relies in providing a basis for the expansion of the proper matrix elements $\langle\psi|S|\phi\rangle$, which can be understood as representing the *out* state in terms of the *in* state as [5]

$$\psi_{\text{out}}(\boldsymbol{p}) = \int d^3p'\,\langle\boldsymbol{p}|S|\boldsymbol{p}'\rangle\,\psi_{\text{in}}(\boldsymbol{p}') \tag{I.24}$$

Another way of visualizing this "improper" S matrix elements is as the probability amplitude that an *in* state of momentum $\boldsymbol{p}$ will lead into an *out* state of momentum $\boldsymbol{p}'$. To further explore the energy conservation mentioned above, let us take advantage again of the commutator of S with the kinetic energy Hamiltonian H_0 and see its implications in its momentum-space matrix representation,

$$\langle\boldsymbol{p}'|[H_0, S]|\boldsymbol{p}\rangle = (E_{p'} - E_p)\langle\boldsymbol{p}'|S|\boldsymbol{p}\rangle \tag{I.25}$$

with the obvious implication that the S-matrix elements are always zero except when $E_{p'} = E_p$, leading to the momentum-space expression of energy conservation

$$\langle\boldsymbol{p}'|S|\boldsymbol{p}\rangle \propto \delta(E_{p'} - E_p) \tag{I.26}$$

The T-matrix formulation

In the absence of interactions $S = 1$, so a way of exploring the nature of the momentum-space S matrix previously defined is to introduce the operator R in such a way that $S = 1 + R$, that said, R represents the difference between the value of S

9

and its value in the absence of interactions. And as with for the matrix elements in S, we can write

$$\langle \boldsymbol{p'}| R |\boldsymbol{p}\rangle = -2\pi i \delta(E_{p'} - E_p)t(\boldsymbol{p'} \leftarrow \boldsymbol{p}). \tag{I.27}$$

The details of this expression can be read in Taylor [5], but the expression for the S matrix becomes,

$$\langle \boldsymbol{p'}| S |\boldsymbol{p}\rangle = \delta^3(\boldsymbol{p'} \leftarrow \boldsymbol{p}) - 2\pi i \delta(E_{p'} - E_p)t(\boldsymbol{p'} \leftarrow \boldsymbol{p}) \tag{I.28}$$

In Equation (I.28) the first term corresponds to the amplitude for the particle to pass the interaction center without being scattered, and the second term is therefore the amplitude for scattering the particle. As it was seen to happen in Equation (I.25) for the S matrix, where the delta function caused it to be zero every time but when energies between states were the same, the quantity $t(\boldsymbol{p'} \leftarrow \boldsymbol{p})$ is only defined when $E_{p'} = E_p$. This statement can be understood as having $t(\boldsymbol{p'} \leftarrow \boldsymbol{p})$ defined only "on-shell" when $|\boldsymbol{p'}| = |\boldsymbol{p}|$, which is the reason that $t(\boldsymbol{p'} \leftarrow \boldsymbol{p})$ is called the on-shell T matrix. There is also the possibility of defining the matrix $\langle \boldsymbol{p'}| T |\boldsymbol{p}\rangle$ for all $\boldsymbol{p'}$ and $\boldsymbol{p}$, and it is called the "off-shell T matrix".

Evaluation of the on-shell T matrix determines the S matrix through Equation (I.28) and is closely related to the scattering amplitude (which will be used among other things to compute cross sections) by

$$f(\boldsymbol{p'} \leftarrow \boldsymbol{p}) = -(2\pi)^2 m \; t(\boldsymbol{p'} \leftarrow \boldsymbol{p}) \tag{I.29}$$

and the off-shell T matrix will prove to be of great importance since it satisfies the Lippmann-Schwinger equation which provides one of the variational integral principles used to solve scattering problems, and the one we employ throughout this work. Finally by means of Equations (I.28) and (I.29) the S matrix can be expressed in terms of the amplitude as

$$\langle \boldsymbol{p'}| S |\boldsymbol{p}\rangle = \delta^3(\boldsymbol{p'} \leftarrow \boldsymbol{p}) + \frac{i}{2\pi m}\delta(E_{p'} - E_p)f(\boldsymbol{p'} \leftarrow \boldsymbol{p}) \tag{I.30}$$

I.1.3   Variational methods

Variational methods are in general used to provide approximate solutions to a variety of differential and integral equations. In that sense, variational methods can

10

be classified into differential or integral forms. A variational principle is said to be differential if its based on the differential equation and requires its trial functions to satisfy boundary conditions of the problem. On the other hand, when a variational principle is said to be of the integral form is based on the integral equation and most important, the boundary conditions need not to be included in the trial function, as they are taken into account through the Green's function. From the methods to be described in the next sections, the Kohn variational principle is of the differential form, and the Schwinger variation principle, based on the Lippmann-Schwinger equation, is of the integral form [11]. As is the case with variational methods in a diverse number of applications, the starting point is to guess a trial function, and from there continue through a well defined procedure to modify the trial until this variations converge within a certain criteria into the desired value or function. The theoretical computation of the relevant quantities in scattering, such as the S, K or T matrices, are based upon variational methods.

In a variational calculation of the ground state energy for a particle with Hamiltonian H, a trial function $\zeta(x)$ for the actual ground state wave function $\psi_0(x)$ needs to be suggested. What follows, is to compute the functional [5]

$$\epsilon[\zeta] = \frac{\langle \zeta | H | \zeta \rangle}{\langle \zeta | \zeta \rangle} \tag{I.31}$$

Some properties should be fulfilled by the computed functional, first, $\epsilon[\zeta]$ should be independent of the normalization of the trial function; also if $\zeta_{ex}(x)$ is proportional to the exact ground state wave function, that will imply that $\epsilon[\zeta_{ex}]$ is precisely the ground state energy E_0. The second property implies the functional $\epsilon[\zeta]$ to be stationary with respect to variations of $\zeta(x)$ about the exact wave function, that is, if

$$\zeta(x) = \zeta_{ex}(x) + \delta\zeta(x) \tag{I.32}$$

then

$$\epsilon[\zeta] = \epsilon[\zeta_{ex}] + O(\delta\zeta)^2 \tag{I.33}$$

And lastly, the functional $\epsilon[\zeta]$ has to be a minimum at the exact wave function, besides being stationary. This last property allows to determine uniquely the best function from a family of trial functions as the one for which $\epsilon[\zeta]$ is a minimum.

The scattering variational methods are different from the usual energy varia-

tional methods. The variational calculations to study electron-molecule scattering and photoionization processes in molecules include the Schwinger variational method, the R-matrix method and the Kohn variational method among others [12]. In the present work, we use the Schwinger variational method, and therefore a more complete description of it is given below together with brief outline of the other methods mentioned above.

Schwinger variational method

The Schwinger variational principle [12] solves the Lippmann-Schwinger integral equation instead of the Schrödinger equation to derive a stationary expression for the scattering amplitude. The formalism can be applied in a number of different ways, in terms of the K matrix, or $\tan \nu$ for single-channel scattering, for example. As defined by Taylor [5] the partial wave amplitude given in terms of the radial wave function is given by,

$$f_l(p) = -\frac{1}{p^2} \int_0^\infty \hat{j}_l(pr) U(r) \psi_{l,p}(r) dr \tag{I.34}$$

where $U(r) = 2mV(r)$, $\hat{j}_l(pr)$ is the Riccati-Bessel function and the other quantities take their usual meaning. To find the correct guess ζ for the wave function, the Schwinger method starts from the functional,

$$\alpha[\zeta] = -\frac{1}{p^2} \frac{\left(\int dr \hat{j}_l U \zeta\right)^2}{\int dr \zeta (U - U G^0 U) \zeta} \tag{I.35}$$

where $G^0 \equiv G^0_{l,p}$ is the free Green's operator for angular momentum l and $\zeta(r)$ is a trial function. Using the properties outlined in the previous section for variational methods and its functionals, it can be shown [5] that the Schwinger variational expression for the partial-wave amplitude is,

$$f_l(p) = -\frac{1}{p^2} \frac{\left(\int dr \hat{j}_l U \zeta\right)^2}{\int dr \zeta (U - U G^0 U) \zeta} + O(\delta \zeta)^2 \tag{I.36}$$

It has been shown elsewhere that the Schwinger variational principle is a powerful formulation of the scattering problem, and that it has several advantages over other

variational methods. One of the most important advantages for real applications, is that the trial wave function need not to satisfy any specific asymptotic boundary conditions [12–14]. Just as it was shown, the variational expression for the partial-wave amplitude, the Schwinger variational expression for the T-matrix can be written as [13],

$$\langle \phi_k | T | \phi'_k \rangle = \frac{\left\langle \phi_k \left| \boldsymbol{U} \right| \Psi_k^{(+)} \right\rangle \left\langle \Psi_k^{(-)} \left| \boldsymbol{U} \right| \phi'_k \right\rangle}{\left\langle \Psi_k^{(-)} \left| \boldsymbol{U} - \boldsymbol{U}\boldsymbol{G}^0\boldsymbol{U} \right| \Psi_k^{(+)} \right\rangle} \tag{I.37}$$

where $\boldsymbol{U}$ is the potential and $|\Psi_k\rangle$ can be expanded in a set of basis functions $|\alpha\rangle$ as

$$|\Psi_k\rangle = \sum_\alpha a_\alpha(k) |\alpha\rangle \tag{I.38}$$

Requiring that Equation (I.37) be stationary with respect to variation of the coefficients, $a_\alpha(k)$, leads to the Schwinger variational expression

$$\langle \phi_k | T | \phi'_k \rangle = \sum_{\alpha,\beta} \langle \phi_k | \boldsymbol{U} | \alpha \rangle \, (\boldsymbol{D}^{-1})_{\alpha,\beta} \, \langle \beta | \boldsymbol{U} | \phi'_k \rangle \tag{I.39}$$

where $(\boldsymbol{D}^{-1})_{\alpha,\beta}$ denotes the (α, β) element of the matrix $\left\langle \alpha \left| \boldsymbol{U} - \boldsymbol{U}\boldsymbol{G}^0\boldsymbol{U} \right| \beta \right\rangle$.

Kohn variational method

Just as the Schwinger variational method depends on the exact wave function satisfying the integral Lippmann-Schwinger equation, the Kohn method is based on solving the Schrödinger differential equation. In contrast to the Schwinger variational method, the Kohn method does not provide a stationary expression for the amplitude itself, but for the tangent of the phase shift. Following Taylor [5], we start again with a trial radial function $\zeta(r)$ that satisfies $\zeta(0) = 0$ and with the asymptotic condition:

$$\zeta(r) \xrightarrow[r\to\infty]{} \frac{1}{p}\sin(pr - \frac{1}{2}l\pi) + \tau\cos(pr - \frac{1}{2}l\pi) \tag{I.40}$$

and where the exact radial function $\zeta_{\text{ex}}(r)$ satisfies

$$\left[-\frac{d^2}{dr^2} + \frac{l(l+1)}{r^2} + U(r) - p^2 \right] \zeta_{\text{ex}}(r) = 0 \tag{I.41}$$

where we will call the term between square brackets D. It can be seen that the constant term τ_{ex} in Equation (I.40) for the exact wave function will be $\tau_{\text{ex}} = \frac{1}{p} \tan \delta_l$, where δ_l is the exact phase shift. Considering the functional

$$\beta[\zeta] = \tau - \int_0^\infty dr \zeta(r) D\zeta(r) \tag{I.42}$$

from the functional of Equation (I.42) and Equation (I.41) it follows that for the exact radial function $\beta[\zeta_{\text{ex}}] = \tau_{\text{ex}} = \frac{1}{p} \tan \delta_l$. The stationarity of $\beta[\zeta]$ with respect to arbitrary variations of the radial function about its exact value allows to write

$$\beta[\zeta] = \beta[\zeta_{\text{ex}}] + O(\delta\zeta)^2 \tag{I.43}$$

which by simple substitution with the definition of the functional β at the exact value of the radial function gives,

$$\frac{1}{p} \tan \delta_l = \tau - \int_0^\infty dr \zeta(r) D\zeta(r) + O(\delta\zeta)^2 \tag{I.44}$$

which is the expression for the phase shift from the Kohn variational principle. Equation (I.44) can be reduced to

$$\frac{1}{p} \tan \delta_l \approx -\frac{1}{p^2} \int_0^\infty dr \hat{j}_l U \hat{j}_l \tag{I.45}$$

when the trial function is taken to be the free radial function,

$$\zeta r = \frac{1}{p} \hat{j}_l(pr) \xrightarrow[r\to\infty]{} \frac{1}{p} \sin(pr - \frac{1}{2} l\pi) \tag{I.46}$$

which has $\tau = 0$. One important point to note and for which the full explanation won't be given here, but can be found elsewhere [5] is that the Kohn expression with the free trial function $\hat{j}_l$ is equivalent to the first Born approximation, and the corresponding Schwinger expression is equivalent, under the same conditions, to the second Born approximation, so that for a trial function the Schwinger principle will give superior results than the Kohn method. The relation between these two methods has been explored with more detail by Takatsuka *et al.* [15] and Lucchese *et al.* [11] concluding and demonstrating that the Schwinger variational principle is one rank higher than the Kohn principle, so that, if the same trial scattering

wave function is used within these two principles, the Schwinger principle should lead to a superior result. Also, it should not be overlooked the occurrence in the Schwinger variational principle of a double integral involving the Green's function $\boldsymbol{G}_0$ (see Equations (I.37) and (I.36)) which, unless the trial function is relatively simple, can prove to be difficult to evaluate specially on realistic applications. In any case, that *inconvenience* should not prevent its use, since there are several numerical approaches in solving the integral equations appearing from its application.

I.2 Molecular photoionization

It was mentioned before that one of the possible outcomes of the interaction of light with matter is the absorption of energy and, consequentially, the excitation of matter. By looking at Table I.1 one of the processes depicted is the photoionization of a molecule, in which a photon with energy greater than the ionization potential of the molecule is absorbed by an isolated molecule, leading to ionization with the emission of a photoelectron. In this sense, it is important to mention that the study of molecular photoionization requires special methods due to the continuous energy spectrum and the asymptotic boundary conditions required to describe the photoelectron produced within the photoionization process [16]. The difference in energy between the initial photon energy and the measured photoelectron kinetic energy provides the energy difference between the molecule and the ion in its final rotational, vibrational and electronic states. The study of photoionization processes leads to understanding highly excited states of molecules, and so the understanding of these states, the cross sections for their production and its dynamics are of great use in fields including astrophysics [17], atmospheric chemistry [18], and materials processing [19] among others.

I.2.1 Cross sections

As mentioned above, one important quantity to measure or compute is the photoionization cross section. In the weak field limit, it is given by [16]

$$\frac{d\sigma}{d\Omega_{\hat{k}}} = \frac{4\pi^2}{cE}|T_{\mathrm{i,f},\vec{k}}|^2 \tag{I.47}$$

where E is the photon energy $\hbar\omega$, $\Omega_{\hat{k}}$ is the solid angle in the direction of the unit vector $\hat{k}$ and c is the speed of light. The transition matrix elements between the initial and final ionized states can be expanded as,

$$T_{i,f,\vec{k}} = \left\langle \Psi_i \left| \sum_{j=1}^{N} \exp\left(i\frac{\omega}{c}\hat{s}\cdot\vec{r}_j\right) \hat{n}\cdot\nabla_{r_j} \right| \Psi_{f,\vec{k}}^{(-)} \right\rangle \tag{I.48}$$

where N is the number of electrons, Ψ_i is the initial state of the system, and $\Psi_{f,\vec{k}}^{(-)}$ represents the final ionized state of the system, with the photoelectron having asymptotic momentum $\vec{k}$. Equation (I.48) gives the transition matrix element for the interaction of the molecule with a single-frequency electromagnetic field.

I.2.2 Dipole approximation

It is important to observe that the exponential factor in Equation (I.48) has a value tending to unity for small energies, less than 100 eV, so when that exponential factor is replaced by 1, this is known as the dipole approximation, which leads to the following expression for the dipole velocity matrix element [16]

$$T_{i,f,\vec{k},\hat{n}}^{V} = \left\langle \Psi_i \left| \sum_{j} \hat{n}\cdot\nabla_{r_j} \right| \Psi_{f,\vec{k}}^{(-)} \right\rangle. \tag{I.49}$$

It is important to note that at higher photon energies the electric-quadrupole and magnetic dipole transitions may contribute giving non-dipolar effects that can affect the angular distributions of photoelectrons [16]. By integration of Equation (I.48) over all angles $\vec{k}$ and averaging over all orientations of the polarization of light, it is possible to obtain the total photoionization cross section,

$$\sigma_{i,f} = \frac{\pi}{cE} \int d\Omega_{\hat{k}} \int d\Omega_{\hat{n}} |T_{i,f,\vec{k},\hat{n}}|^2 \tag{I.50}$$

An alternative form of the transition dipole matrix elements given in Equation (I.49) can be formulated when the exact eigenfunctions of the molecular Hamiltonian are used for the initial and final states, and is called the length form [16]

$$T_{i,f,\vec{k},\hat{n}}^{L} = E \left\langle \Psi_i \left| \sum_{j} \hat{n}\cdot\vec{r}_j \right| \Psi_{f,\vec{k}}^{(-)} \right\rangle \tag{I.51}$$

Of course, the differential cross section can then be constructed from either of the two equivalent formulations of the transition dipole matrix element leading to,

$$\frac{d\sigma^{\mathrm{L(V)}}}{d\Omega} = \frac{4\pi^2}{cE} \left| T^{\mathrm{L(V)}}_{\mathrm{i,f},\vec{k},\hat{n}} \right|^2 \tag{I.52}$$

Finally, a useful form of the differential cross section is the *mixed* form, which can be constructed from this two transition dipole matrix elements in the form,

$$\frac{d\sigma^{\mathrm{M}}}{d\Omega} = \frac{4\pi^2}{cE} \mathrm{Re} \left\{ \left[T^{\mathrm{L}}_{\mathrm{i,f},\vec{k},\hat{n}} \right]^* T^{\mathrm{V}}_{\mathrm{i,f},\vec{k},\hat{n}} \right\} . \tag{I.53}$$

The different forms of the cross section are also said to be different *gauges*. If all forms have the same value, then the method used is said to be gauge invariant [16]. For methods that are not gauge invariant, the difference between them can be used to estimate the minimum error in the calculations.

I.2.3 The Born-Oppenheimer approximation

The molecular Hamiltonian (including nuclei and electrons) is a much more complicated expression than its atomic counterpart. When the spin is eliminated from the Hamiltonian and only the one and two electron terms are kept, the molecular Hamiltonian has the form,

$$\mathscr{H} = -\frac{\hbar^2}{2m} \sum_i \nabla_i^2 - \sum_A \frac{\hbar^2}{2M_A} \nabla_A^2 - \sum_{A,i} \frac{Z_A e^2}{r_{Ai}} + \sum_{A>B} \frac{Z_A Z_B e^2}{R_{AB}} + \sum_{i>j} \frac{e^2}{r_{ij}} \tag{I.54}$$

In this expression, indices i and j are used to label electrons and A and B for nuclei, whereas r and R are used for the distances between electrons and nuclei as labeled, and all the other variables take the usual meaning. The solution to the corresponding Schrödingier can in general not be obtained directly. As can be readily seen $\mathscr{H}$ incorporates the electron kinetic energy and the electron-electron repulsion on the first and last terms, the nuclear kinetic energy and the nuclear-nuclear repulsion, in the second and fourth terms, and finally the electron-nuclear attractions in the third term [7]. The Born-Oppenheimer approximation [20] consists in assuming that the total wave function is separable into the nuclear and electronic components,

$$\Psi_{\mathrm{molecular}}(\boldsymbol{r}, \boldsymbol{R}) = \psi_{\mathrm{e}}(\boldsymbol{r}; \boldsymbol{R}) \chi_{\mathrm{N}}(\boldsymbol{R}) \tag{I.55}$$

Equation (I.55) implies that the motions of the electrons, with general coordinates $\boldsymbol{r}$, are unaffected by the momentum of the nuclei, with general coordinates $\boldsymbol{R}$, and that they depend only parametrically on the nuclear positions [7, 21]. Using this product wave function in the Schrödinger equation, the total Hamiltonian, $\mathscr{H}$, can be written as the sum of electronic, $\mathscr{H}_\mathrm{e}$, and nuclear, $\mathscr{H}_\mathrm{N}$, Hamiltonians,

$$\mathscr{H} = \mathscr{H}_\mathrm{e} + \mathscr{H}_\mathrm{N}. \tag{I.56}$$

Thus, two independent expressions can be written for the electronic and nuclear components,

$$\mathscr{H}_\mathrm{e}\psi_\mathrm{e} = E_\mathrm{e}\psi_\mathrm{e} \tag{I.57a}$$

$$\mathscr{H}_\mathrm{N}\chi_\mathrm{N} = E_\mathrm{N}\chi_\mathrm{N} \tag{I.57b}$$

The Born-Oppenheimer separation is based on the relative velocities of the nuclei and electrons, and thus on their relative masses.

In the study of molecular photoionization and electron-molecule scattering [22], the Born-Oppenheimer approximation or adiabatic approximation consists of two approximations, the decoupling of the electronic state of the molecular ion from the nuclear motion, and the separation of the photoelectron and nuclear motions. It is also usually assumed that the effects of rotation can be separated from the electronic and vibrational motion and that by an appropriate orientational averaging of fixed orientation results they can later be incorporated [16]. So, following Equation (I.55), we can write in a very similar way the fixed-nuclei Hamiltonian depending only parametrically on the geometry for the target initial state as

$$\Psi_\mathrm{i}(\boldsymbol{r}, \boldsymbol{R}) = \psi_\mathrm{i}(\boldsymbol{r}; \boldsymbol{R})\chi_{\mathrm{i},v}(\boldsymbol{R}) \tag{I.58}$$

where $\chi_{\mathrm{i},v}(\boldsymbol{R})$ is the vibrational wave function of the initial state with quantum number v. Following this, the final state wave function can then be written as

$$\Psi_{\mathrm{f},\vec{k}}^{(-)}(\boldsymbol{r}, \boldsymbol{R}) = \psi_{\mathrm{f},\vec{k}}^{(-)}(\boldsymbol{r}; \boldsymbol{R})\chi_{\mathrm{f},v'}(\boldsymbol{R}) \tag{I.59}$$

where $\chi_{\mathrm{f},v'}(\boldsymbol{R})$ is a vibrational wave function of the final ion state f with quantum number v'. An important result from the Born-Oppenheimer or adiabatic approx-

imation is the form that the dipole velocity matrix elements (see Equation (I.49))
take, and are given by,

$$M_{\text{i,f},\vec{k},\hat{n}}^{\text{V}}(\boldsymbol{R}) = \left\langle \psi_{\text{i}}(\boldsymbol{r};\boldsymbol{R}) \left| \sum_j \hat{n} \cdot \nabla_{r_j} \right| \psi_{\text{f},\vec{k}}^{(-)}(\boldsymbol{r};\boldsymbol{R}) \right\rangle_{\boldsymbol{r}}$$ (I.60)

and

$$T_{\text{i},v,\text{f},v',\vec{k},\hat{n}}^{\text{V}} = \left\langle \chi_{\text{i},v}(\boldsymbol{R}) \left| M_{\text{i,f},\vec{k},\hat{n}}^{\text{V}}(\boldsymbol{R}) \right| \chi_{\text{f},v'}(\boldsymbol{R}) \right\rangle_{\boldsymbol{R}}.$$ (I.61)

With these expressions in mind, the total vibrationally specific cross sections can be
obtained from

$$\sigma_{\text{i},v,\text{f},v'} = \frac{\pi}{cE} \int d\Omega_{\hat{k}} \int d\Omega_{\hat{n}} \left| T_{\text{i},v,\text{f},v',\vec{k},\hat{n}}^{\text{L(V)}} \right|^2.$$ (I.62)

The use of Equation (I.62) allows for the computation of the relative cross sections for
excitation to different final vibrational states, called branching ratios. The branching
ratios $B_{v',v''}$ for the excitation of the v' state relative to the v'' state can be defined
as,

$$B_{v',v''} = \frac{\sigma_{\text{i},v,\text{f},v'}}{\sigma_{\text{i},v,\text{f},v''}}.$$ (I.63)

There are many conditions in which the dependence of the electronic matrix element
$M_{\text{i,f},\vec{k},\hat{n}}^{\text{V}}(\boldsymbol{R})$ on the molecular geometry $\boldsymbol{R}$ is very weak over a range of geometries. If
this assumption is true, the transition matrix element $T_{\text{i},v,\text{f},v',\vec{k},\hat{n}}$ can be approximated
assuming the independence of $M_{\text{i,f},\vec{k},\hat{n}}^{\text{V}}(\boldsymbol{R})$ from $\boldsymbol{R}$ leading to the expression,

$$T_{\text{i},v,\text{f},v',\vec{k},\hat{n}} \approx M_{\text{i,f},\vec{k},\hat{n}}(\boldsymbol{R}_0) \left\langle \chi_{\text{i},v}(\boldsymbol{R}) \right| \chi_{\text{f},v'}(\boldsymbol{R}) \right\rangle$$ (I.64)

where $\boldsymbol{R}_0$ represents a fixed geometry, usually the equilibrium geometry of the initial
state. This approximation is called the *Frank-Condon approximation* and will be
addressed in more detail in Chapter II.

Computing matrix elements

The computation of photoionization cross sections as described in the previous sec-
tion requires the computation of the dipole photoionization matrix elements. There
are several theoretical approaches towards this objective and also a number of numer-
ical techniques to implement such theoretical frameworks. Following the description
by Lucchese [16], we consider the problem that arises when continuum electrons are

involved, as is the case with molecular photoionization, in which the one-electron basis sets based on Gaussian functions do not provide an adequate description of the scattering wave functions. In such a case, alternative ways for describing the continuum functions must be used. One way of representing the scattering wave functions is by means of single center expansions (SCEs) [11]. A SCE of a function of the spherical coordinates $f(r, \theta, \phi)$ is obtained by using the spherical harmonics $Y_{lm}(\theta, \phi)$, which is a complete set of angular functions. So, an arbitrary function in three dimensions can be written as

$$f(r, \theta, \phi) = \sum_{lm} \frac{1}{r} f_{lm}(r) Y_{lm}(\theta, \phi) \tag{I.65}$$

and

$$f_{lm}(r) = r \int \sin\theta d\theta d\phi Y_{lm}^*(\theta, \phi) f(r, \theta, \phi). \tag{I.66}$$

It is important to note that in Equation (I.65) the expansion is in principle infinite, however for obvious reasons, in computations the expansion has to be truncated at some $l_{\max}$ value, which should be chosen to be large enough so that convergence is achieved. For nonlinear molecular systems, a symmetry adapted harmonic basis set is used and Equation (I.65) is written as

$$f^{p\mu}(r, \theta, \phi) = \sum_{l=0}^{l_{\max}} \sum_{h=1}^{n_l^{p\mu}} \frac{1}{r} f_{lh}^{p\mu}(r) X_{lh}^{p\mu}(\hat{r}) \tag{I.67}$$

and the symmetry adapted functions $X_{lh}^{p\mu}(\hat{r})$ are expanded in terms of spherical harmonics as

$$X_{lh}^{p\mu}(\hat{r}) = \sum_{m=-l}^{l} b_{lmh}^{p\mu} Y_{lm}(\hat{r}) \tag{I.68}$$

where p indicates the irreducible representation (IR) to which the functions belong in the molecule's point group, μ is the component of the pth IR that the functions belong to, and $n_l^{p\mu}$ is the number of angular functions that can be constructed from the spherical harmonics with the l index belonging to the μth component of the pth IR. If all the functions are expanded using the SCE, then the Schrödinger's equation for the close-coupling expansion can be written as a set of integro-differential equations for the radial functions, ultimately leading to the compact integral equation (for

20

details see [16]),

$$|\psi\rangle = |\psi^0\rangle + \boldsymbol{G}(E)\boldsymbol{V}|\psi\rangle \qquad (\text{I.69})$$

where the $|\psi\rangle$ is a vector of partial-wave radial functions. One approach to solve Equation (I.69) is to employ the Schwinger variational method, described above. The matrix elements given in Equations (I.49) and (I.51) can be written in a simplified bracket notation as $\langle\bar{\psi}_i|\,\psi\rangle$ and then a variational expression can be written by expanding the wave function in a basis set $g_i(\vec{r})$ to give

$$\langle\bar{\psi}_i|\,\psi\rangle \approx \langle\bar{\psi}_i|\,\psi^0\rangle + \sum_{i,j}\langle\bar{\psi}_i|\,\boldsymbol{GV}\,|g_i\rangle\,(\boldsymbol{D}^{-1})_{i,j}\,\langle g_j|\,\boldsymbol{V}\,|\psi^0\rangle \qquad (\text{I.70})$$

where $\boldsymbol{D}_{i,j} = \langle g_i|\,\boldsymbol{V} - \boldsymbol{VGV}\,|g_j\rangle$.

I.2.4 Resonances

Resonances are one of the most striking phenomena within molecular photoionization and scattering. In the simplest case, a resonance leads to a sharp peak in the total cross section as a function of energy [5]. Resonances are closely related to structural and dynamical properties of the target initial and final states. Although there are different theoretical approaches to study resonant phenomena, they all have in common the understanding that the sharp variation in the cross section at a certain energy E_{R} is somehow related to the existence of a nearly bound state of the collisional system with energy E_{R}. That means that when the projectile approaches the target with energy E_{R} there is the possibility of getting captured temporarily within the potential of the target forming a metastable state and leading to a "resonant" effect that can be observed as a rapid variation in the cross section. Analytically, it has been shown [5] that as bound states of angular momentum l are related to poles of the S matrix, $s_l(p)$ in the upper half plane $\{\mathrm{Im}\,p\} > 0$; resonances of angular momentum l are related to poles of the S matrix in the lower, negative, half plane $\{\mathrm{Im}\,p\} < 0$. This two relations clearly create a connection between bound states and resonant states. However, one should note that the relation described between resonant states and poles in the lower plane of p is not exact, and requires first, a reasonable potential that allows continuation into the lower half of the plane $\{\mathrm{Im}\,p\}$ and second that there are "mathematical artifacts" and other non-resonant effects that may cause such poles without a resonance effect being observed, this is specially

true for poles far from the real axis. Conversely there can be potentials displaying resonant effects without any poles whatsoever in the S matrix.

There are some important quantities to know when characterizing resonances, one of those is the *phase shift*, $\delta(p)$, which is defined as

$$\delta(p) \approx -\arg\left(\frac{d\mathfrak{F}}{dp}\right)_{\bar{p}} - \arg(p - \bar{p}) \equiv \delta_{\text{bg}} + \delta_{\text{res}}(p) \tag{I.71}$$

where $\mathfrak{F}$ is the Jost function (see [5,8]) and $\bar{p} = p_{\text{R}} - ip_{\text{I}}$, with R standing for real or resonance, and I for imaginary. The quantity δ_{res} is called the resonant phase shift, and is the angle from the "horizontal" axis to the vector going from p to $\bar{p}$. So, as p increases past the location of the zero in the Jost function, the resonant part of the phase shift, $\delta_{\text{res}}(p)$ increases from 0 to π. The closer the zero is to the real axis, the more sudden is the increase. This rapid increase of $\delta_l(p)$ by π in Equation (I.71) can be understood as the definition of a resonance of angular momentum l. Furthermore, we can note that the behavior of the scattering partial cross section $\sigma_l(p)$ near a resonance will depend on the value of the background phase shift δ_{bg},

$$\sigma_l(p) = \frac{4\pi(2l+1)}{p^2} \sin^2 \delta_l(p) \tag{I.72}$$

Just as all the equations related to the resonances have been shown to depend on p, similar expressions can be derived in terms of $E = \frac{p^2}{2m}$, and the bound states and resonant states can therefore be placed on the imaginary E plane as well. One important quantity to look at is $\bar{E}$,

$$\bar{E} = E_{\text{R}} - i\frac{\Gamma}{2} \tag{I.73}$$

As a function of energy, which usually provides a more practical representation to know than that in terms of p, the peak of a resonance will be expected to happen at E_{R} and will have an approximate width of Γ. When a resonance in potential scattering is due to an angular momentum barrier it is known as a shape resonance.

Shape resonances in molecular photoionization

Shape resonances can be described as a one electron continuum state phenomenon in which the ejected photoelectron is resonantly trapped by a potential barrier through

which it eventually tunnels into the continuum. This dynamical centrifugal barrier temporarily traps the electron in the region of the molecule. The barrier is determined by both the sensitive interaction of the Coulombic screening and the centrifugal forces acting on the ionized electron in the proximity of the molecule. It is important to recall that such forces only produce shape resonance effects under particular circumstances of symmetry and angular momentum of the continuum channel. These centrifugal barriers occur in the perimeter of the molecule, because there is where angular momentum is approximately a good quantum number thus allowing the radial and angular motion to be decoupled [23]. This results in low barriers due to the relatively weak attractive forces. Thus shape resonances usually occur only at energies close to threshold and to depend sensitively on the characteristics of the molecular potential. It is important to note that shape resonances are not the only possible resonant processes above an ionization threshold. Other processes that can induce a rise in the cross section in isolated molecules are multi electron resonances, and shape resonances are a one-electron process, and even non-resonant phenomena such as satellite thresholds can induce sudden rises in the cross section. Although it has been more common to find shape resonances localized along bond axes it should not be assumed that they will always be of σ symmetry, since there is no fundamental reason to assume that. Piancastelli [23] mentions as the two main criteria to assign a resonance as a shape resonance the following:

1. Confirm the one-electron character of the resonant process, the resonant enhancement should be exhibited only by the main line channel.

2. Perform the corresponding theoretical calculations for comparison.

Dehmer *et al.*, [24] showed how shape resonances in molecular photoionization induce strong coupling between vibrational and electronic motion over a spectral range broader than the half-width (see second term of Equation (I.73)). This coupling is enhanced by the time delay in the photoelectron escape. In the next chapters, effects of this conclusion are shown to happen in the systems studied and to have different degrees of impact on each case.

I.3 Overview of research projects

I.3.1 Derivation of electronic factors as a framework for comparison between theory and experiments of photoionization where non-Franck-Condon behavior prevails

The Franck-Condon approximation is said to hold when the electronic transition matrix elements do not depend on the geometry of the molecule. Deviations from the Franck-Condon principle can have a variety of origins, such as shape resonances and inter channel continuum coupling effects [25], auto ionization [26], geometry dependent interference effects [27] and Cooper minima [28] among others. The evaluation of the effects of such non-Franck-Condon features is of great use to characterize them, and get a qualitative and quantitative estimate of their magnitude. There are several methods for the evaluation of the Franck-Condon and non-Franck-Condon factors [29–31] for different systems (polyatomic molecules, harmonic oscillators, Morse potentials, etc.). Here we derive, and in the following sections implement, two approximations to this problem, considering first an expansion of the matrix element of the dipole operator $\vec{\mu}$ up to first order terms and second, an extension where we also assume harmonic oscillator functions and the same frequencies in the initial and final vibrational states.

I.3.2 Study of the mechanisms of Franck-Condon breakdown on diatomic linear molecules

The interpretation of the vibrational structure of photoelectron spectra is usually made using the adiabatic approximation, in which the time scale of the ionization process is assumed to be so short that the motions of the nuclei are effectively frozen during this process, *i.e.* that the bond length remains basically constant during the transition (see for example [32]). With the additional approximation that electronic transition matrix elements do not depend on the geometry, *i.e.* the Franck-Condon approximation, the relative intensity of ionization to different final vibrational states of the same electronic state can be then understood by considering the overlap between the vibrational wave functions of the initial and final states.Observations of how vibrational branching ratios vary as a function of photon energy from the corresponding Franck-Condon values provide a good indication of the geometry dependence of a specific electronic transition. In this direction, we studied the molecular

photoionization of N_2 leading to the $3\sigma_g^{-1}$ and $2\sigma_u^{-1}$ ion states and CO leading to the isoelectronic valence states. The vibrational branching ratios were computed and the analysis of the ratios for these processes showed a breakdown in the Franck-Condon approximation. Some of the deviations have been well documented as shape resonances, but we also found by means of a partial wave analysis, that the partial wave cross sections have an interference pattern similar to a Young-type interference, which are related to molecular Cooper minima. Such features were also seen to induce non-Franck-Condon effects in the vibrational branching ratios at higher energies. The use of an electronic factor F, described in Chapter II of this work, proved to be of great use to compare both experiments and theory.

I.3.3 Vibrationally specific photoionization cross sections from low energy electrons on low-symmetry molecular systems

The discovery that low-energy electron collisions with DNA can lead to single and double strand breaks [33] has led to much interest in the study of such collisions with molecules which are models for fragments of DNA [34] and more generally of collisions with larger, low-symmetry molecular systems. We have studied such low symmetry systems by specifically looking at the vibrational branching ratios in the photoionization of acrolein for ionization leading to the $\tilde{X}\ ^2A'$ ion state. The method outlined in Chapter II is employed to compute logarithmic derivatives of the cross sections and to compare the theoretical data obtained in this work with the experimental measurements done by our collaborators. From the analysis, we located two shape resonances near photon energies of 15.5 and 23 eV in the photoionization cross sections and they were demonstrated to originate from the partial cross section of the A' scattering symmetry. The use of the electronic factor F in this work provided, furthermore, a qualitative reference for the strength of a shape resonance and a measure of the sensitivity of the cross section to geometry changes in acrolein.

I.3.4 Effects of rotational motion between ionization and fragmentation on non-linear molecules

One of the experimental methods widely used for studying photoionization dynamics is the measurement of photoelectron angular distributions (PADs), being the observables giving the best insight on the transition matrix elements A molecular photoionization experiment is said to achieve "completeness" when it determines all

the information needed for the theoretical description of such process, which means to provide all the significant matrix elements or dynamic parameters [35]. There are different experimental methods for obtaining the matrix elements from the PADs for molecular ionization, depending on the frame of reference used. When a measurement is done on a fixed-in-space oriented molecule, it is referred to as the molecular frame photoelectron angular distribution (MFPAD) and if the direction of emission of the recoil fragment is taken as reference it is named the recoil frame photoelectron angular distribution (RFPAD). Non-linear systems, as mentioned above, show special difficulties compared to linear molecules due to the extra angular and spatial coordinate(s) that must be considered when studying the MFPADs and RFPADs. Additional complications come into play when considering systems dissociating in two fragments and those with dissociative lifetimes that are long compared to the rotational period. Chapter V and Appendix A, a model is derived to predict the effects of rotational motion between the ionizing events and fragmentation of non-linear systems with lifetimes of the metastable molecular ions not short compared to the rotational periods of the molecule. We considered as a relevant system to study the C $1s$ ionization of the methane molecule, for which previous work has been done without the consideration of the rotational effects, providing a suitable framework of comparison.

CHAPTER II

A SCALED FRANCK-CONDON FACTOR TO STUDY THE MECHANISMS OF FRANCK-CONDON BREAKDOWN*

II.1 Introduction

In the previous chapter we described molecular photoionization, and discussed some of the methods and approximations required to deal with the continuous energy spectrum and the asymptotic boundary conditions necessary to describe the photoelectron produced within the photoionization process. In this chapter we explore in more detail the transitions expected in a photoionization process, and how by means of the Born-Oppenheimer approximation and the Franck-Condon approximation one can simplify its study. Furthermore we discuss how the breakdown of the Franck-Condon approximation can be used to characterize and identify different features common in ionizing processes. We introduce the notion of an *electronic factor*, F, that provides a common framework to compare experimental and theoretical results, helps to evaluate quantitatively the deviations from the expected Frank-Condon values for the vibrational branching ratios, and provides a qualitative measure of the relative effect that features causing non-Franck-Condon behavior have in general.

II.1.1 Ro-vibronic transitions

Transitions between two different electronic states of a diatomic molecule may also involve changes in both vibrational and rotational state. The analysis of such transitions allows for the determination of equilibrium internuclear distances and dissociation energies of the excited states produced. In this sense, each molecular state contains electronic, T_e, vibrational, G_v, and rotational, $F_v(J)$, contributions to the total energy [7]. The actual transition and energy difference between upper (single

---

primed) and lower (double primed) states will be given by,

$$h\nu = (T_e' - T_e'') + (G_{v'} - G_{v''}) + (F_{v'}(J') - F_{v''}(J'')) \tag{II.1}$$

II.1.2 The Franck-Condon approximation

As was mentioned in Chapter I, when Equation (II.1.2) is valid, it is assumed that matrix element $M_{\mathrm{i,f},\vec{k},\hat{n}}(R_0)$ is independent of R. One important consequence of the Franck-Condon (FC) approximation is that the branching ratios, defined in Equation (I.63), are reduced to energy independent ratios of squares of vibrational overlap integrals, and will have the form

$$B_{v',v''}^{\mathrm{FC}} = \frac{|\langle \chi_{\mathrm{i},v}(R) | \chi_{\mathrm{f},v'}(R) \rangle|^2}{|\langle \chi_{\mathrm{i},v}(R) | \chi_{\mathrm{f},v''}(R) \rangle|^2} \tag{II.2}$$

Each of the integrals in the branching ratio $B_{v',v''}^{\mathrm{FC}}$ is called a FC overlap, and provides an expression to determine the relative final state intensities as a function of v. By looking at Figure II.1 this "overlap" takes a more physical meaning, since it is clear as indicated by the blue arrow, that a transition between two vibrational levels (from different electronic states) will be favored when there is an *overlap* between the two vibrational envelopes. In the example depicted, such transition goes from $v'' = 0$ to $v' = 2$, and purely from this perspective the probability of a transition from $v'' = 0$ to either $v' = 0$ or $v' = 1$ is very low, since there is a very small overlap between the two vibrational wave functions. If an absolute probability is desired, then the electronic matrix element is needed. In the evaluation of the FC overlap integrals, symmetry is not always useful, since the symmetry of initial, i, and final, f, electronic states may not be the same. If the overlap integral is to be non-zero, both electronic states must belong to the same irreducible representation [36].

For diatomic molecules, the dependence of the overlap on the final electronic and vibrational state can be determined qualitatively by looking at the electronic potential energy curves, where usually the excited state equilibrium geometry is displaced with respect to the initial ground state (see in Figure II.1 the displacement labeled as q_{01}). When there is a considerable overlap between an initial bound state

---
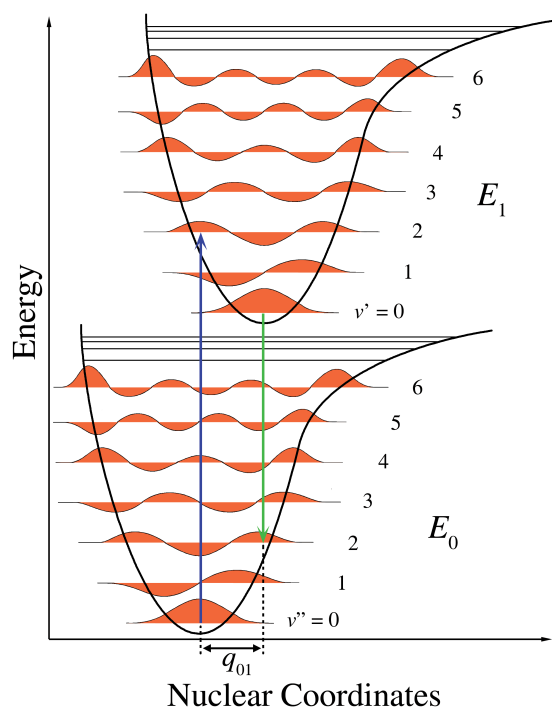
Figure II.1: Franck-Condon principle energy diagram. Since electronic transitions are very fast compared with nuclear motions, vibrational levels are favored when they correspond to a minimal change in the nuclear coordinates. From the overlaps depicted it is clear that the transition from $v = 0$ to $v' = 2$ is favored.[2]

and a final dissociative continuum state, a portion of the band spectrum will be expected to be continuous. It is important to note that the square of the overlap of initial and final states gives the probability of the transition to happen (we can understand Equation (II.2), as a ratio of two probabilities).

In cases where the overlap is very small, near to zero, even if symmetry allowed, its said to be FC forbidden, and as may be deduced from the qualitative definition of the overlap integral, this will occur when the initial and final states have very different equilibrium geometries. In contrast, there are many cases for polyatomic molecules, within the FC approximation, where the cross sections leading to certain vibrational states of the ion can be zero by symmetry, and thus, the transition will be a forbidden one. In those cases if there is a break down of the FC approximation it can lead to a vibronic transition induced by the lowering of the symmetry of the molecule by the vibrational motion. This is known as a *type 'a' vibronic transition* [37]. As expected those types of transitions are stronger near resonances in the photoionization process. Breakdown of the FC approximation is not the only reason that may lead to the observation of an otherwise forbidden transition. If it is due to a breakdown in the Born-Oppenheimer approximation for the final ionic state, it is known as *type 'b' vibronic transition*, and the molecular state is thus a mixture of states with same vibronic symmetry but from electronic states of different symmetry [16]. When there is a strong geometry dependence of an electronic transition moment $M_{i,f,\vec{k},\hat{n}}(R_0)$, then the FC approximation no longer holds and breaks down. This phenomena can happen for different reasons, one of the most prominent being that the photoionization energies are near to the energies of resonant processes. Two important examples that have become standards to exemplify this behavior are the photoionization of N_2 and CO, that will be addressed with detail in the next chapter [16].

II.1.3 Franck-Condon factors

According to the FC principle the transfer of excitation in an electronic transition occurs in a time that is short compared with that required for vibrational motion to take place. Assuming that a transition moment $T_{e',e''}$ varies slowly with internuclear coordinates, q, the absolute probability, $P_{v',v''}$ for the transition mentioned before, is given by [38],

$$P_{v',v''} = [T_{e',e''}]^2 \, |\langle \chi_{i,v}(R) | \, \chi_{f,v'}(R)\rangle|^2 \tag{II.3}$$

The second term of the product is referred to as the FC factor, and it is obvious from Equation (II.3) that it will be proportional to $P_{v',v''}$ when $T_{e',e''}$ is constant.

Theoretically, the evaluation of this FC factors requires to know the vibrational wave functions for the initial and final states. These wave functions can be obtained using a number of different assumptions and approximations of which the use of a harmonic oscillator normal mode basis is probably the best known. Although the use of the harmonic basis has proven its utility particularly at low energies, it is clear that the assignment of normal-modes for individual states become more difficult due to anharmonicity effects as vibrational energy increases, so that the use of other approximations such as the Morse potential, or more complex functions are required. In this context, there have been a number of functions proposed to evaluate the FC factors. López *et al.* [31] suggested a model to calculate 1-D Morse functions overlaps, using the Morse potential eigenstates. Starting from the one dimensional Morse potential function,

$$V(x) = \mathcal{D}[(1 - e^{-\beta x})^2 - 1], \quad (x = R - R_e) \tag{II.4}$$

where $\mathcal{D}$ is the bonding energy and $x = R - R_e$ is the position with respect to the equilibrium geometry, R_e. The energy spectrum is described by $E_v = -\frac{\hbar^2 \beta^2}{2\mu}(j - v)^2$, with $j = \frac{\sqrt{2\mu\mathcal{D}}}{\beta\hbar} - 1/2$. Taking this potential as a starting point, they define an overlap integral $f_{1,2}$, and consequently FC factors which depends on the number of anharmonic phonons ν and other quantities defined within the Morse energy expression, to give an explicit formula (see Equation (20) on reference [31]). Different approaches have been taken by Frank *et al.* [30], who started from a harmonic oscillator potential and defined overlap integrals for diatomic molecules based on the so called Bogoliubov algebraic transformations [30]. Also, using two one-dimensional harmonic oscillators Castañeda and co-workers [39], derived an algebraic self contained method to compute FC overlaps and factors in the form of sums of products of Hermite polynomials. As can be seen, there are several methods for the evaluation of the Franck-Condon and non-Franck-Condon factors [29–31, 39] for different systems (polyatomic molecules, harmonic oscillators, Morse potentials, etc.). Here we derive and implement two new approximations to this problem, considering first an expansion of the matrix element of the dipole operator $\vec{\mu}$ up to first order terms, and second an extension where we also assume harmonic oscillator functions and the

same frequencies in the initial and final vibrational states. This approach will be tested later in Chapter III in the study of photoionization of systems of very high symmetry and in the Chapter IV on a larger system with lower symmetry and in a range of photon energies of more than 100 eV.

II.2   Theory

Within the Born-Oppenheimer or Chase approximation [22], widely used in molecular photoionization theory (see Section I.2.3), both the bound electronic state and the photoelectron wave function only depend on the position of the nuclei and not on their momenta. Then, the initial state and final total scattering state wave functions may, respectively, be written as [16],

$$\Psi_{\rm i}(r,q) = \psi_{\rm i}(r;q)\chi_{v,{\rm i}}(q) \tag{II.5}$$

$$\Psi_{{\rm f},\vec{k}}^{(-)}(r,q) = \psi_{{\rm f},\vec{k}}^{(-)}(r;q)\chi_{v^+,{\rm f}}(q) \tag{II.6}$$

where r represents the electronic coordinates, q represents the generalized normal mode nuclear coordinates, and $\chi_{v,{\rm i}}(q)$ and $\chi_{v^+,{\rm f}}(q)$ are the initial and final state vibrational wave functions, note these two equations are the same as Equations (I.58) and (I.59) just with different selection of coordinates. Here, the $(-)$ symbol is used in the conventional way to denote an outgoing asymptotic wave within the total scattering $(\Psi_{{\rm f},\vec{k}}^{(-)}(r,q))$ or continuum $(\psi_{{\rm f},\vec{k}}^{(-)}(r;q))$ states.

In photoionization, the transition matrix elements in the dipole length form can be expressed as [40, 41],

$$f_{\vec{k},\hat{n}}^{({\rm f}\leftarrow{\rm i})} = (k)^{1/2} \left\langle \Psi_{\rm i} \middle| \vec{\mu} \cdot \hat{n} \middle| \Psi_{{\rm f},\vec{k}}^{(-)} \right\rangle \tag{II.7}$$

where $\vec{k}$ is the momentum of the photoelectron, $\hat{n}$ is the direction of the polarization of the light, and $\vec{\mu}$ is the dipole operator. The $(k)^{1/2}$ factor changes the normalization of continuum functions $\Psi_{{\rm f},\vec{k}}^{(-)}$ from momentum to energy normalization [41]. Then applying Equations (II.5) and (II.6) to the transition matrix element we get

$$f_{\vec{k},\hat{n}}^{(v^+\leftarrow v)} = \left\langle \chi_{v,{\rm i}}(q) \middle| \mu\left(\vec{k},\hat{n},q\right) \middle| \chi_{v^+,{\rm f}}(q) \right\rangle_q \tag{II.8}$$

where

$$\mu\left(\vec{k}, \hat{n}, q\right) = \left\langle \psi_{\mathrm{i}}(r; q) \left| \sum_j e\vec{r}_j \cdot \hat{n} \right| \psi_{\mathrm{f},\vec{k}}^{(-)}(r; q) \right\rangle_r \qquad \text{(II.9)}$$

Then by using Equation (II.8), the vibrationally specific cross sections are obtained by averaging over all orientations of the field and integrating over the emission direction of the photoelectron, yielding the expression,

$$\sigma_{v^+ \leftarrow v} = \frac{\pi}{cE} \int d\Omega_{\hat{k}} \int d\Omega_{\hat{n}} \left| f_{\vec{k},\hat{n}}^{(v^+ \leftarrow v)} \right|^2 \qquad \text{(II.10)}$$

where $\Omega_{\hat{j}}$ is the solid angle in the $\hat{j}$ direction, c is the speed of light and E is the energy of the photon. Thus, from this definition, the branching ratio $R_{v_j^+ \leftarrow v/v_i^+ \leftarrow v}$ for the excitation of the v_j^+ state, relative to the v_i^+ state is defined as

$$R_{v_j^+ \leftarrow v/v_i^+ \leftarrow v} = \frac{\sigma_{v_j^+ \leftarrow v}}{\sigma_{v_i^+ \leftarrow v}}. \qquad \text{(II.11)}$$

II.2.1   Breakdown of the Franck-Condon approximation

By considering the expansion of the dipole matrix element with respect to q around the equilibrium internuclear distance q_0 we obtain,

$$\mu\left(\vec{k}, \hat{n}, q\right) = \mu\left(\vec{k}, \hat{n}, q_0\right) + \left[\frac{\partial \mu\left(\vec{k}, \hat{n}, q\right)}{\partial q}\right]_{q_0} (q - q_0) + \dots \qquad \text{(II.12)}$$

Introducing Equation (II.12) into the total cross section allows us to rewrite it as,

$$\begin{aligned}
\sigma_{v^+ \leftarrow v} = \frac{1}{4\pi} \iint d\Omega_{\hat{k}} d\Omega_{\hat{n}} \Big| &\mu(\vec{k}, \hat{n}, q_0) \left\langle \chi_{v^+,\mathrm{f}}(q) | \chi_{v,\mathrm{i}}(q) \right\rangle \\
&+ \left[\frac{\partial \mu(\vec{k}, \hat{n}, q)}{\partial q}\right]_{q_0} \left\langle \chi_{v^+,\mathrm{f}}(q) | (q - q_0) | \chi_{v,\mathrm{i}}(q) \right\rangle + \cdots \Big|^2
\end{aligned} \qquad \text{(II.13)}$$

If this expansion is truncated at the first derivative and only the first order terms are retained, Equation (II.13), when all vibrational integrals are real valued, can be expressed as

$$\sigma_{v^+\leftarrow v} = \left[\frac{1}{4\pi}\iint d\Omega_{\hat{k}}d\Omega_{\hat{n}}\left|\mu(\vec{k},\hat{n},q_0)\right|^2\right]\langle\chi_{v^+,\mathrm{f}}(q)|\,\chi_{v,\mathrm{i}}(q)\rangle^2$$

$$+\left\{\frac{1}{4\pi}\iint d\Omega_{\hat{k}}d\Omega_{\hat{n}}2\mathbb{R}\left[\mu^*(\vec{k},\hat{n},q_0)\left[\frac{\partial\mu(\vec{k},\hat{n},q)}{\partial q}\right]_{q_0}\right]\right\} \qquad \text{(II.14)}$$

$$\times\,\langle\chi_{v,\mathrm{i}}(q)|\,\chi_{v^+,\mathrm{f}}(q)\rangle\,\langle\chi_{v^+,\mathrm{f}}(q)|\,(q-q_0)\,|\chi_{v,\mathrm{i}}(q)\rangle.$$

For simplicity, we define the integral factors multiplying the vibrational wave function matrix elements on Equation (II.14) as $\sigma^{(0)}$ and $\sigma^{(1)}$,

$$\sigma^{(0)} = \frac{1}{4\pi}\iint d\Omega_{\hat{k}}d\Omega_{\hat{n}}\left|\mu(\vec{k},\hat{n},q_0)\right|^2$$

$$\sigma^{(1)} = \frac{1}{4\pi}\iint d\Omega_{\hat{k}}d\Omega_{\hat{n}}2\mathbb{R}\left[\mu^*(\vec{k},\hat{n},q_0)\left[\frac{\partial\mu(\vec{k},\hat{n},q)}{\partial q}\right]_{q_0}\right] \qquad \text{(II.15)}$$

where $\sigma^{(0)}$ is the total cross section at q_0 and $\sigma^{(1)}$ is the first derivative of the total cross section with respect to q at q_0. Higher order terms coming from the original expansion might be written as $\sigma^{(j)}$ with $j > 1$ and can provide more accurate expressions for the photoionization matrix elements if the $\mu(\vec{k},\hat{n},q_0)$ have significant geometry dependence in the range of vibrational integrals. Now the total cross section from Equation (II.13) can be rewritten in terms of Equation (II.15) to become,

$$\sigma_{v^+\leftarrow v} = \sigma^{(0)}\langle\chi_{v^+,\mathrm{f}}(q)|\,\chi_{v,\mathrm{i}}(q)\rangle^2 + \sigma^{(1)}\langle\chi_{v,\mathrm{i}}(q)|\,\chi_{v^+,\mathrm{f}}(q)\rangle\,\langle\chi_{v^+,\mathrm{f}}(q)|\,(q-q_0)\,|\chi_{v,\mathrm{i}}(q)\rangle \tag{II.16}$$

When the Franck-Condon branching ratio is not zero, it is useful to write $R_{v_1^+\leftarrow v/v_0^+\leftarrow v}$ in terms of the Franck-Condon branching ratio

$$R_{v_1^+\leftarrow v/v_0^+\leftarrow v} = R^{(\mathrm{FC})}_{v_1^+\leftarrow v/v_0^+\leftarrow v}\times\frac{1+\dfrac{\sigma^{(1)}\left\langle\chi_{v_1^+,\mathrm{f}}(q)\left|(q-q_0)\right|\chi_{v,\mathrm{i}}(q)\right\rangle}{\sigma^{(0)}\left\langle\chi_{v_1^+,\mathrm{f}}(q)\left|\chi_{v,\mathrm{i}}(q)\right.\right\rangle}}{1+\dfrac{\sigma^{(1)}\left\langle\chi_{v_0^+,\mathrm{f}}(q)\left|(q-q_0)\right|\chi_{v,\mathrm{i}}(q)\right\rangle}{\sigma^{(0)}\left\langle\chi_{v_0^+,\mathrm{f}}(q)\left|\chi_{v,\mathrm{i}}(q)\right.\right\rangle}} \tag{II.17}$$

where

$$R^{(FC)}_{v_1^+ \leftarrow v/v_0^+ \leftarrow v} = \frac{\left\langle \chi_{v_1^+,f}(q) \middle| \chi_{v,i}(q) \right\rangle^2}{\left\langle \chi_{v_0^+,f}(q) \middle| \chi_{v,i}(q) \right\rangle^2}. \tag{II.18}$$

Keeping only first-order terms, together with the already defined Franck-Condon vibrational branching ratio in last equation, we have [42]

$$
\begin{aligned}
&R_{v_1^+ \leftarrow v/v_0^+ \leftarrow v} \\
&= R^{(FC)}_{v_1^+ \leftarrow v/v_0^+ \leftarrow v} \\
&\times \left[1 + \frac{\sigma^{(1)} \left\langle \chi_{v_1^+,f}(q) \middle| (q - q_0) \middle| \chi_{v,i}(q) \right\rangle}{\sigma^{(0)} \left\langle \chi_{v_1^+,f}(q) \middle| \chi_{v,i}(q) \right\rangle} - \frac{\sigma^{(1)} \left\langle \chi_{v_0^+,f}(q) \middle| (q - q_0) \middle| \chi_{v,i}(q) \right\rangle}{\sigma^{(0)} \left\langle \chi_{v_0^+,f}(q) \middle| \chi_{v,i}(q) \right\rangle} \right]
\end{aligned}
\tag{II.19}
$$

We can define the electronic contribution to the non-Franck-Condon behavior as

$$F = \frac{\sigma^{(1)}}{\sigma^{(0)}}, \tag{II.20}$$

which using the first-order expansion in Equation (II.19) can be written as

$$
\begin{aligned}
F &= \left[\frac{R_{v_1^+ \leftarrow v \backslash v_0^+ \leftarrow v}}{R^{(FC)}_{v_1^+ \leftarrow v \backslash v_0^+ \leftarrow v}} - 1 \right] \\
&\times \left[\frac{\left\langle \chi_{v_1^+,f}(q) \middle| (q - q_0) \middle| \chi_{v,i}(q) \right\rangle}{\left\langle \chi_{v_1^+,f}(q) \middle| \chi_{v,i}(q) \right\rangle} - \frac{\left\langle \chi_{v_0^+,f}(q) \middle| (q - q_0) \middle| \chi_{v,i}(q) \right\rangle}{\left\langle \chi_{v_0^+,f}(q) \middle| \chi_{v,i}(q) \right\rangle} \right]^{-1}
\end{aligned}
\tag{II.21}
$$

II.3   Harmonic approximation

Equations (II.20) and (II.21), provide a way to analyze experimental and theoretical branching ratio data to emphasize the geometry dependence of the transition moment and factor out the effects of the change in geometry and frequency of vibrations when going from the initial state to the ion state. A more compact and easily applied form can be obtained by assuming the same frequency for the initial and final vibrational states and harmonic oscillator vibrational wave functions, for $(1 \leftarrow 0/0 \leftarrow 0)$ and

$(2 \leftarrow 0/0 \leftarrow 0)$ reducing Equation (II.20) to [42]

$$F = \pm \left(2R_{1\leftarrow 0/0\leftarrow 0}^{(FC)} \right)^{\frac{1}{2}} \left[\frac{R_{1\leftarrow 0/0\leftarrow 0}}{R_{1\leftarrow 0/0\leftarrow 0}^{(FC)}} - 1 \right] \tag{II.22}$$

and

$$F = \pm \left(\frac{R_{2\leftarrow 0/0\leftarrow 0}^{(FC)}}{2} \right)^{\frac{1}{4}} \left[\frac{R_{2\leftarrow 0/0\leftarrow 0}}{R_{2\leftarrow 0/0\leftarrow 0}^{(FC)}} - 1 \right] \tag{II.23}$$

where the sign depends on the direction of displacement of the ion state potential energy function from that of the neutral state. These expressions were derived assuming that $q = \pm 1$ correspond to the inner and outer classical turning points of the initial state vibrational wave function. It is noteworthy from these expressions that $F = 0$ corresponds to the Franck-Condon behavior, as can be seen from the terms in the square brackets in Equations (II.21) to (IV.5), when $R_{i\leftarrow 0/0\leftarrow 0} = R_{i\leftarrow 0/0\leftarrow 0}^{(FC)}$, for $i = 1, 2$.

II.4 Conclusion

We showed how the F factor can be related to the deviation of the branching ratios from their Franck-Condon value allowing the experimental data to be presented as measured F factors. In particular, when $F = 0$, the Franck-Condon approximation is valid. Then the deviation from zero indicates the extent of the breakdown of the Franck-Condon approximation.

CHAPTER III

MECHANISMS OF FRANCK-CONDON BREAKDOWN ON HIGHLY SYMMETRIC MOLECULES[*]

III.1   Introduction

We mentioned in Chapter II how the behavior of vibronic intensities within the Franck-Condon approximation provides a good insight into the geometry dependence of electronic transitions. In this chapter we explore this phenomena in close connection to resonances but even more in connection to molecular Cooper minimum [28,43]. The main focus is on highly symmetric systems, and for such purpose we take as benchmarks the well known molecular photoionization of two isoelectronic diatomic molecules: N_2 and CO.

The molecular photoionization of N_2 leading to the $3\sigma_g^{-1}$, $2\sigma_u^{-1}$ ion states and CO leading to the valence isoelectronic $5\sigma^{-1}$, $4\sigma^{-1}$ ion states is studied using theoretical methods, and the results are compared with the experimental results obtained by our collaborators giving a picture of the utility of the methods derived in this work [42]. The vibrational branching ratios were obtained in the 15 to 200 eV photoelectron energy range. The analysis of the computed branching ratios for these processes showed a breakdown in the Franck-Condon approximation in the range of energies studied. Some of the deviations at lower energies are well documented as being due to shape resonances, in such cases we found good agreement between the present work and previous experimental and theoretical investigations of these photoionization channels. Besides the shape resonances, both N_2 and CO ionization showed that the partial wave cross sections have an interference pattern similar to a Young-type interference [44,45], which are related to molecular Cooper minima [46–49]. Such features are seen to induce non-Franck-Condon effects in the vibrational branching ratios at higher energies.

The interpretation of the vibrational structure of photoelectron spectra is usually

made using the adiabatic, or Born-Oppenheimer, approximation (see Section I.2.3), in which the time scale of the ionization process is assumed to be so short that the motions of the nuclei are effectively frozen during this process, *i.e.* that the bond length remains basically constant during the transition (see for example [32]). With the additional approximation that electronic transition matrix elements do not depend on the geometry, *i.e.* the Franck-Condon approximation (see section II.1.2), the relative intensity of ionization to different final vibrational states of the same electronic state can be then understood by considering the overlap between the vibrational wave functions of the initial and final states. Furthermore, the ratio of cross sections between different final vibrational levels will then not depend on the photon energy. Observations of how vibrational branching ratios vary as a function of energy from the corresponding Franck-Condon values provide a good indication of the geometry dependence of a specific electronic transition. Deviations from the Franck-Condon principle can have a variety of origins, such as shape resonances and interchannel continuum coupling effects [25], autoionization [26], geometry dependent interference effects [27] and Cooper minima [28] among others. In this chapter we focus on the breakdown of the Franck-Condon approximation related to the appearance of Cooper minima in the photoionization total cross sections. This phenomenon is characterized by a change of sign in a dipole matrix element as a function of photon energy. Therefore at a Cooper minimum a particular matrix element goes through zero, which in certain circumstances can be accompanied by a rapid change in the photoelectron asymmetry parameter β [49,50].

Originally Cooper minima were observed as an atomic phenomena [43] on multiple atoms and later were studied in a more systematic manner for atoms throughout the periodic table, finding them in ionization from subshells with nodes in their wave functions [50]. As a molecular feature, a general review was presented by Carlson *et al.* [49] who studied Cooper minima as a function of atomic number, subshell and molecular environment for the case where the initial orbital is nearly atomic. Such atomic-like Cooper minima are relatively insensitive to geometry and are thus not expected to lead to the breakdown of the Franck-Condon principle. In contrast to this case, there are also molecular Cooper minima which arise from the geometry dependence of the initial or final state wave functions. Geometry dependence of Cooper minima in molecules has been observed by Stephens and McKoy [46], and others.

The molecular photoionization of CO and N_2 has been widely studied, both theoretical and experimentally [28, 41, 51–58]. In particular, previous experiments and theoretical studies of the vibrational branching ratios at low energy for the $X^2\Sigma_g^+$ state of N_2^+ and $X^2\Sigma^+$ state of CO^+ [52] and the $B^2\Sigma_u^+$ state of N_2^+ and $B^2\Sigma^+$ state of CO^+ [51] and high energy for the $B^2\Sigma_u^+$ state of N_2^+ [28] have been performed. Here, along with our theoretical calculations, we include data from newly measured high energy experimental vibrational branching ratios for the X and B ion states of N_2^+ and CO^+ obtained from photoelectron spectroscopy (done by our experimental collaborators at Louisiana State University), allowing for a consistent treatment of the four states considered here [42]. The N_2 and CO A states appearing at intermediate ionization potentials are not considered in the present work where we have focused on the electronic X and B states. These two states have very similar ionic potential energy curves and are related by the fact that in the CO molecule the X and B states are of the same symmetry and can be thought of as a linear combination of the corresponding states in N_2. In any case, the A states have been extensively studied by other authors [52].

We proposed in Chapter II an alternative presentation of vibrational branching ratios which is directly related to the logarithmic derivatives of the cross section with respect to bond length (see Equations (II.19) to (IV.5)). This provides a mean to compare the breakdown of the Franck-Condon approximation across systems with differing frequencies and bond shifts upon ionization. We have additionally analyzed the resulting non-Franck-Condon behavior at higher energy in terms of Cooper minima within the Cohen-Fano framework. Cohen and Fano [53] showed that photoelectrons emitted from more than one atomic center can exhibit interference effects related to the well known Young's double slit experiment [44]. Evidence of interference phenomena may be seen from the total cross section reported there as $\sigma = \sigma_0[1 + (\sin kR)/(kR)]$ where σ_0 is the atomic photoionization cross section (for a hydrogen-like atom of atomic number Z^*), k is the electron wave vector and R the internuclear distance.

More recently it has been reported that the photoionization of H_2 and H_2^+ oriented perpendicularly to the polarization direction of the light exhibit a typical Young's double-slit interference pattern [45, 59–62]. Similar studies support the interpretation of the photoemission from homonuclear diatomic molecules, such as N_2, in terms of a double-slit experiment [63]. The case of heteronuclear diatomic molecules has

been less explored, although also in the original work by Cohen and Fano [53], it was proposed that for this type of systems the modulation interference will proceed approximately as $\sin 2kR$ since parity considerations have less relevance than in the case of homonuclear systems. The recent work by Canton *et al.* [52] suggests that having non identical centers, the interferences should differ from those coming from homonuclear molecules (just like having two different slits in the Young's experiment), but that coherent emission of the electron wave is still possible given a sufficiently delocalized ionized molecular orbital over the two nuclei.

The systems studied here, N_2 and CO are a good benchmark for photoionization studies, especially with respect to using molecular probes as interference modulators, since both are small enough for accurate calculations providing a definitive interpretation. Another interesting feature that makes these two molecules suitable for a comparison between homonuclear and heteronuclear centers is the fact they are isoelectronic, having basically the same electronic ground state configuration, $1\sigma_g^2\ 1\sigma_u^2\ 2\sigma_g^2\ 2\sigma_u^2\ 1\pi_u^4\ 3\sigma_g^2$ for N_2 and $1\sigma^2\ 2\sigma^2\ 3\sigma^2\ 4\sigma^2\ 1\pi^4\ 5\sigma^2$ for CO.

III.2   Calculations

In this study, we used a range of geometries (bond lengths) of N_2 and CO including the corresponding equilibrium values, $R_{N-N}/\text{Å} = 0.8763$, 0.9206, 0.9649, 1.0091, 1.0534, 1.0977 (equilibrium), 1.1419, 1.1861, 1.2304, 1.2746, 1.3189 and $R_{C-O}/\text{Å} = 0.9179$, 1.00194, 1.04396, 1.08598, 1.12800 (equilibrium), 1.17002, 1.21204, 1.25406, 1.29608, 1.33810 respectively. All the electronic structure calculations on the bound states have been done with the MOLPRO suite of programs [64]. The systems were studied at the Hartree-Fock (HF) level for both the initial and ion states. The scattering calculations were performed using a single channel frozen-core Hartree-Fock approximation (SCFCHF) with the ePolyScat suite of programs [65, 66]. For these calculations, the maximum l in the partial wave expansion of the scattering wave functions and orbitals is 75. The vibrational wave functions for the initial $\chi_v(q_i)$ and ion states $\chi_{v^+}(q_i)$ were taken to be the Morse oscillator eigenfunctions with the parameter obtained from Herzberg and Huber [67]. The electronic factor F was calculated using two approaches. First we directly computed F using Equation (II.20), where the derivatives were computed by numerical differentiation. Second, we computed F using Equation (II.22), where the branching ratios were computed using

Equations (II.8) and (II.11) with the full q dependent transition matrix elements and using Morse oscillators functions for the vibrational wave functions. These two approaches for computing F should give the same values to the extent that the oscillators are nearly harmonic and the higher order terms, which were neglected in the derivation of Equation (II.22), are indeed small. Finally, the experimental data was treated by using Equaiton (II.22) to express vibrational branching ratios in terms of the F electronic factors. The experimental methods used to produce the results that we show here in comparison of the theoretical calculations, were done by the group of Professor Erwin Poliakoff in the Chemistry Department at Louisiana State University, and the details can be found in reference [42].

III.3 Results and Discussions

In Figures III.1, III.2, III.3 and III.4 we present the experimental and computed electronic factors leading to the X and B states of N_2 and CO. In each case we have only considered the $(0 \leftarrow 1)/(0 \leftarrow 0)$ ratio and we have used Equation (II.22) to convert the experimental branching ratios to experimental electronic factors using computed Franck-Condon branching ratios. In Figure III.1 we give the data for the N_2^+ X state, where we have converted the experimental data to electronic factors using the computed Franck-Condon value of 0.0854. In this figure we see the strong deviation from the Franck-Condon value at low energy with only a weak energy dependence above 100 eV. In Figure III.2 we present the electronic factor for the ionization leading to the X state of CO^+ where we have used the computed Franck-Condon branching ratio of 0.03713 to compute the experimental F. In this case, there is both a strong resonance feature at low energy and a deviation from the constant Franck-Condon at high energy. In Figures III.3 and III.4, the corresponding electronic factors for ionization leading to the B states of N_2^+ and CO^+ are also given. In case of the N_2^+ B state, the Franck-Condon ratio used was 0.12478 and in the case of the CO^+ B state we used 0.36544. Plotted in terms of the electronic factors (F), the high energy deviations from the constant Franck-Condon result is seen fairly similar for these two cases, in contrast to how these results appear when the branching ratios are plotted [51] where there appears to be much less variation in the case of CO at high energy when compared to the ionization to the N_2^+ B state. Here, we convert experimental branching ratios to the F factors by scaling the
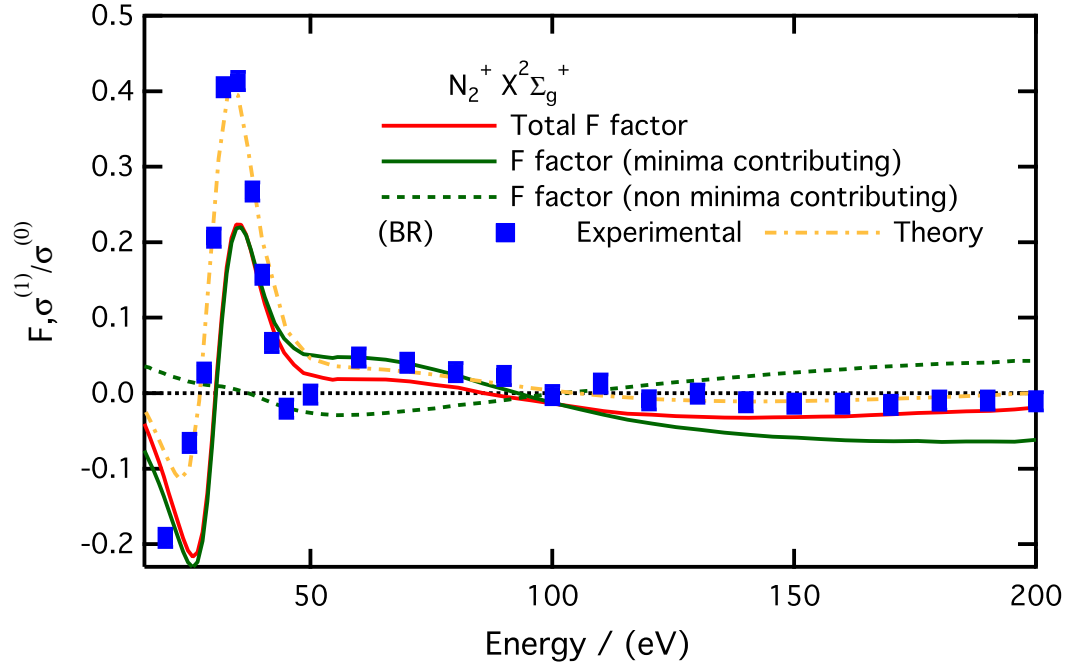
Figure III.1: Theoretical and experimental F factors for photoionization leading to the N_2^+ $X^2\Sigma_g^+$ ion state. The analysis of the experimental data was based on the computed $R^{(\text{FC})} = 0.0854$. The dot-dash gold line is the F factor computed using Equation (II.22). The red line is the F factor computed using Equation (II.20). The solid green line is the partial wave contribution to the F factor in Equation (II.20) from partial waves that have Cooper minima. The dashed green line is the contribution to F from the partial waves without a Cooper minimum. In this figure experimental errors are approximately the same size as the symbols used to plot the data.

branching ratios relative to the Franck-Condon value by the factor $\left(2R^{(\text{FC})}\right)^{(1/2)}$ as indicated in Equation (II.22). The relative errors are also scaled by the same factor. The scatter in the experimental branching ratio data is nominal (*i.e.*, relative errors are on the order of 4-6 %), however the scaling used to compute the F factor leads to larger experimental errors in the derived F values for the states which have the larger Franck-Condon branching ratio, *e.g.* in the CO B state case where $R^{(\text{FC})}$=0.36544.
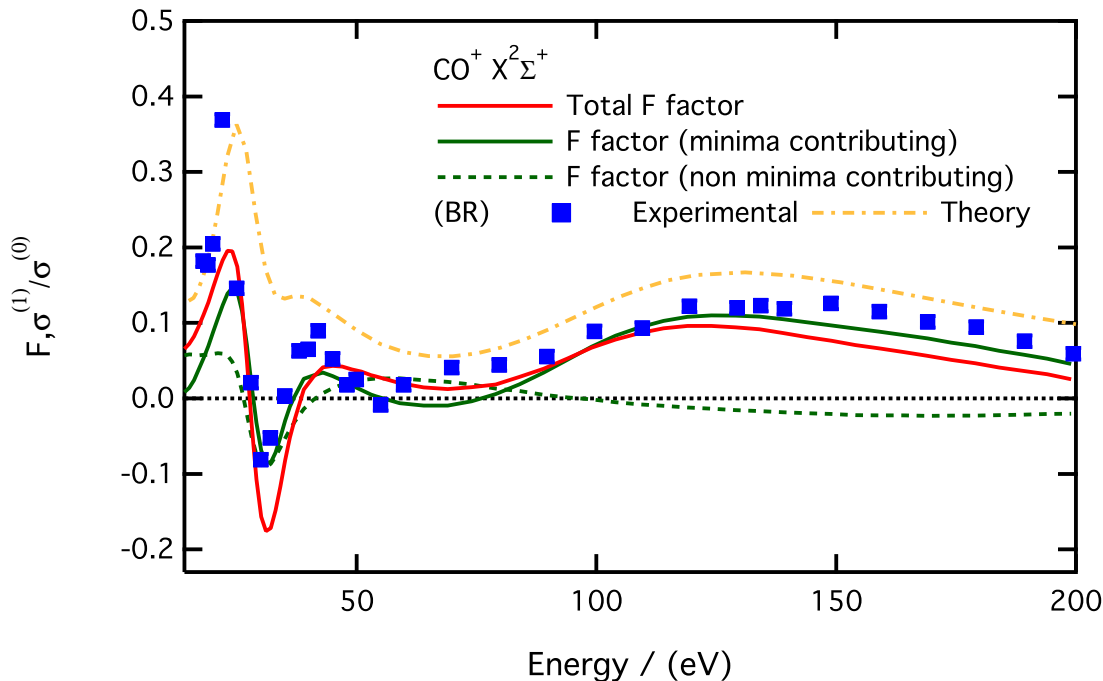
Figure III.2: Theoretical and experimental F factors for the photoionization leading to the CO$^+$ $X^2\Sigma^+$ ion state. Experimental values were derive assuming $R^{(\text{FC})} = 0.03713$. The definitions of the lines are the same as in Figure III.1.

III.3.1 The effects of shape resonances in the photoionization branching ratios of N$_2$ $3\sigma_g$ and CO 5σ orbitals

Both N$_2$ and CO are known to have prominent σ^* shape resonances which contribute to the photoionization of the X $(3\sigma_g)^{-1}$ ground state of N$_2^+$ and the X $(5\sigma)^{-1}$ ground state of CO$^+$ [23, 24, 68–70]. Due to the sensitivity of the resonant state energies to bond length, there are also significant non-Franck-Condon effects in the corresponding branching ratios [28, 51]. These features appear in the present calculations. The top panels of Figures III.5 and III.6 show the geometry depen-
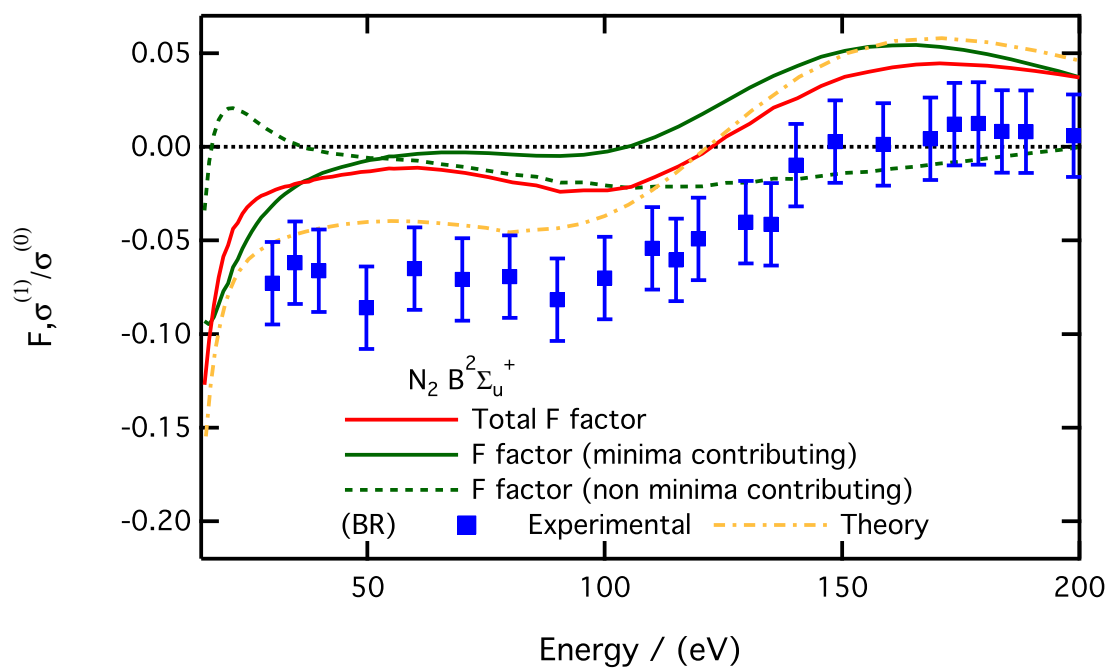
Figure III.3: Theoretical and experimental F factors for photoionization leading to the N_2^+ $B^2\Sigma_u^+$ ion state. Experimental values were derive ssuming $R^{(FC)} = 0.12478$. The definitions of the lines are the same as in Figure III.1.
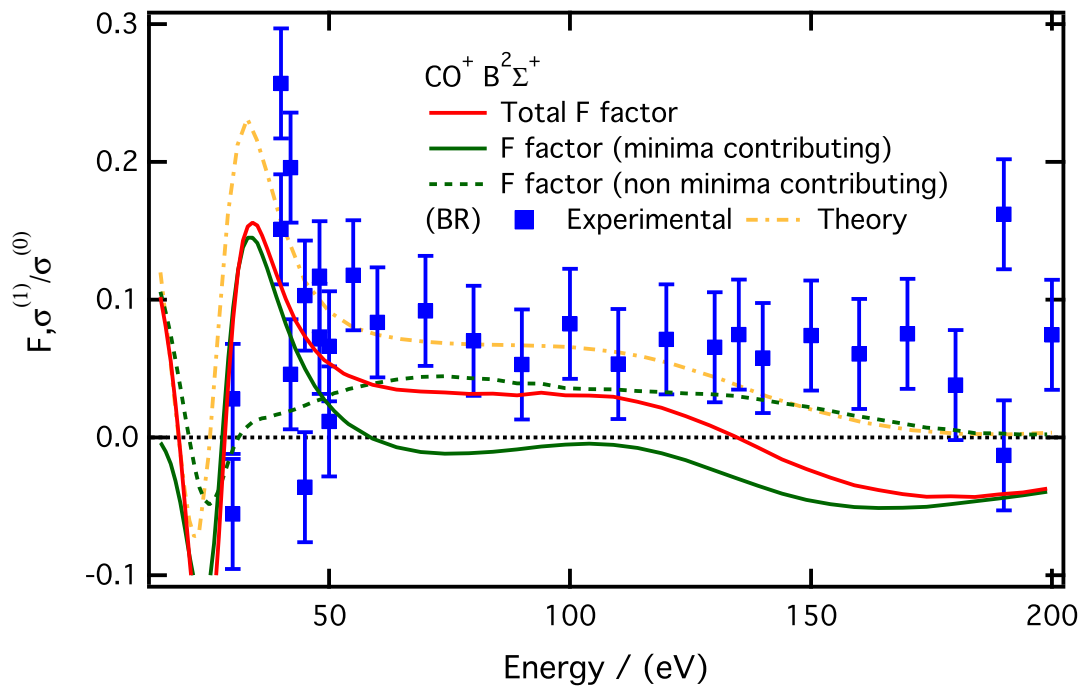
Figure III.4: Theoretical and experimental F factors for photoionization leading to the CO^+ $B^2\Sigma^+$ ion state. Experimental values were derive ssuming $R^{(FC)} = 0.36544$. The definitions of the lines are the same as in Figure III.1.

dence of the total fixed nuclei cross sections for these two molecules. At low energy, the cross sections are rapidly changing with geometry, leading to the large deviations of the electronic factor from zero seen in Figures III.1 and III.2. Qualitatively, the geometry dependence of the shape resonance feature can be understood with a particle-in-a-box model [71] with longer (shorter) bond lengths leading to lower (higher) resonance energies. The one-electron photoionization processes for these two isoelectronic molecules have very similar patterns, although all *shared* features appear shifted to lower energies (by about 10 to 15 eV) in CO compared to the corresponding features in N_2. One reason for this shift can be the difference in equilibrium bond lengths ($R_{CO,eq} = 1.12800\mathring{A}$ and $R_{N_2,eq} = 1.0977\mathring{A}$) which pulls the shape resonance and other non-Franck-Condon effects to lower energies for the CO.

III.3.2 The effect of shape resonances in the photoionization of the N_2 $2\sigma_u$ and CO 4σ orbitals

In the ionization from the 4σ orbital in CO leading to the B state, we can also see the effects of the shape resonance. In contrast, the ionization from the corresponding $2\sigma_u$ orbital of N_2 does not have a shape resonance, since the $2\sigma_u \rightarrow k\sigma_u$ channel is symmetry forbidden and we have neglected interchannel coupling, leading to much smaller non-Franck-Condon effects than in the case of ionization of CO leading to the B state [51].

III.3.3 High energy non-Franck-Condon effects analyzed by partial waves

To understand the non-Franck-Condon effects at energies above the shape resonances, it is helpful to consider the partial wave expansion of the cross sections. The total molecular photoionization cross section as expressed in Equation (II.16) can also be regarded as the sum of the contributions from different partial waves (l, m) (see for example [5]) that can be written as,

$$\sigma_{v^+ \leftarrow v} = \sum_{l,m} \sigma_{l,m}. \tag{III.1}$$

Any feature appearing in the total cross section may then be understood as reflecting a similar behavior in one, several, or all of the partial waves contributions $\sigma_{l,m}$. In Figure III.5, we see the geometry dependence of the total fixed nuclei cross
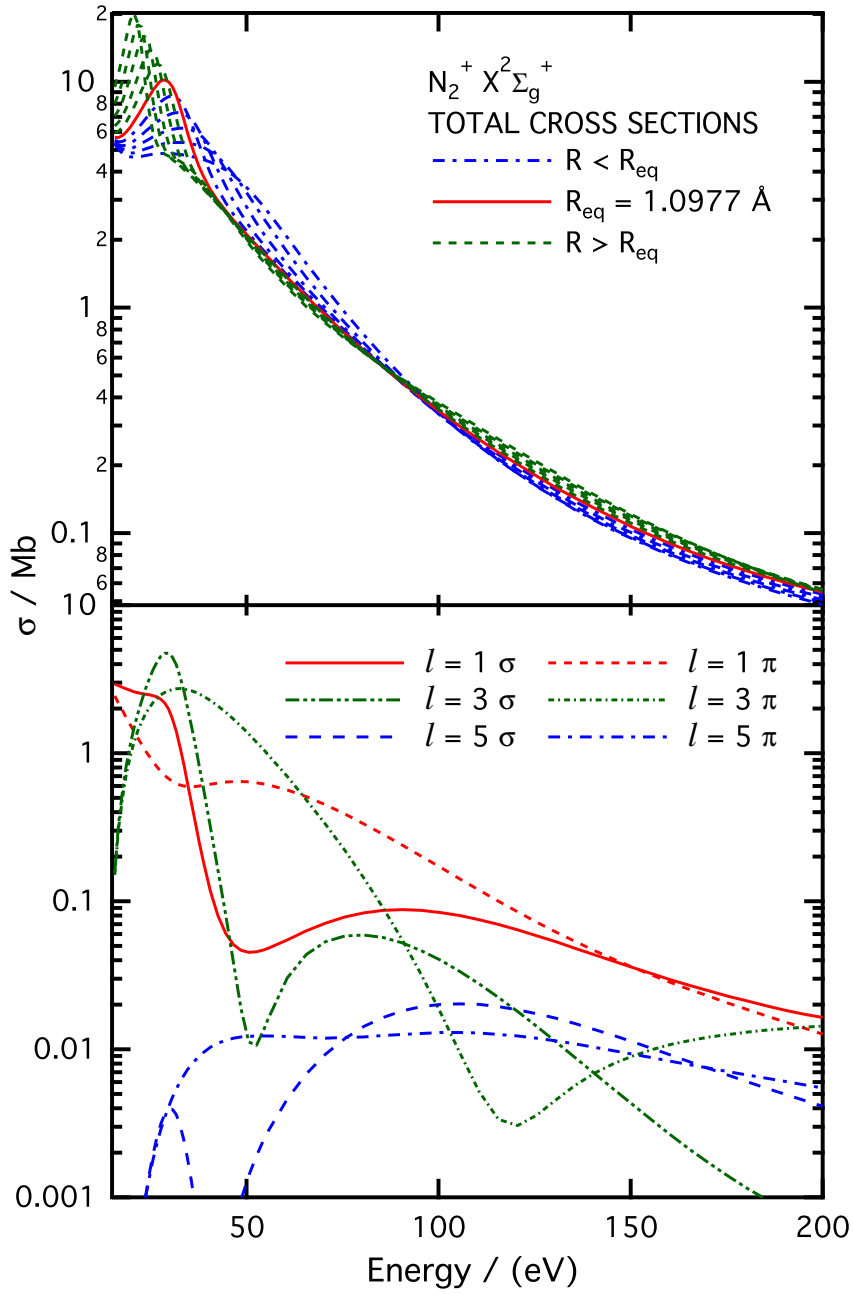
Figure III.5: Total cross sections for the photoionization leading to the N_2^+ $X^2\Sigma_g^+$ ion state at different values of internuclear distance R (*top*); and *relevant* partial cross sections of the same transition for the $\sigma l = 1, 3, 5$ and $\pi l = 1, 3, 5$ partial waves (*bottom*) at the equilibrium bond length ($R_{eq} = 1.0977 \overset{\circ}{A}$).
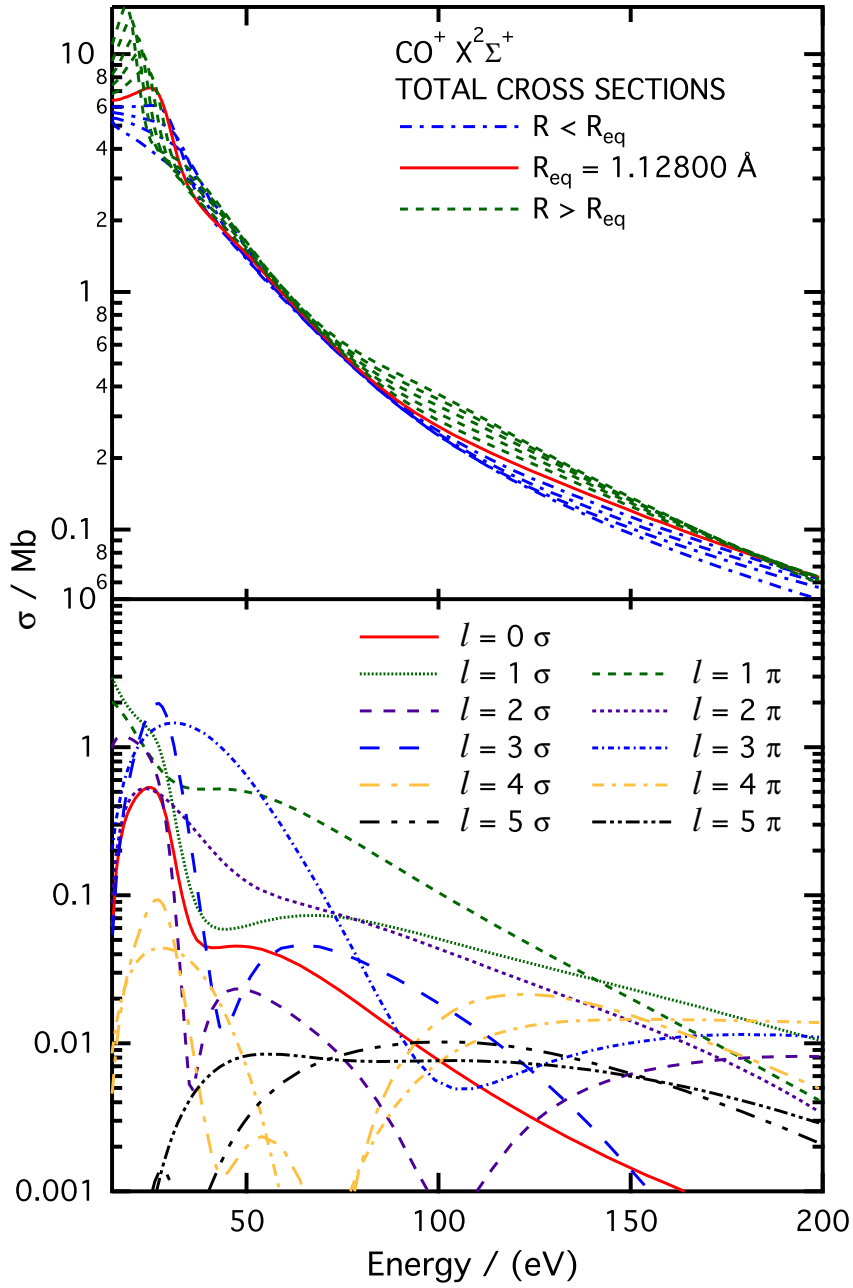
Figure III.6: Total cross sections for the photoionization leading to the CO$^+$ $X^2\Sigma^+$ ion state at different values of internuclear distance R (*top*); and *relevant* partial cross sections of the same transition for the $\sigma l = 0, 1, 2, 3, 4, 5$ and $\pi l = 1, 2, 3, 4, 5$ partial waves (*bottom*) at the equilibrium bond length ($R_{\text{eq}} = 1.12899\AA$).
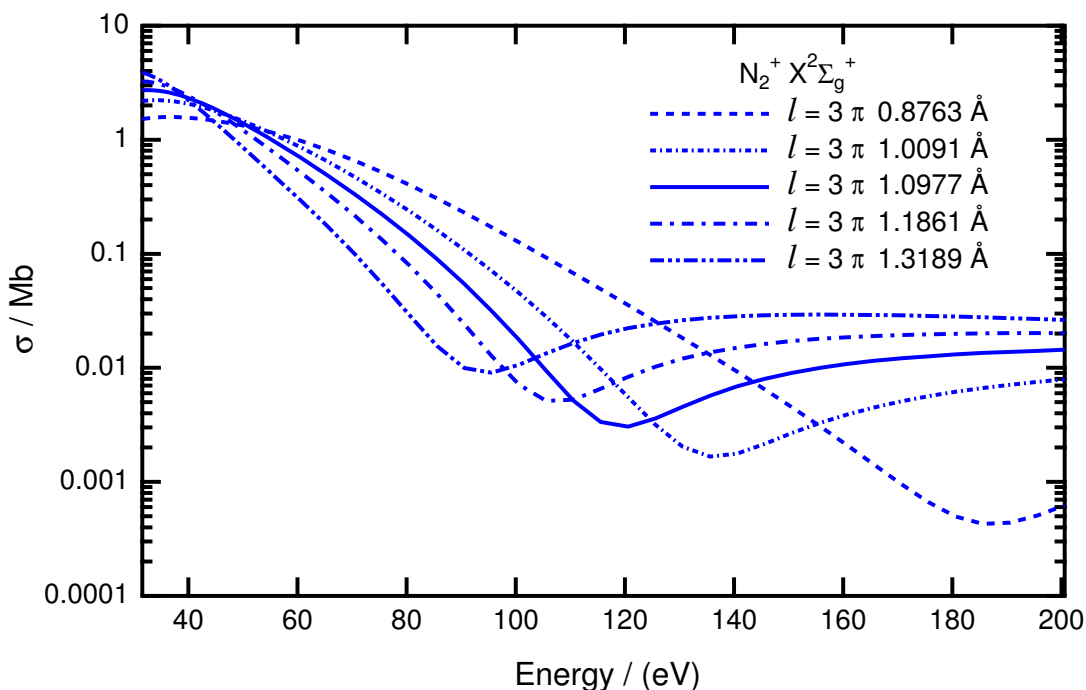
Figure III.7: Calculated photoionization partial cross sections (of the $l = 3$ partial wave) at different internuclear distances of N_2 leading to the $X^2\Sigma_g^+$ state of N_2^+.

section and the important partial wave contributions to the N_2^+ X state. At high energies the geometry dependence mainly comes from the $3\sigma_g \rightarrow k\pi_u$ channel. We show in Figure III.7 how the $(l, m) = (3, 1)$ partial cross section shifts as a function of the internuclear distance (similar behavior is observed in other partial waves not shown here). The corresponding CO total and partial photoionization cross sections leading to the corresponding X state are given in Figure III.6. Here we see that two prominent partial waves with strong Cooper minima features are the $(l, m) = (3, 1)$ and $(l, m) = (4, 0)$. In Figure III.8, we can again see strong dependence on the internuclear distance in the $(l, m) = (3, 1)$ and $(l, m) = (4, 0)$ partial cross sections. A reason for the weak geometry dependence in the photoionization leading to the X state of N_2^+ at around 100 eV compared to the corresponding dependence observed for CO, is the lack (for symmetry reasons) of the $(4, 0)$ partial wave being excited in the N_2 ionization, and being responsible a great part of the Franck-Condon departure for CO in this channel. In Figures III.1 and III.2 we decompose the computed F factors for ionization leading to the X states of N_2 and CO into the contribution from partial waves that do and do not contain Cooper minima. To compute the partial
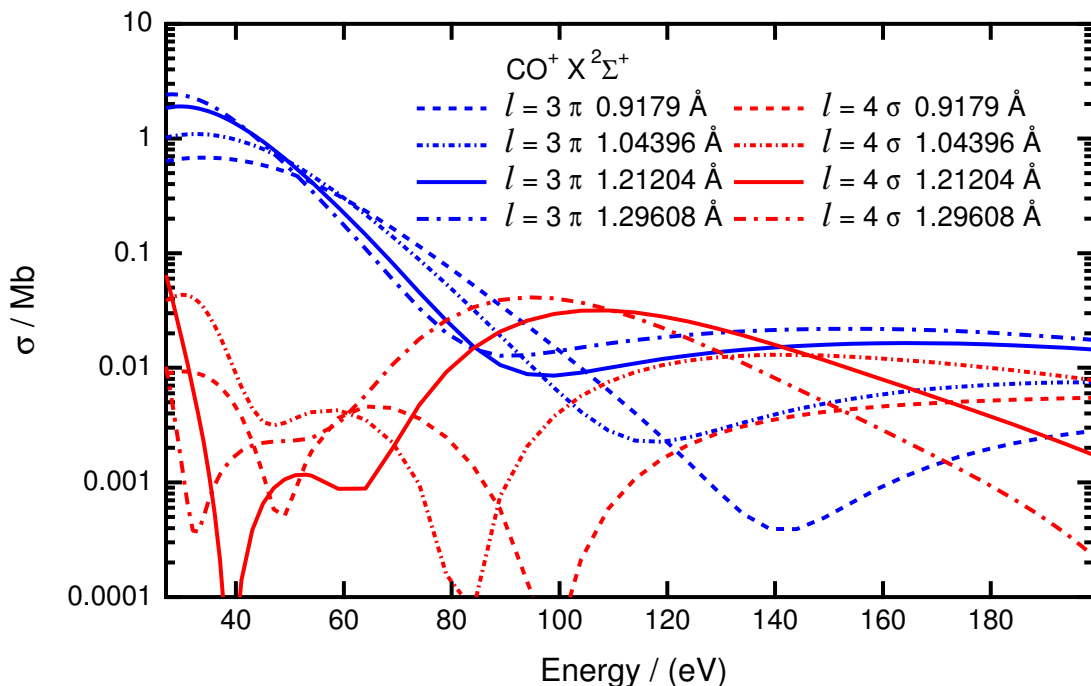
Figure III.8: Calculated photoionization partial cross sections (of the $l = 3$, blue, and $l = 4$, red, partial waves) at different internuclear distances of CO leading to the $X^2\Sigma^+$ state of CO^+.

wave contributions to F, as defined in Equation (II.20), we partial wave expand the derivative of the cross section found in the numerator but then divide it by the total cross section. In this way the different partial wave contributions to F will sum to the correct total value. For ionization leading to the X states of N_2 and CO we see that the deviations of F from zero are dominated by partial waves which contain a Cooper minimum like structure.

A similar partial wave analysis has been performed for the ionization leading to the B states of N_2 and CO. In Figures III.3 and III.4 the electronic factor, F (Equation (II.20)), was calculated separately for those waves containing a Cooper minima and for those not exhibiting such Cooper minima. In the case of the CO molecule, it can clearly be seen that the non-Franck-Condon behavior is due to a large contribution from the Cooper minima but there is also a mixed effect from non-Cooper-minima partial waves. One possible source for the non-Cooper-minima non-Franck-Condon effects is the sensitivity of the orbital which is being ionized to changing geometry. This is particularly true for the 5σ and 4σ orbitals of CO,

which are ionized to produce the X and B states, that have lower symmetry than the corresponding orbitals in N_2. For the N_2 photoionization from Figure III.3 it is evident that almost all the non-Franck-Condon behavior comes from the Cooper minima and not from other effects.

III.3.4 Cohen-Fano-like interference phenomena from diatomic molecules photoionization

As a way of making a comparison between the Cohen-Fano interference phenomena and the molecular Cooper minima in the photoionization of diatomic molecules, we computed the cross sections using plane waves for the continuum rather than the scattered waves discussed above. A comparison of plane wave and scattered wave cross sections will allow us to consider the extent to which Cooper minima effects seen in this system can be attributed the interference effects in the Cohen-Fano model of photoionization.

In Figure III.9 a single partial wave obtained within the plane wave approximation exhibiting a *Cooper minimum* like phenomena was plotted as a function of geometry. The cross section is highly geometry dependent as can be readily seen, just as its scattered wave analogs (see Figure III.8) but featuring those minima at higher energies. The geometry dependence of this partial wave is close to the Cohen-Fano interference pattern [53] predicted for heteronuclear molecules ($2k_eR \approx l\pi$) with $l = 4$. There are differences in the shape and position of the minima, that should not be overlooked. Thus the non-resonant non-Franck-Condon behavior of the systems considered here can in large part be attributed to an interference phenomena analogous to the Young's Double slit experiment as mentioned elsewhere [47, 52, 54] which appear as Cooper minima in the partial wave expansion.

III.4 Conclusion

The new experimental photoelectron data presented on the vibrational branching ratios for the photoionization of the two outer valence σ orbitals of CO and N_2 for photon energies from threshold to 200 eV was analyzed by a comparison to computed branching ratios. To assist in the comparison between theory and experiment, we use the electronic factor F, which is defined as the logarithmic derivative of the cross section with respect to a scaled bond length (see Chapter II).
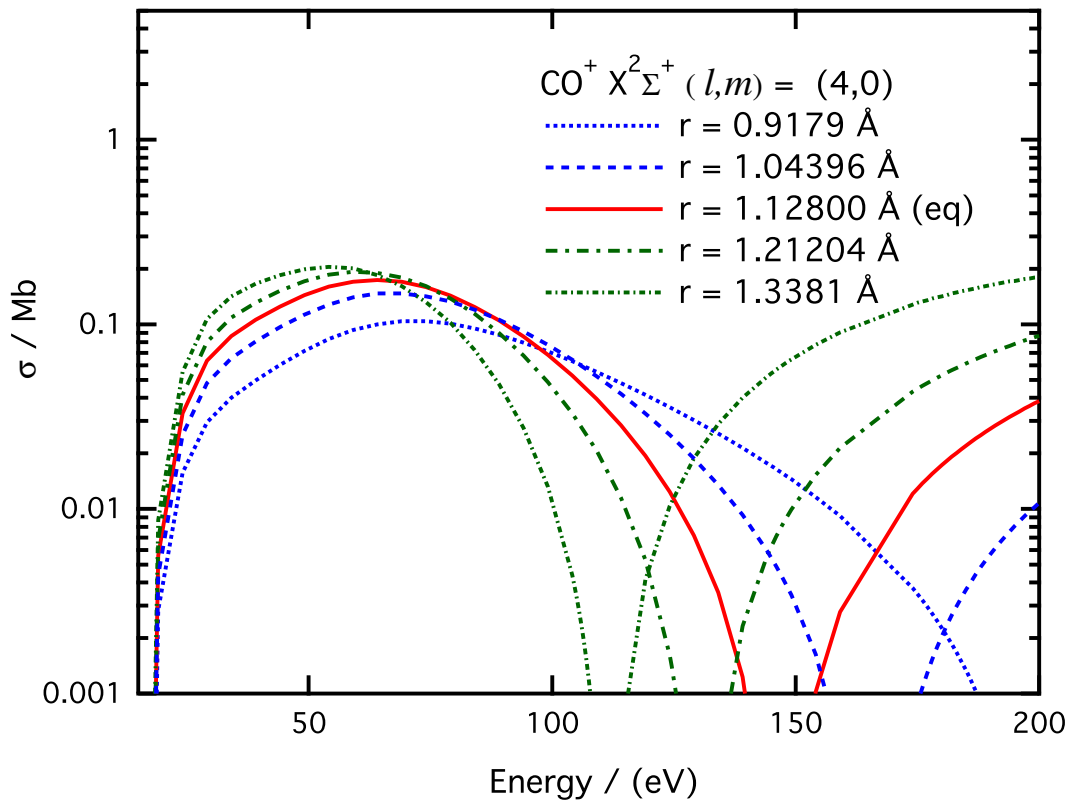
Figure III.9: Partial photoionization cross section using plane waves for the continuum electron, leading to the CO$^+$ $X^2\Sigma^+$ ion state for $(l, m) = (4,0)$ at different bond lengths.

An analysis of the non-Franck-Condon behavior using the electronic factors in these systems shows the effects of the much studied shape resonances at low photon energy. At higher energy, we see the deviations from the Franck-Condon value that have been previously described as being due to molecular Cooper minima [28, 55] and as being due to interference from the ionization from two centers as described by Cohen and Fano [53]. We find that in N_2 and CO, these two descriptions are related by the fact that the partial wave matrix elements obtained from decomposition of the plane-wave matrix elements used in the Cohen-Fano analysis also have energies at which they change sign which is the characteristic of a Cooper minimum. The resulting minima of the plane-wave partial cross sections then correlate with the oscillations in the total cross sections seen in the Cohen-Fano analysis. A comparison of the four cases considered shows that, except for the X state of N_2^+, all have similar F factors at high energy in the region of the Cooper minima or equivalently the Cohen-Fano oscillations. A comparison of the X states for N_2^+ and CO^+ at these energies shows that the $(l, m) = (4, 0)$ partial wave in the CO cross section makes a significant contribution to the geometry dependence of the cross section. By symmetry this partial wave is not excited in the ionization leading the the X state of N_2^+, so that the F factor is much reduced for N_2 when compared to CO.

VIBRATIONALLY SPECIFIC PHOTOIONIZATION CROSS SECTIONS FROM LOW-SYMMETRY MOLECULAR SYSTEMS *

IV.1 Introduction

In this chapter we study the molecular photoionization of acrolein, a low symmetry molecule, in a range of photon energies ranging from 11 to 100 eV [72]. The vibrational branching ratios in the photoionization of acrolein for ionization leading to the $\tilde{X}\,^2A'$ ion state were studied. Computed logarithmic derivatives (see Chapter II) of the cross section and the corresponding experimental data derived from measured vibrational branching ratios for several normal modes (ν_9, ν_{10}, ν_{11}, and ν_{12}) were found to be in relatively good agreement, particularly for the lower half of the range of photon energies considered. We found two shape resonances near photon energies of 15.5 and 23 eV in the photoionization cross section and we demonstrated they originate from the partial cross section of the A' scattering symmetry. It is important to note that the wave functions computed at the resonance complex energies are delocalized over the whole molecule. By looking at the dependence of the cross section on the different normal mode displacements together with the wave function at the resonant energy, a qualitative explanation is given for the change of the cross sections with respect to changing geometry. The discovery that low-energy electron collisions with DNA can lead to single and double strand breaks [33] has lead to much interest in the study of such collisions with molecules which are models for fragments of DNA [34] and more generally of collisions with larger, low-symmetry molecular systems. The mechanism for the strand breaking is thought to be the resonant capture of the scattered electron, which can lead to bond breaking through dissociation of the metastable negative ion. Of course the probability for this dissociative process depends on the lifetime of the resonant state and the coupling to the vibrational modes of the system. Although electron-molecule collisions and molecular photoion-

---

* "Reproduced in part with permission from "Vibrationally specific photoionization cross sections of acrolein leading to the $\tilde{X}\,^2A'$ ionic state" by Jesús A. López-Domínguez, Robert R. Lucchese, K. D. Fulfer, David Hardy, E. D. Poliakoff, and A. A. Aguilar, *J. Chem. Phys.* **141**, 094301 (2014). Copyright 2014, AIP Publishing LLC". [http://dx.doi.org/10.1063/1.4893702]

ization are not the same process, in many cases the same dynamical mechanisms control them. This is because the short-range potential experienced by a scattered electron and a photoelectron are very similar [73]. Moreover, larger systems have much smaller shifts in the resonance energies between the electron scattering and the photoionization, [73] thus the resonances found in the photoionization will be very close to those that would be experienced in the electron scattering process.

Resonances or in particular shape resonances are one of the most interesting phenomenon within molecular photoionization, and are closely related to structural and dynamical properties of the target initial and final states (see Section I.2.4). A shape resonance occurs when the ejected photoelectron is temporarily trapped in the region of the molecule by a dynamical centrifugal barrier [23] and eventually tunnels or is scattered out into the free continuum. In molecular photoionization, the time delay produced by such metastable states formed by the target and the ejected electron can induce strong coupling between electronic and vibrational motions [24], making the electronic transition matrix elements very sensitive to geometry changes and thus, leading to deviations from the expected Franck-Condon behavior [24, 74], as mentioned before. In this chapter, we present a study of the valence shell photoionization of acrolein, CH_2=CHCHO, where theoretical calculations are compared with experimental results (which were measured in the experimental group of Professor E. Poliakoff at Lousiana State University) to better understand the resonant states and the coupling of the resonances to the vibrational modes of the molecule. A combination of the measured vibrationally resolved spectra and theoretical geometry-specific cross sections are analyzed together with computed resonant wave functions.

It has been shown that in the vicinity of a resonance there is a sudden rise in the eigenphase sum, $\delta(E)$ [5, 75, 76]. The eigenphase sum is computed from the eigenvalues of the scattering S-matrix [76]. An isolated pole in the S scattering matrix in the complex energy plane, on the unphysical sheet at an energy, E from Equation (I.73) is generally associated with a resonance [5, 77] (see also [78] and [79], which discuss exceptional cases where the existence of S matrices producing sharp resonances with no poles in the unphysical sheet) and thus with a rising eigenphase sum. To understand the qualitative behavior of a resonant state it is interesting to see the spatial location, nodal structure, and extent of the resonant state. By computing the Siegert state wave function [80–82] at the complex energy where the resonance is centered, $i.e.$, at a pole of the S-matrix, and if the resonance is

sufficiently narrow, one expects the electron density of the state to be well localized in a specific region (or bond) of the molecule [74]. This has been shown to be particularly true for linear molecules and diatomics. Although a quantitative rule for the relation between energy position of a shape resonance and bond length is not possible (see [23]), for diatomics at least, a qualitative relation between these two quantities holds, specifically for σ resonances (localized on the bond axis). The case for polyatomic molecules turns out to be more complicated, and even sometimes the specific localization of the dynamical barrier that causes the resonant state within the molecule's framework cannot be located with the same degree of certainty as in diatomic (or linear) molecules. The greater number of vibrational degrees of freedom may increase the number of modes coupled to a given resonant state, thus complicating its analysis. Here, we address the issue of the extent to which we can extract information such as geometry sensitivity from the photoelectron scattering dynamics of the dipolar low-symmetry polyatomic molecule, acrolein.

IV.1.1 Molecular model of study: acrolein

In the $\tilde{X}\ ^1A'$ electronic ground state both *s-cis* and *s-trans* isomers of acrolein, also known as 2-propenal or prop-2-enal, have a planar equilibrium structure with a C_s symmetry point group and electronic configuration

$$(1a')^2(2a')^2(3a')^2(4a)^2(5a')^2(6a')^2(7a')^2(8a')^2(9a')^2$$
$$(10a')^2(11a')^2(12a')^2(1a'')^2(13a')^2(2a'')^2. \tag{IV.1}$$

It is important to note that this ordering, based on the calculated Hartree-Fock orbital energies (Koopmans' theorem), suggests that the HOMO-1 and HOMO are of a' and a'' symmetries respectively (see also [83, 84]), nevertheless it has been shown that the first band in the photoelectron (PE) spectrum corresponds to ionization from the oxygen in plane lone-pair (n_O that is the $13a'$ orbital) [85, 86] as opposed to ionization from the π(C=C) molecular orbital ($2a''$). The matter of the ordering and energetics of the three HOMO's has been extensively discussed [87, 88], and it has been shown that Koopmans' theorem breaks down in the case of the ordering of ion states in acrolein, where relaxation is smaller in the $^2A''$ ($2a''$) ion state than in the $^2A'$ ($13a'$) state, due in part to the bonding and non-bonding nature of the two orbitals respectively and the strong localization of the n_O orbital [89]. Acrolein

Table IV.1: Vibrational normal modes for the ground state under consideration in the present study.

Mode	Symmetry	Assignment
ν_9	a'	CH vinyl bending
ν_{10}	a'	C-C vinyl stretching
ν_{11}	a'	=CH$_2$ rocking
ν_{13}	a'	C=C-C bending
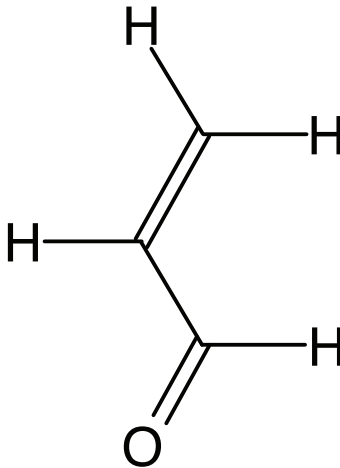
Figure IV.1: Structural formula of the *s-trans*-acrolein molecule.

has eighteen vibrational normal modes in the ground state (which are described completely elsewhere [90–93]) of which the in-plane vibrations have A' symmetry and the out-of-plane vibrations have A'' symmetry. We investigated the sensitivity of the dynamics of the molecular photoionization from the $13a'$ orbital of *s-trans*-acrolein to the A' vibrations indicated in Table IV.1.

In this study we have concentrated on the *s-trans* isomer of acrolein since the experimental portion of the work was carried out at room temperature and it is well known that the *s-cis* isomer's zero-point level lies approximately 770 cm^{-1} above the *s-trans* form, so that the *s-cis* form is only four percent of the population at room temperature [94]. Throughout this chapter, we report theoretical results accompanied by experimental measurements for the photoionization dynamics of *s-trans*-acrolein (which we will refer to as just acrolein for convenience), with the structure shown in Figure IV.1, leading to the $\tilde{X}\,^2A'$ ion state. The experimental and theo-

retical results are compared within the framework of logarithmic derivatives of the cross sections with respect to geometry, previously reported as the electronic factor F [42] (see Chapter II), providing a better understanding of the relation between experiment and theory.

IV.2 Calculations

The photoionization calculations were performed within the Born-Oppenheimer or Chase adiabatic approximation [22] (Section I.2.3). In the Chase approximation the electronic ground state and photoelectron wave functions depend parametrically on the nuclear coordinates allowing for the initial and the final total scattering state wave functions to be written as [16],

$$\Psi_{\mathrm{i}}(r,q) = \psi_{\mathrm{i}}(r;q)\chi_{\nu,\mathrm{i}}(q) \tag{IV.2}$$

$$\Psi_{\mathrm{f},\vec{k}}^{(-)}(r,q) = \psi_{\mathrm{f},\vec{k}}^{(-)}(r;q)\chi_{\nu^+,\mathrm{f}}(q) \tag{IV.3}$$

which are Equations (II.5) and (II.6). A set of fixed nuclear positions were used to compute the vibration-state specific transitions within the normal mode coordinates (q_i) in a wide range of values, from $q_i = -3$ to $q_i = +3$ in one unit steps, where $q_i = \pm 1$ corresponds to the classical turning point in the ith mode. The initial and final electronic state wave functions were calculated at the Hartree-Fock level of theory, using the augmented correlation-consistent polarized valence triple-ζ [95, 96] (aug-cc-pVTZ) basis set and were computed using the Gaussian09 suite [97].

The photoionization cross sections have been computed using the Schwinger variational method [98, 99] (see Section I.1.3) with an $l_{\mathrm{max}} = 90$ for the single-center expansion of the electronic wave functions within the single channel frozen core Hartree-Fock approximation (SCFCHF) using the ePolyScat suite of programs [65, 66]. The ground state of the acrolein molecule (*cis-* or *trans-* forms) and the final $\tilde{X}\,^2\mathrm{A}'$ electronic state belong to the C_s (planar) symmetry point group. The ionization potential used for the calculation and to determine the photoelectron kinetic energies was 10.11 eV [86, 100, 101] (some values in the references are within ± 0.02 eV). The photoionization calculations were performed for photon energies from 10.2 to 100 eV. Additionally, within this range of energies a search for poles of the scattering S matrix in the complex plane were performed using a local exchange potential and

the local adiabatic static model-exchange method (ASME) [102, 103]. The position of the resonance structures in the cross sections and the computed poles from the complex energy plane were compared. The wave functions of the resulting Siegert states were plotted at the resonance energies and analyzed to better understand the dynamics of the resonance.

As a means of comparing the theoretical and experimental results we computed the electronic factor F and calculated its corresponding value from the experimental results using Equations (II.20) and (II.22) [42] (see Chapter II) respectively,

$$F = \frac{\sigma^{(1)}}{\sigma^{(0)}} = \left(\frac{d}{dq}\ln\sigma(q)\right)_{q=0} \tag{IV.4}$$

and

$$F = \pm(2R_{1\leftarrow0/0\leftarrow0}^{(\text{FC})})^{1/2}\left[\frac{R_{1\leftarrow0/0\leftarrow0}}{R_{1\leftarrow0/0\leftarrow0}^{(\text{FC})}} - 1\right]. \tag{IV.5}$$

In Equation (IV.4), $\sigma^{(i)}$ is the ith derivative of the computed total fixed nuclei cross section with respect to the normal mode coordinate q evaluated at its equilibrium $q = 0$. Thus F is the logarithmic derivative of the cross section with respect to the coordinate q. For the analysis of the experimental data, Equation (IV.5) was used, where the different R values correspond to the usual vibrational branching ratios for the specified transition and the $R^{(\text{FC})}$ are the expected Franck-Condon vibrational branching ratio values. As explained elsewhere (see Chapter II and reference [42]), Equation (IV.4) gives the same result as Equation (IV.5) when harmonic oscillator vibrational states are assumed and the cross section is expanded as $\sigma = \sigma^{(0)} + q\sigma^{(1)}$. Note that $F = 0$ in Equation (IV.4) when σ is independent of geometry (that is $\sigma^{(1)} = 0$) and equivalently when $R = R^{(\text{FC})}$ in Equation (IV.5).

The use of electronic factors to analyze non-Franck-Condon effects allows for the interpretation of an observable, the vibrational branching ratio, which contains contributions from a number of factors, in terms of a simple quantity with physical significance, the logarithmic derivative of the cross section. There are two limitations of this approach: the $R^{(\text{FC})}$ factor must be non-zero and the assumed linear geometry dependence of the cross section must be a good approximation. Within those limitations, the F factor removes the structural effects, *i.e.*, the shift in geometry upon ionization, leaving only the differential geometry sensitivity of the cross section. In the present study, this facilitates the analysis of non-Franck-Condon effects which
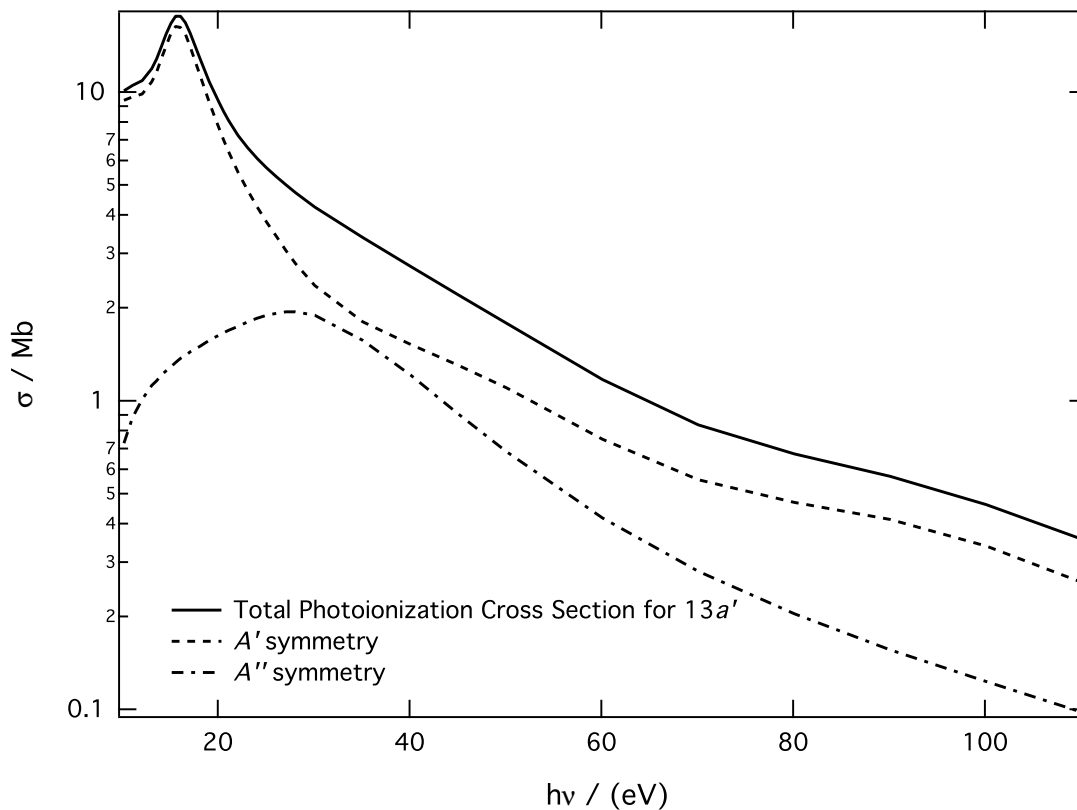
Figure IV.2: Theoretical photoionization cross sections for ionization from the $13a'$ orbital of acrolein, with the contributions from the A' and A'' scattering symmetries and the corresponding total cross section.

are fairly weak, allows for the direct comparison of the non-Franck-Condon effects in different modes, and allows for a decomposition of the sources of the non-Franck-Condon into contributions from different partial waves. In other applications [42], the electronic factors are also useful since they put branching ratios from different vibrational quanta, *e.g.* $\nu = 1$ and $\nu = 2$, on the same scale.

IV.3 Results and Discussions

IV.3.1 Valence shell molecular photoionization of acrolein and electronic factors

In Figure IV.2 we show the calculated total cross section for the photoionization of acrolein from the $13a'$ orbital leading to the X $^2A'$ ionic state, together with the corresponding cross sections from the two scattering symmetries (A' and A'') present

Table IV.2: Calculated poles of the S-matrix for the A' scattering symmetry with possible physical significance.

$E_{\mathrm{Re}}/\mathrm{eV}^3$ $(h\nu/\mathrm{eV})$	$E_{\mathrm{Im}}/\mathrm{eV}^4$
5.39 (15.5)	-2.24
12.9 (23.01)	-3.78
73.8 (83.91)	-11.13

in the process which add up to the total (solid line). From this plot, the presence of at least one shape resonance at low energy is evident, peaking at around 16 eV, clearly caused by the partial waves with A' symmetry. The low energy peak actually is the combination of two shape resonances that are close in energy. Additionally, there is a much broader resonance which occurs at the high end of the energies investigated. In Table IV.2, the corresponding resonance energies computed using the ASME model are given.

In Figure IV.3 we present experimental electronic factors [42] in comparison to computed values. To present the experimental data in this fashion we need to assume values of the Franck-Condon $R_{\nu_i}^{(\mathrm{FC})}$. In the results given we have used $R_{\nu_9}^{(\mathrm{FC})} = 0.096$, $R_{\nu_{10}}^{(\mathrm{FC})} = 0.18$, $R_{\nu_{11}}^{(\mathrm{FC})} = 0.079$ and $R_{\nu_{13}}^{(\mathrm{FC})} = 0.217$, which were chosen in order to give the best agreement between experiment and theory. From Figure IV.3 we see that the resonances present in the low energy region, visible in Figure IV.2, have an effect on the electronic factor values (and thus in the vibrational branching ratios), making them depart from the expected Frank-Condon value (corresponding to an $F = 0$), in that low energy region. Also, as important is the fact that the magnitude of that deviation is not as large as that seen in F in smaller and more symmetrical systems such as the prototypical examples of N_2 or CO [42] shown in Chapter III. If we take as reference the values of F found in [42] for the photoionization leading to the N_2 X $^2\Sigma_g^+$ ion state, we see that a strong and well defined resonance in N_2 leads to a large deviation from the expected Franck-Condon behavior with $F = 0.4$ in the resonance. The value of $|F|$ in acrolein, as seen from Figure IV.3, never goes beyond 0.1 and most of the time is significantly smaller. In this sense, we can roughly expect to see dramatic effects in the branching ratios when $|F| > 0.2$. It is evident from Figure IV.3 that all the vibrational modes studied exhibit an effect due to the low energy resonances, and thus a displacement from the expected Franck-Condon value of $F = 0$, and a relatively good agreement with experiments up to the middle

61

Figure IV.3: Comparison between experimental and theoretical results for the photoionization of acrolein leading to the $\tilde{X}$ $^2A'$ ion state, using the previously described electronic factors, given in Equations (IV.4) and (IV.5) and reference [42] for the vibrational specific modes, ν_9, ν_{10}, ν_{11} and ν_{13}, as labeled in the plots.
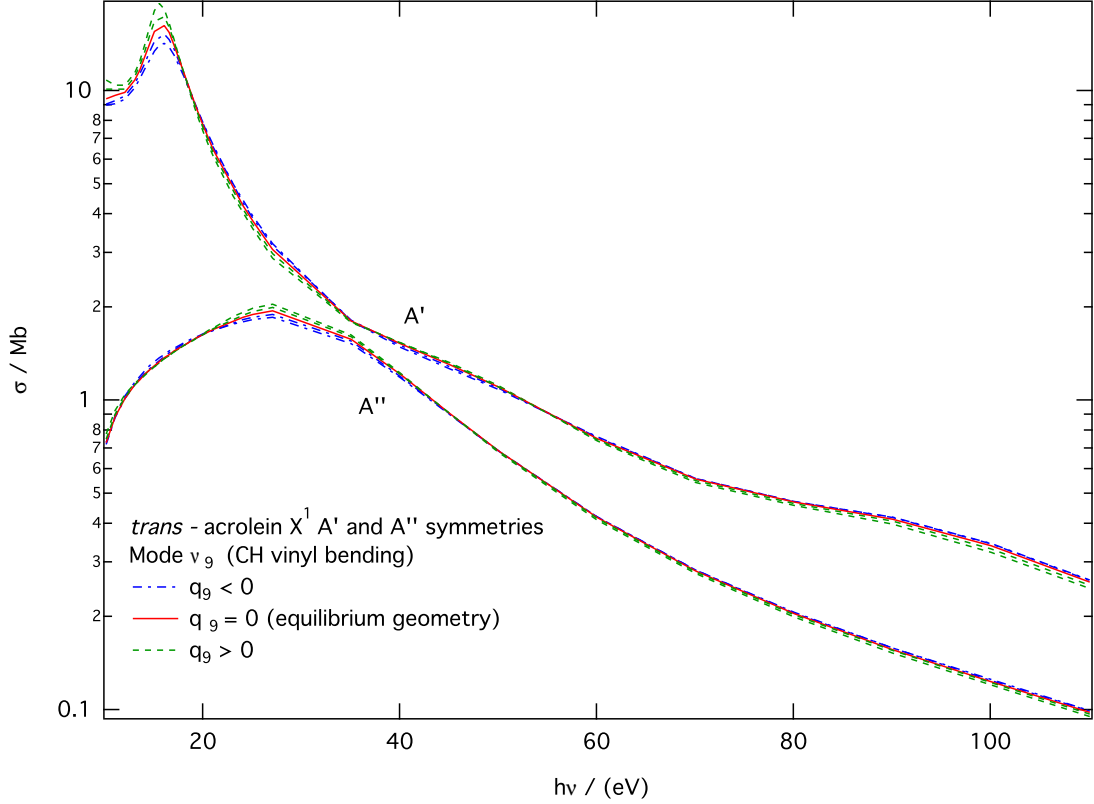
Figure IV.4: Normal mode specific partial cross sections for the A' and A'' scattering symmetries for the photoionization of acrolein leading to the $\tilde{X}\ ^2A'$ ion state, showing the effect of the variation in the normal mode coordinate q_9 for the ν_9 mode: $q_9 < 0$, dash-dotted blue lines; equilibrium, $q_9 = 0$, solid red line; and $q_9 > 0$, dashed green lines.

of the energy range considered here; at higher energies there is a larger scatter of the measured branching ratios which makes it difficult to compare experiment to theory. It is also important to note that the computed values of F in a given mode, as given by Equation (IV.4), have an overall arbitrary factor of ± 1 relative to the experimental data. We have chosen the phase in each case to give the best overall agreement between theory and experiment.

To provide a better perspective on the non-Franck-Condon effects in the low energy resonance in this system we show in Figures IV.4 and IV.5 the case of the ν_9 and ν_{10} modes respectively (see Figure IV.3 top left and top right panels) as the corresponding normal mode coordinate q_i varies from -2 to +2 in one unit steps. Since the ν_9 mode is a bending mode from the vinyl group (see Table IV.1), changes
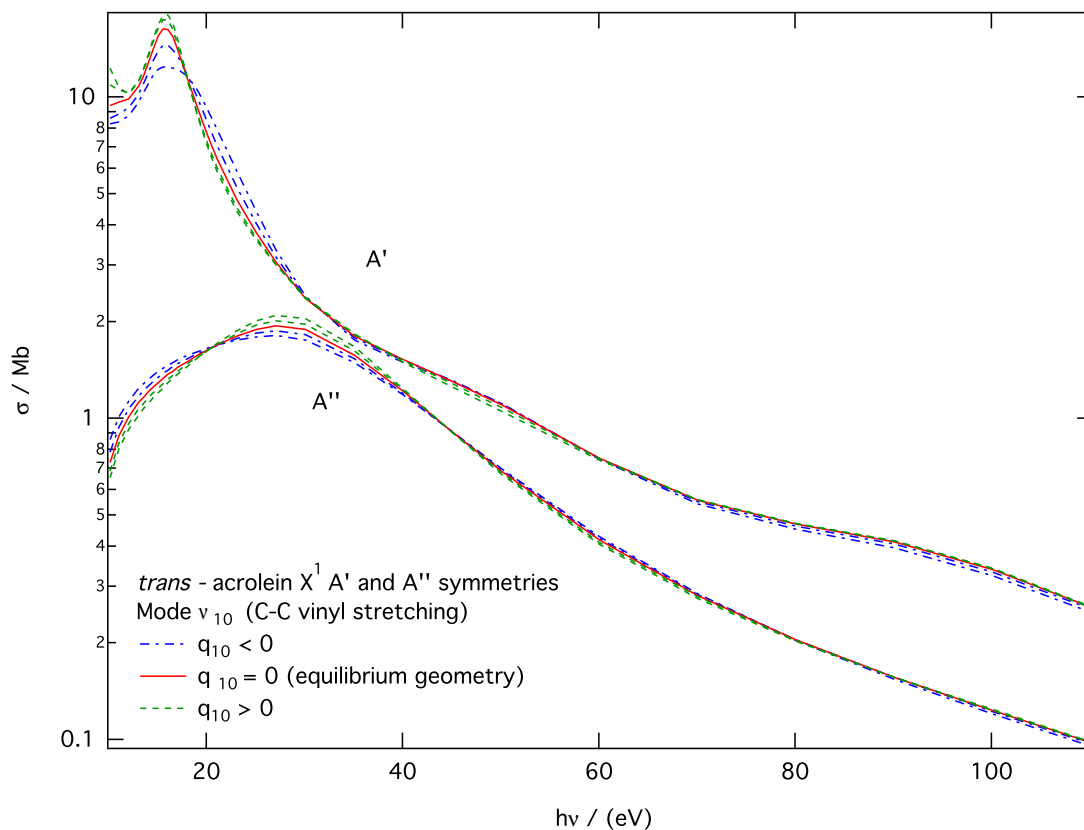
Figure IV.5: Normal mode specific partial cross sections for the A' and A'' scattering symmetries for the photoionization of acrolein leading to the $\tilde{X}\ ^2A'$ ion state, showing the effect of the variation in the normal mode coordinate q_{10} for the ν_{10} mode: $q_{10} < 0$, dash-dotted blue lines; equilibrium, $q_{10} = 0$, solid red line; and $q_{10} > 0$, dashed green lines.

in q_9 have no net effect in the length of the internuclear distances specially, thus a displacement of the position of the resonance won't be expected, but a change in the magnitude of the cross section due to a changing lifetime is reasonable (as can be readily seen from Figure 3), as the molecule distorts its shape. As for the ν_{10} plot (Figure IV.5), although not as dramatic as in the previously mentioned examples of diatomics, there is a displacement of the position of the low energy resonances as q_{10} changes from $q_{10} > 0$ to $q_{10} < 0$ compared to what is seen for ν_9 (Figure IV.4). This observation is very reasonable since ν_{10} is a stretching mode (see Table IV.1) and by increasing the size of the effective box that is trapping the electron a shift in the position of the resonances to lower energies is expected. Looking at the A' symmetry waves in Figures IV.4 and IV.5, one would expect to have zeros in the F factor in Figure IV.3 at the energy values where the cross sections follow a Frank-Condon behavior, $i.e.$ where the cross section does not depend on geometry. The apparent discrepancies between the actual position of the zeroes in the F factors and the behavior of the A' cross section can be explained by the contribution that the A'' symmetry waves make to the total F factor where the magnitude of both scattering symmetries are comparable, $i.e.$, approximately between 30 and 45 eV.

IV.3.2   Orbitals analysis and MBS calculations

A qualitative understanding of the resonant states can be obtained by examining the orbitals and resonant state wave functions involved. From the plot of the ionized $13a'$ orbital in Figure IV.6 we see first that the orbital is more localized near to the oxygen on what looks like a p-type orbital, and extends toward the carbonyl and central carbon atom. That this orbital is primarily a lone pair on the O atom is consistent with the fact that $R^{(\text{FC})}$ are relatively small for all vibrations, since this is neither a bonding nor an antibonding orbital. In Figure IV.7 the nodal structure from the A' resonance wave function with an energy near 23 eV suggests a centrifugal barrier localized near the vinyl group. It has been shown that minimum basis set (MBS) virtual orbitals of molecules [103] can often resemble the symmetry of one-electron resonances. Thus to better understand this resonance, we computed the MBS virtual orbitals of acrolein. As can be seen from comparing the resonance wave function obtained at 23.01 eV and the MBS ninth virtual orbital in Figure IV.7, they share a very similar structure, which can be characterized as an out-of-phase combination of two σ^* antibonding orbitals. This can be compared with the behavior
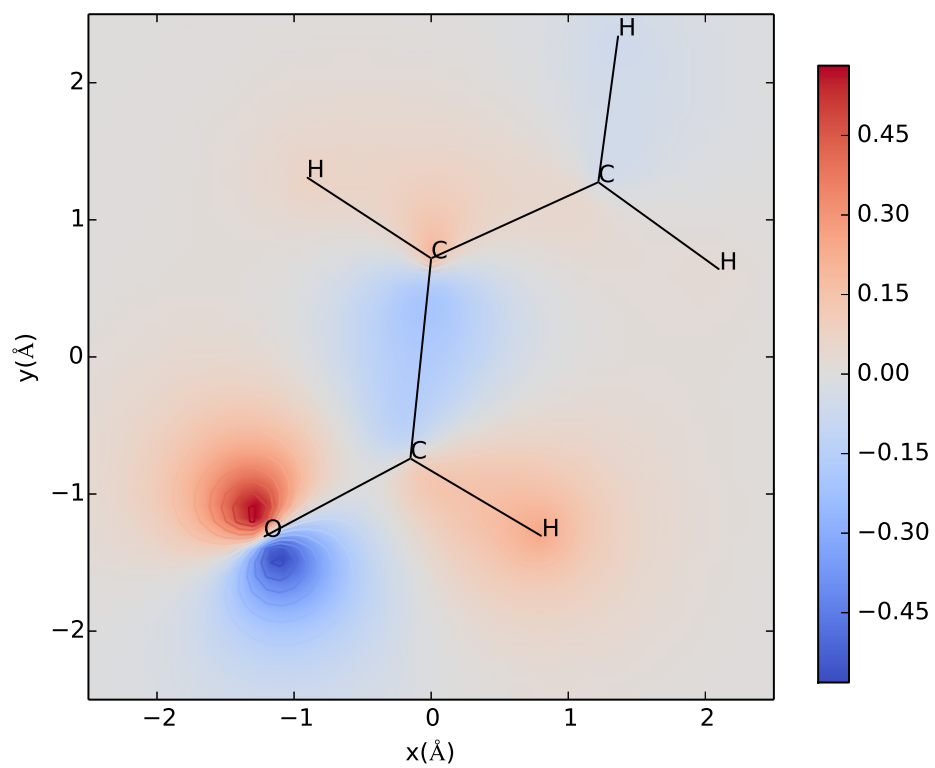
Figure IV.6: Contour plot of the wave function of the ionized $13a'$ orbital in the photoionization of acrolein leading to the $\tilde{X}\,^2A'$ ionic state. The contour is plotted in the plane of the molecule.
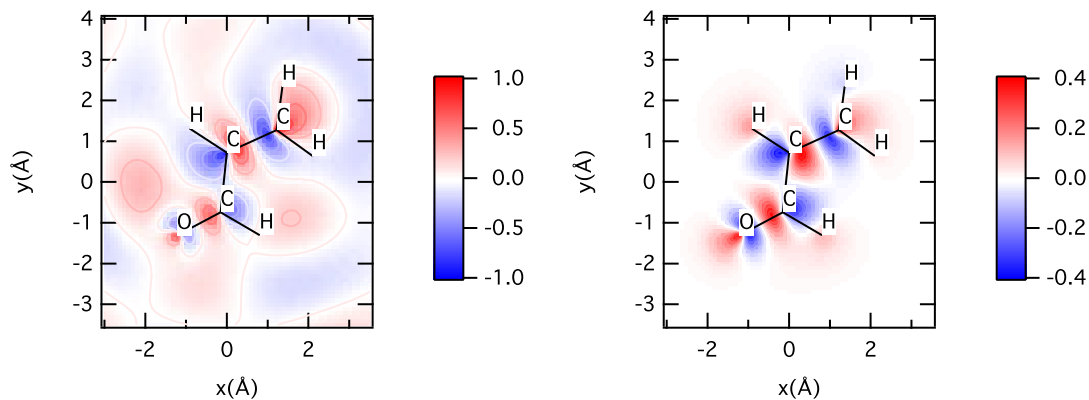
Figure IV.7: Comparison between the real component of the A' resonant wave function at 23.01 eV photon energy, showing the nodal structure for photoionization leading to the $\tilde{X}\ ^2A'$ ionic state (left panel) and the contour plot of the wave function of the 9th virtual orbital of the ground state acrolein, computed using a MBS (right panel).

of the lower energy resonance occurring near 15.5 eV shown in Figure IV.8. In this case the resonant wave function obtained at 15.5 eV and the MBS seventh virtual orbital are more localzed on the carbonyl group with a weaker in-phase contribution on the vinyl group. The MBS calculation for the plotted virtual orbitas gave orbital energies of 23.63 and 28.94 eV, for the seventh and ninth virtual orbitals respectively. It is important to note that, as would be expected, the actual scattering resonances are shifted to lower energies, since the MBS calculation corresponds to the neutral molecule and to the use of a restricted basis set. It is also important to note that there are many other A' virtual MBS orbitals which do not correspond to resonances.

IV.4   Conclusions

The computed vibrational branching ratios were compared to experimental measurements for the photoionization of *trans*-acrolein from the $13a'$ orbital, leading to the $\tilde{X}\ ^2A'$ ionic state. We found shape resonances near threshold and confirmed their presence by computing the poles in the scattering S matrix. The electronic factor F in this work allowed us to compare computed and measured results and provided a qualitative reference for the strength of a shape resonance and a measure of the sensitivity of the cross section to geometry changes in acrolein. It was observed, as we

67
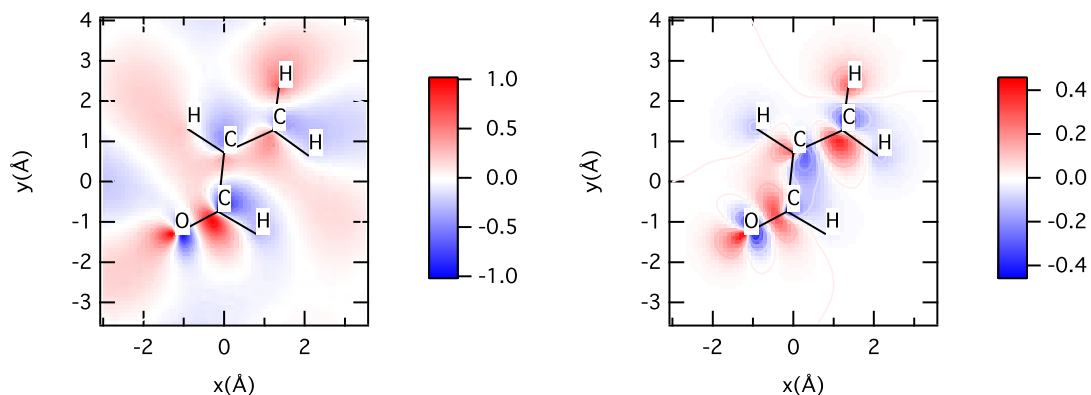
Figure IV.8: Comparison between the real component of the resonant wave function at 15.5 eV photon energy, showing the nodal structure for photoionization leading to the $\tilde{X}\ ^2A'$ ionic state (left panel) and the contour plot of the wave function of the 7th virtual orbital of the ground state acrolein, computed using a MBS (right panel).

mentioned above, that as a molecule becomes more complex with lower symmetry, the resonant states become more delocalized within the molecule, and their position and widths become less sensitive to changes in specific normal modes. Th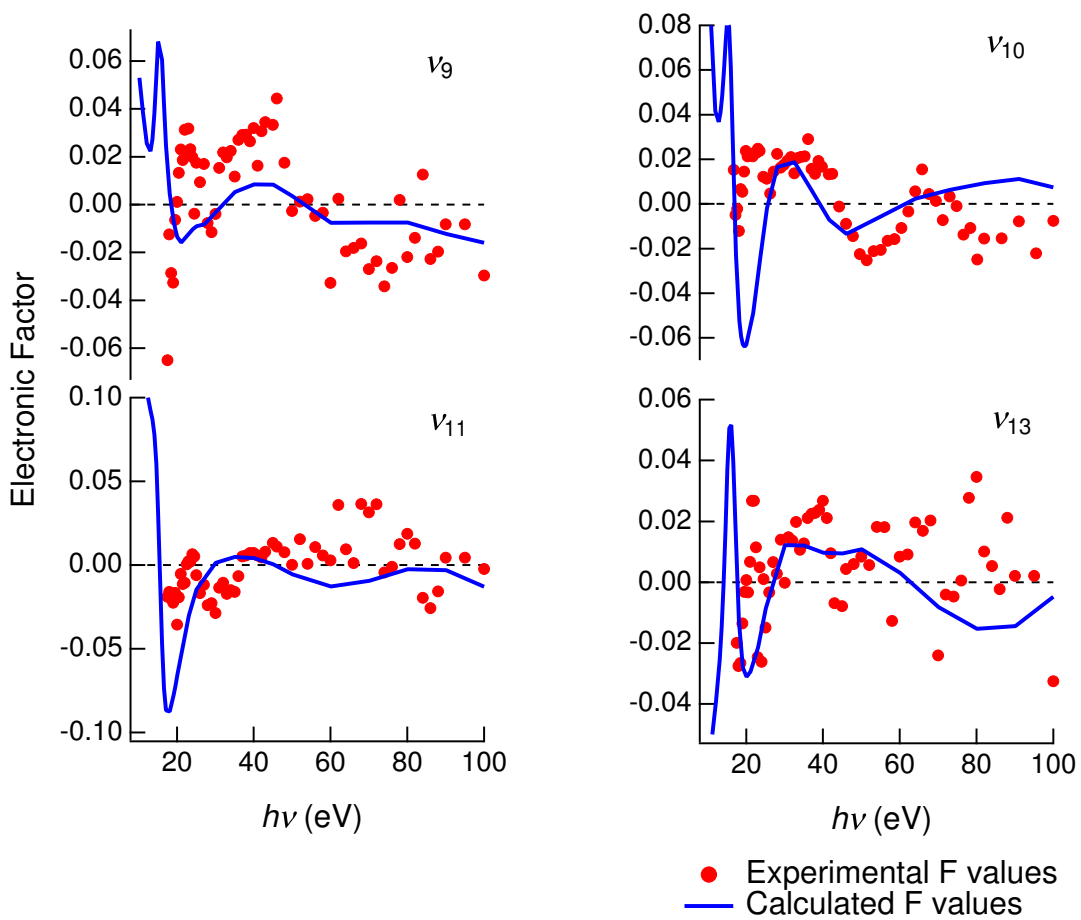e comparison between experiments and theory for the photoionization of acrolein leading to the $\tilde{X}\ ^2A'$ ionic state, showed a good agreement, especially in the low (near to threshold) and mid-energy regions.

CHAPTER V

EFFECTS OF ROTATION BETWEEN IONIZATION AND FRAGMENTATION FOR NON-LINEAR MOLECULES

V.1 Introduction

V.1.1 Molecular frame photoelectron angular distributions

The study and understanding of molecular photoionization is of great importance considering the number of phenomena directly or indirectly related to it. One of the experimental methods widely used for studying photoionization dynamics is the measurement of photoelectron angular distributions (PADs), being the observables giving the best insight on the transition matrix elements [35]. It has being observed that the PAD of the fragments on molecular photoionization can be peaked parallel or perpendicular to the incident light beam. This anisotropy depends on the orientation of the electronic dipole moment within the molecule, the polarization of the light beam and in general on the dynamics of the specific dissociation process [104]. The theoretical description of the one photon photoionization processes in first order of time dependent perturbation theory involves a representation of the initial state (prior to the interaction) and the scattering state when the photoelectron is leaving the target [105]. The PAD, $I(\theta_k, \phi_k)$, can be expanded in the spherical harmonics basis, $Y_{LM}(\theta_k, \phi_k)$,

$$I(\theta_k, \phi_k) \propto \sum_{L=0}^{L_{\max}} \sum_{M=-L}^{L} B_{LM} Y_{LM}(\theta_k, \phi_k) \tag{V.1}$$

where the angles correspond to the orientation of the emitted particles after ionization. The coefficients B_{LM} depend on the dynamics of the photoionization, the experimental geometry, the orbital from which the electron is ejected and the photoionization energy [106].

A molecular photoionization experiment is said to achieve "completeness" when it determines all the information needed for the theoretical description of such process, which means to provide all the significant matrix elements or dynamical parameters [35]. There are different experimental methods for obtaining the matrix elements

from the PADs for molecular ionization, depending on the frame of reference used. When the measurement is done on a fixed-in-space oriented molecule, it is referred to as the molecular frame photoelectron angular distribution (MFPAD) and, can be written as [105–110],

$$I(\theta_k, \phi_k, \theta_n, \phi_n) = \frac{4\pi^2}{c} E \sum_{L,M,L',M'} A_{LML'M'} Y_{LM}(\theta_k, \phi_k) Y_{L'M'}(\theta_n, \phi_n) \qquad (V.2)$$

where θ_n and ϕ_n are the polar and azimuthal angles for the direction of the polarization of the light. For linear molecules in the dipole approximation (see Section I.2.2), the expression is limited by the constraints $M = -M'$ and $0 \leq L' \leq 2$. For the linearly polarized light induced photoionization, the MFPADs depend on the angles giving the direction of emission (θ_k, ϕ_k) of the photoelectron in the molecular frame, and on the polar angle θ_n describing the orientation of the molecular axis with respect to the direction of polarization.

Measuring the MFPADs directly is not always possible. However, there are a number of other methods that can give information which can be related to the MFPADs. One way of measuring the MFPAD is through dissociative photoionization (DPI). If the dissociation event is rapid in comparison to the rotation period of the molecular ion, then the axial-recoil approximation (ARA) [104,111] (see Section V.1.2 below) may be valid [107]. This approximation assumes that the recoil direction of the ionic fragment is along the molecular axis at the time of the initial ionization [105, 111]. When the ARA is not valid it is necessary to take another frame of reference. One approach is by measuring the recoil-frame photoelectron angular distribution (RFPAD), which later can be related to the MFPAD. In the case of non-linear molecules, which are the main subject of this chapter, even if the ARA is still valid, when only two fragments are produced from photodissociation, it is not possible to measure the MFPAD, and the RFPAD measurement is the only one possible. This is due to the azimuthal angle giving the orientation about the recoil axis, which cannot be determined when only two fragments are produced [105]. If the molecule breaks into three or more fragments then the full MFPAD, as shown below, can be determined, as long as the number of fragments minus one are detected in coincidence with the photoelectron. The full MFPAD with linearly polarized light

has the form [105, 112],

$$I(\theta_k, \phi_k, \theta_n, \phi_n) = \sum_{L=0,2} \sum_{N'=0}^{L} \sum_{N'=0,\pm 1,\pm 2,\cdots} F^{(c)}_{LNN'}(\theta_k) P^N_L(\cos\theta_n) \cos(N'\phi_k - N\phi_n)$$
$$+ \sum_{L=0,2} \sum_{N'=0}^{L} \sum_{N'=0,\pm 1,\pm 2,\cdots} F^{(s)}_{LNN'}(\theta_k) P^N_L(\cos\theta_n) \sin(N'\phi_k - N\phi_n)$$

$$(\text{V}.3)$$

where the $F_{LNN'}$ functions can be expanded in the usual Legendre polynomials, $P^{N'}_{L'}(\cos\theta_k)$, and the coefficients $C_{L'LN'}$ depend on the dipole matrix elements $T^{M_i M_f}_{lm\mu}$ (defined elsewhere [41, 108]) and are given by [109],

$$F_{LNN'}(\theta_k) = \sum_{L'} C_{L'NN'} P^{N'}_{L'}(\cos\theta_k) \qquad (\text{V}.4)$$

The mathematical expressions presented above and similar ones have been used to study a variety of linear systems PADs in the molecular and recoil frames of reference [35, 40, 108, 109, 113–118]. Lafosse *et al.*, [108, 115] have studied the dissociative photoionization (DPI) of O_2 initially ionized to O_2^+ in the B $^2\Sigma_g^-$, 3 $^2\Pi_u$ and c $^4\Sigma_u^-$ states that subsequently dissociate to $O + O^+$ in various atomic states. The analysis of the directions of the ion and electron velocity vectors allowed the authors to determine a complete angular distribution $I(\chi_{O^+}, \theta_e, \phi_e)$ for each process, where χ_{O^+} is the polar angle of the velocity vector of the O^+ fragment referred to the axis parallel to the direction of linear polarization, at the instant of the photoionization. The inclusion of the effect of the molecular rotation gave a good agreement between the theory and experiments.

The non-linear systems, as mentioned above, show special difficulties compared to linear molecules due to the extra angular and spatial coordinate(s) that must be considered when studying the MFPADs and RFPADs. Additional complications come into play when considering systems dissociating in two fragments (See above) and those with dissociative lifetimes that are long compared to the rotational period. Several attempts have been made to study these systems [105, 119–124] both experimentally and theoretically. In this chapter, we develop similar expressions for the MFPADs and RFPADs as the ones shown above for linear molecules. This mathematical expressions will allow one to consider dissociative states where the lifetime of

the metastable molecular ions is not short compared to the rotational periods of the molecule and thus where the axial recoil approximation (see Section V.1.2) cannot be used [108]. This consideration will extend the number of states which can be studied and may improve the agreement between theory and experiment.

For linear systems, the effects of rotational motion on the derivation of the MF-PADs results in the expression [108]:

$$I_{\mu_0}(\theta_k, \phi_k, \theta_n, \phi_n) = \sum_{L',L,N} H_{L'LN}^{\mu_o\tau} Y_{L'N}(\Omega_{\hat{k}}) Y_{LN}^*(\Omega_{\hat{n}}) \tag{V.5}$$

where the index μ_0 represents the state of polarization of the light, $\Omega_{\hat{n}} = (\theta_n, \phi_n)$ and $\Omega_{\hat{k}} = (\theta_k, \phi_k)$ define the orientation of polarized light and direction of emission of the photoelectron respectively in the recoil frame, the $Y_{L'N}$ and Y_{LN}^* are spherical harmonic functions and the coefficients $H_{L'LN}^{\mu_o\tau}$ (where τ is the lifetime of the ion state) contain the information of the distribution of rotational states, the matrix elements and several transformations involving the polarization of light and angular momentum, the full details can be found elsewhere [108]. A smiler formalism is developed in this chapter and later implemented in the study of the C $1s$ photoionization of CH_4.

V.1.2 Axial-recoil approximation

It was shown by Zare [104] that for photodissociation, unless the recoil velocity is very large compared to the angular velocity of molecular rotation, the angular distribution of products of a photodissociation will be modified by the molecular rotation. He showed that if a molecular ensemble is randomly oriented having equal M state populations the photofragment angular distribution is obtained by summing over all the M sub levels of the initial state,

$$I(\theta, \phi) = \sum_M \left| \sum_{J'M'} \mathscr{R}_{J'} \langle J \quad 1, J' \quad 0| M, 0 \rangle \langle J \quad 1, J' \quad 0| 0, \lambda \rangle D_{M'\Omega}^{J'}(\phi, \theta, 0) \right|^2 \tag{V.6}$$

where $\mathscr{R}_{J'}$ is the 'rotational term' and $D_{M'\Omega}^{J'}(\phi, \theta, 0)$ is a rotational matrix as defined elsewhere [125–127]. When explicit algebraic expressions are substituted for the Clebsch-Gordan coefficients, the well known [128] expression for $I(\theta, \phi)$ having the form $[1 + \beta P_2(\cos(\theta))]/4\pi$ arises. The evaluation of the photo fragment distribution

of Equation (V.6) requires the knowledge of the rotational radial term $\mathscr{R}_{J'}$ over the range of permitted J' transitions. However, if the kinetic energy of the fragments is much larger than the rotational energy it can be shown that $\mathscr{R}_{J'}$ is effectively a constant over the rotational structure and can be taken outside of the sum in Equation (V.6) leading ultimately [104, 111] to the reduced expression for the photofragment angular distribution

$$I(\theta, \phi) = \left| D_{0\lambda}^1(\theta, \phi, 0) \right|^2 . \tag{V.7}$$

Thus axial-recoil approximation is valid when $\mathscr{R}_{J'+1} = \mathscr{R}_{J'-1}$. In Section V.2 we consider the effects of rotation on the evaluation of molecular and recoil frame photoelectron angular distributions when the effect of the rotational motion is not negligible, that is when the axial-recoil approximation breaks down.

V.2   Theory: expressions for MFPADs and RFPADs [1]

The analysis of the MFPADs for non-linear polyatomic molecules follows closely the work that has been done previously for linear systems [107,108]. Here we will consider MFPADs for elliptically polarized light. For the case that the light is either linearly polarized or circularly polarized, the state of the light can be characterized by a single parameter μ_0. If the light is linearly polarized, the index $\mu_0 = 0$, if the light is circularly polarized then $\mu_o = \pm 1$. The index μ_0 is defined for circularly polarized light as being $\mu_0 = +1$ for left circularly polarized light having positive helicity, and $\mu_0 = -1$ for right circularly polarized light with negative helicity. Throughout this model we have used different coordinate systems for convenience depending on the frame of reference used.

   As mentioned above, if the lifetime of a molecular ion state represents a significant fraction of the rotational period of the molecule, then the axial-recoil approximation breaks down, and the effects of the rotational motion should be included when computing the cross sections. For this purpose, we assume a Boltzmann distribution of the rotational states [129], and followed a similar treatment as the one used for rotational motion in photodissociation by Jonah [130], assuming that the population of initial rotational states is thermal. After the molecule is ionized the density matrix elements for the rotational states is propagated in time. A Poisson distribution is assumed for the distribution of decay times.

---

[1]Full details of the derivation of the model can be found on Appendix A at the end of this work.

V.2.1 Ionization of non-linear molecules and rotational state specific matrix elements

Here we will consider the photoionization of non-linear molecules in the dipole approximation (see Section I.2.2), and later on, the analysis of the angular distributions with respect to the direction of propagation of the light for two cases: linearly and circularly elliptically polarized light. The dipole matrix elements for photoionization going from an initial state i to a final state f by either polarized light or circularly polarized light can be written as,

$$T_{\lambda,\delta}^{(\zeta',\zeta'')}(\Omega_K, \hat{R}) = \sum_{l,m,n,\mu} \frac{1}{\sqrt{2}} \left\{ B_+ D_{\mu,-1}^{(1)}(\hat{R}) - B_- D_{\mu,1}^{(1)}(\hat{R}) \right\} I_{lm\mu}^{(\zeta',\zeta'')} Y_{ln}^*(\Omega_K) D_{m,n}^l(\hat{R})$$

(V.8)

in this expression, the indices ζ' and ζ'' indicate a component of a degenerate set of orbitals for the initial and final state respectively, and λ and δ are the angles used to characterized the polarized light by the Stokes parameters (see Equation (A.1) in Appendix A). This expression is already transformed from the molecular frame (MF) into the field frame (FF) using the inverse transformation defined by the Euler angles [126] $\hat{R}^{-1} = (-\beta, \chi, \gamma)$. In the FF the direction of emission of the photoelectron is defined by the coordinates $\Omega_K = (\theta_K, \phi_K)$. The field is defined by B, and the D's are the usual rotational matrices defined elsewhere [125–127]. The dipole matrix element of Equation (V.8) can then be written as:

$$I_{lm\mu}^{(\zeta',\zeta'')} = \sqrt{\frac{2}{\pi}} i^l \left\langle \Psi_{\zeta'}^{(i)} \left| e_\mu \right| \Phi_{\zeta''}^{(f)} \psi_{lm}^{(-)}(\vec{r}) \right\rangle$$

(V.9)

where the continuum scattering wave function $\psi_{\vec{k}}^{(-)}(\vec{r})$ can be expanded as [41],

$$\psi_{\vec{k}}^{(-)}(\vec{r}) = \sqrt{\frac{2}{\pi}} \sum_{l,m} i^l \psi_{lm}^{(-)}(\vec{r}) Y_{lm}^*(\Omega_k)$$

(V.10)

The rotational wave function for an asymmetric top, $\psi_{J,M_J,\kappa}$, can be written as a linear combination of symmetric top wave functions $\phi_{J,M_J,H}$ [21],

$$\psi_{J,M_J,\kappa} = \sum_H C_{H,\kappa}^J \phi_{J,M_J,H}$$

(V.11)

74

where the symmetric top wave functions have the well known form,

$$\phi_{J,M_J,H} = \left(\frac{2J+1}{8\pi^2}\right)^{\frac{1}{2}} D^J_{-M_J,-H}(\hat{R}_M) \tag{V.12}$$

In this way, we can construct the rotation state specific matrix elements for the transitions $(\zeta, J, M_J, \kappa \leftarrow \zeta'', J'', M_{J''}, \kappa'')$ using the asymmetric top wave functions from Equation (V.11) for the specific rotational states to get,

$$T_{\lambda,\delta}^{(\zeta,J,M_J,\kappa\leftarrow\zeta'',J'',M_{J''},\kappa'')}(\Omega_K) = \int \left[\psi_{J'',M_{J''},\kappa''}(\hat{R})\right]^* \psi_{J,M_J,\kappa}(\hat{R}) T_{\lambda,\delta}^{(\zeta'',\zeta)}(\Omega_K,\hat{R}) d\hat{R} \tag{V.13}$$

where by substitution of Equation (V.8) leads to the desired result.

V.2.2 Thermal average and propagation into time

In this section we assume that the population of initial rotational states is thermal, and thus that under equilibrium it follows a Boltzmann distribution. This assumption allows us to write the density matrix before the interaction with light similarly to the treatment of the rotational motion in photodissociation by Jonah [130],

$$\rho = \frac{1}{g_i Q(T)} \left\{ \sum_{\substack{\zeta'',J'' \\ M_{J''},\kappa''}} \left|\psi_{J'',M_{J''},\kappa''}\Psi_{\zeta''}^{(i)}\right\rangle g_{\kappa''} \exp\left(-\frac{E_{J'',\kappa''}}{k_B T}\right) \left\langle\psi_{J'',M_{J''},\kappa''}\Psi_{\zeta''}^{(i)}\right| \right\} \tag{V.14}$$

where g_i is the degeneracy of initial electronic states, $\Psi_{\zeta''}^{(i)}$, and $Q(T)$ is the rotation partition function for the initial state for an asymmetric-top molecule (see [131] and Equation (A.33) in Appendix A) and $g_{\kappa''}$ is the nuclear-spin statistical weight, which depends on the parities of the quantum numbers K_p and K_o, collectively labeled here as κ, (which are the quantum numbers on the prolate and oblate limits of the asymmetric rotor).

After the interaction with the light, with a field operator B as defined in Equation (A.2) of Appendix A, we have the density matrix that propagates in time to give,

$$\rho''(t) = \frac{4\pi^2 E}{c} \exp\left(\frac{-iH_{\mathrm{rot}}t}{\hbar}\right) B^*\rho B \left(\frac{iH_{\mathrm{rot}}t}{\hbar}\right) \tag{V.15}$$

where E is the photon energy and c is the speed of light.

V.2.3 MFPADs and RFPADs functional form

To evaluate Equation (V.15), we expand it into final states, which are rotational eigenfuncitons of the rotational Hamiltonian, to give only the diagonal elements of the density matrix for the ionization in the coordinate representation at a particular time t after the excitation. Finally, the usual molecular frame photoelectron angular distribution (MFPAD), $I(\Omega_K, \hat{R})$, can be defined as the differential cross section for the emission of the photoelectron in the direction Ω_K for a fixed orientation of the molecule in the field frame as defined by the Euler angles $\hat{R}$. The usual integrated target distribution [128] would be obtained by an orientation average of the target [132], and thus, the final total cross section would be given by

$$\sigma = \int \frac{d\sigma}{d\Omega_K} d\Omega_K = \frac{1}{8\pi^2} \int \int I(\Omega_K, \hat{R}) d\hat{R} d\Omega_K \tag{V.16}$$

and the total cross section at $t = 0$ would be given by

$$\sigma = \int \int \rho''(\Omega_K, \hat{R}, \Omega_K, \hat{R}, t = 0) d\Omega_K d\hat{R} \tag{V.17}$$

and thus, the RFPAD $I(\Omega_K, \hat{R}, t)$ for the fragmentation after time t is related to the diagonal matrix elements of the density by

$$I(\Omega_K, \hat{R}, t) = 8\pi^2 \rho''(\Omega_K, \hat{R}, \Omega_K, \hat{R}, t) \tag{V.18}$$

Finally, assuming a Poisson distribution of decay times $(1/\tau)\exp(-t/\tau)$, the density matrix can be averaged over decay time, to become,

$$I_\tau(\Omega_K, \hat{R}, t) = \frac{1}{g_i Q(T)} \sum_{\substack{\zeta,\zeta'' \\ J,J',J'' \\ \kappa,\kappa',\kappa''}} g_{\kappa''} \exp\left(-\frac{E_{g_s, J'', \kappa''}}{k_B T}\right) \frac{W^{\binom{J,J',J''}{\kappa,\kappa',\kappa''}}_{\lambda,\delta;(\zeta,\zeta'')}}{1 + \frac{i\tau \Delta E^{(J',\kappa',J,\kappa)}}{\hbar}} \tag{V.19}$$

where the explicit expression $W^{\binom{J,J',J''}{\kappa,\kappa',\kappa''}}_{\lambda,\delta;(\zeta,\zeta'')}$ and its solution can be viewed in detail in Appendix A. The expression for the intensity from Equation (V.19) can be written as,

$$I_\tau(\Omega_K, \hat{R}, t) = \frac{1}{g_i Q(T)} \sum_{L',L,N,N_H} Y_{L',-N_H}(\Omega_K) E_{L,N}^{(\lambda,\delta)}(\hat{R}'')$$

$$\times \sum_{\substack{\zeta,\zeta'' \\ J,J',J'' \\ \kappa,\kappa',\kappa''}} g_{\kappa''} \exp\left(-\frac{E_{g_s,J'',\kappa''}}{k_B T}\right) \times \frac{H_{L',N_H,L,N;(\zeta,\zeta'')}^{\binom{J,J',J''}{\kappa,\kappa',\kappa''}}}{1 + \frac{i\tau\Delta E^{(J,\kappa,J',\kappa')}}{\hbar}} \qquad \text{(V.20)}$$

where

$$H_{L',N_H,L,N;(\zeta,\zeta'')}^{\binom{J,J',J''}{\kappa,\kappa',\kappa''}} = \frac{4\pi^2 E}{c} \sum_{l,p,q,l'} \sum_{q''} (2J+1)(2J'+1)(2J''+1) \left[\frac{(2L'+1)(2l+1)}{(2l'+1)(2L+1)}\right]^{1/2}$$

$$\times C_{H_2',\kappa'}^{J'} \cdot C_{H_1,\kappa}^{J*} \times (-1)^{q-N+1} \langle L'\ N_H, l\ -p|\ l', N_H - p\rangle$$

$$\times \langle L'\ 0, l\ 0|\ l', 0\rangle \langle 1-q', 1\ q|\ L, N\rangle$$

$$\times M_{q'',p,q}^{(J,J'',l,\kappa'',\kappa,\zeta'',\zeta)} \left[M_{q'',p',q'}^{(J',J'',l',\kappa'',\kappa',\zeta'',\zeta)}\right]^* \qquad \text{(V.21)}$$

or by defining $H_{L',N_H,L,N}^{(\tau,T)}$ as

$$H_{L',N_H,L,N}^{(\tau,T)} = \frac{1}{g_i Q(T)} \sum_{\substack{\zeta,\zeta'' \\ J,J',J'' \\ \kappa,\kappa',\kappa''}} g_{\kappa''} \exp\left(-\frac{E_{g_s,J'',\kappa''}}{k_B T}\right) \frac{H_{L',N_H,L,N;(\zeta,\zeta'')}^{\binom{J,J',J''}{\kappa,\kappa',\kappa''}}}{1 + \frac{i\tau\Delta E^{(J,\kappa,J',\kappa')}}{\hbar}} \qquad \text{(V.22)}$$

we can write the intensity as

$$I_\tau^{(\lambda,\delta)}(\Omega_K, \hat{R}) = \sum_{L',L,N,N_H} Y_{L',-N_H}(\Omega_K) E_{L,N}^{(\lambda,\delta)}(\hat{R}'') H_{L',N_H,L,N}^{(\tau,T)} \qquad \text{(V.23)}$$

suming over L' and N_H we can define $G_{L,N}^{(\tau,T)}(\Omega_K)$,

$$G_{L,N}^{(\tau,T)}(\Omega_K) = \sum_{L',N_H} Y_{L',-N_H}(\Omega_K) H_{L',N_H,L,N}^{(\tau,T)} \qquad \text{(V.24)}$$

then the final expression for the intensity becomes,

$$I_\tau^{(\lambda,\delta)}(\Omega_K, \hat{R}) = \sum_{L,N} G_{L,N}^{(\tau,T)}(\Omega_K) E_{L,N}^{(\lambda,\delta)}(\hat{R}'') \qquad (V.25)$$

Lastly, by considering the polarization special cases, Equation (V.25), for the intensiy becomes

$$I_\tau^{(\mu_0)}(\Omega_K, \chi, \gamma) = \sum_{L,N} G_{LN}^{(\tau)}(\Omega_k)[Y_{LN}(\chi, \gamma)]^* (-1)^{\mu_0+1} \langle 1 - \mu_0, 1\, \mu_0 | L, 0 \rangle \qquad (V.26)$$

V.3 Effects of rotational motion on the C 1s photoionization of CH$_4$

V.3.1 Computation of the photoionization dipole matrix elements

The calculation of the dynamical photoionization matrix elements, $I_{lm\mu}^{(\zeta',\zeta'')}$, from Equation (V.8) leading to the C 1s $(1a_1)^{-1}$ state were computed using the Schwinger variational method [12, 98] (see Section I.1.3). An $l_{\max} = 100$ was used for the single-center expansion of the electronic wave functions within the single channel frozen core Hartree-Fock approximation (SCFCHF) using the ePolyScat suite of programs [65, 66]. Using the Born-Oppenheimer or Chase adiabatic approximation [22] (see Section I.2.3). Within this approximation, the initial and final total scattering state wave functions can be expressed as products of vibrational and electronic wave functions, as shown previously in this work in Equations (I.58) and (I.59), and elsewhere [16]. The initial and final electronic state wave functions, $\Psi_i(r, q)$ and $\Psi_{f,\vec{k}}^{(-)}(r, q)$ were calculated at the Hartree-Fock level of theory using the augmented correlation-consistent polarized valence triple-ζ [95, 96] (aug-cc-pVTZ) basis set and were computed using the Gaussian09 program [97]. For this calculations a vertical ionization potential (ionization from the C 1s) of 290.84 eV [133] was used.

V.3.2 MFPADs for CH$_4$

In this section we will examine the MFPADs in the molecular frame for the CH$_4$ C 1s photoionization. The methane molecule has tetrahedral symmetry, since it belongs to the T_d point group, and therefore it has four equivalent C_3 axis of symmetry and three equivalent C_2 axes. Each of the CH bonds lies on a C_3 axis. In Figures V.1 through V.8 the molecule is oriented so that one of the C_2 symmetry axis coincides with the z

cartesian axis. The ground state electronic configuration of CH_4 is $(1a_1)^2(2a_1)^2(1t_2)^6$, where the $1a_1$ orbital is essentially the atomic $1s$ orbital from the central carbon atom.

The MFPADs for the ionization from the $1a_1$ orbital were computed at photoelectron energies $E_k = 0.1, 1.09, 4.35$ and 15.25 eV as described above. These photoelectron kinetic energies are represented in that order in Figures V.1 to V.4 for ionization with linearly polarized light (LP), that is $\mu_0 = 0$ and in Figures V.5 to V.8 for ionization with right circularly polarized light (RCP), that is $\mu_0 = -1$. As it was pointed out by Lucchese [107], the shape of the MFPADs can be, at least qualitatively, understood by considering the angular momentum composition of the initial orbitals and the angular momentum contributed from the different polarizations of the ionizing light. For the case analyzed here, ionization from an s orbital, results in the photoelectron leaving in a p wave, and the orientation of the MFPAD is determined by the orientation of the polarized light. If we look at the first row of Figure V.1, where the lifetime of the pre-dissociative state is assumed to be $\tau = 0$ ps, implying the validity of the axial-recoil approximation (ARA), the MFPADs look different from what was 'predicted' above. As time increases, allowing the meta-stable state to rotate before fragmentation, all the way to an assumed infinit lifetime, $\tau = \infty$ ps, at the bottom row of Figure V.1 the MFPAD shape becomes more isotropic and in better agreement with the expected p wave shape. Williams $et.$ $al.$ [134], have studied the dynamics of dissociation of methane after core ionization by means of measured and computed MFPADs and RFPADs for the aforementioned process. They found that the experimental data with high fragment kinetic energy was in better agreement with the calculated RFPADs, and as they considered lower kinetic energy the RFPADs show a deviation that indicates the fail of the axial-recoil approximation. By including the effects of rotational motion, we are able to explain that deviation. In Figure V.4 it is noticeable that even at a lifetime of $\tau = 0$ ps, the MFPADs look a lot more like the p wave, only observed after letting the pre-dissociative state to rotate when photoionization thames place at lower kinetic energies ($E_k = 0.1, 1.09, 4.25$ eV).

For Figures V.5 through V.8, for circularly polarized light, results also coincide with the effect predicted by Lucchese [107], when the ARA breaks down, showing that as lifetime increases up to infinity, the MFPAD shows a completely uniform distribution of the ejected photoelectron, being a reflection of the isotropic distribution of the initial, $1s$, state. In the case of the figures with circularly polarized light, the

same directions shown in the figures for LP, indicate the propagation vector.

V.3.3   RFPADs for CH$_4$

To compute the RFPADs, it is necessary to include an average of the MFPAD over the azimuthal angle about the recoil direction, and after this average we obtain the expression [135],

$$I_{\mu_0,\beta_R,\alpha_R}^{(ion)}(\theta'_{\hat{k}}, \phi'_{\hat{k}}, \theta'_{\hat{n}}, \phi'_{\hat{n}}) = \sum_{L',L,Q} H_{L',L,Q}^{\mu_0,\beta_R,\alpha_R} Y_{L',Q}(\Omega'_{\hat{k}}) Y_{L,Q}^*(\Omega'_{\hat{n}}) \qquad \text{(V.27)}$$

where the angles β_R and α_R define the recoil direction, and the coefficients $H_{L',L,Q}^{\mu_0,\beta_R,\alpha_R}$ are given by

$$\begin{aligned} H_{L',L,Q}^{\mu_0,\beta_R,\alpha_R} = \sum_{J,N_H,N,P} H_{L',N_H,L,N}^{(\tau,T)} \left[\frac{4\pi(2J+1)}{(2L'+1)^2} \right]^{1/2} \langle J\, 0, L\, Q| \, L', Q\rangle \\ \times \langle J\, P, L\, N| \, L', N_H\rangle Y_{J,P}(\beta_R, \alpha_R) \end{aligned} \qquad \text{(V.28)}$$

where $P = N_H - N$ and $H_{L',N_H,L,N}^{(\tau,T)}$ is given in Equation (V.22). In Figure V.9 we present the RFPADs for the C $1s$ photoionization of methane at a photoelectron energy $E_k = 4.35$ eV, with the vector of polarization of the light in the direction of one of the CH bonds, and averaged over that same axis, which on the figures appears pointing in the z direction. It is noticeable how at a lifetime of $\tau = 0$ ps the RFPAD indicates an axial recoil behavior in the direction of the CH bond, but as the lifetime of the pre-dissociative state is increased to $\tau = 0.32$ ps, exhibits a breakdown of the ARA and shows a better agreement with the experiments [134], revealing the importance that the rotational motion has on the specific dynamics of photoionization from C $1s$ of methane at this particular energy.

V.4   Conclusions

We presented a theoretical model for computing MFPADs and RFPADs for non-linear molecules that allows for the inclusion of the effect of rotational motion between ionization and fragmentation. This model has proven to predict the photoionization dynamics of the photoelectron through the three dimensional MFPADs for systems where the axial-recoil approximation breakdown. The predicted MFPADs for the

τ/ps	$\parallel C_2(z)$	$\perp C_2(z)$	$\perp C_3$ near a CH	$\parallel C_3$
0				
0.16				
0.32				
3.15				
∞				
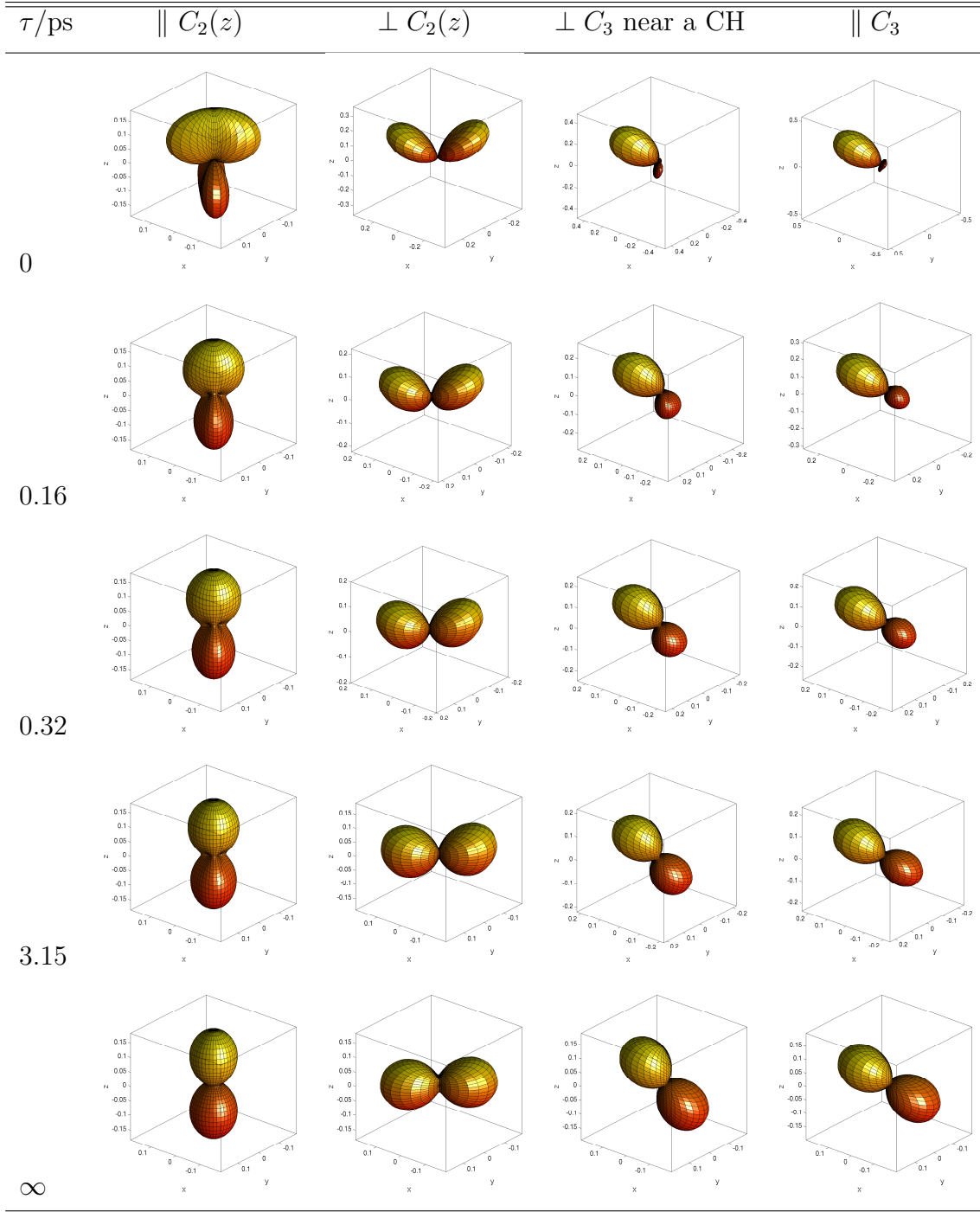
Figure V.1: MFPADs for the photoionization of the C $1s$ orbital of CH_4 molecule. Results computed at $E_k = 0.1$ eV for linearly polarized light (LP). In each column the polarization vectors change: first parallel to the C_2 axis in the z direction; second, perpendicular to the $C_2(z)$ axis and in the plane with two CH bonds; third, perpendicular to a C_3 axis but close to a CH bond, and fourth parallel to a C_3 axis (CH bond). Lifetimes of the pre-dissociative state are indicated for each row.

τ/ps	$\parallel C_2(z)$	$\perp C_2(z)$	$\perp C_3$ near a CH	$\parallel C_3$
0				
0.16				
0.32				
3.15				
∞				
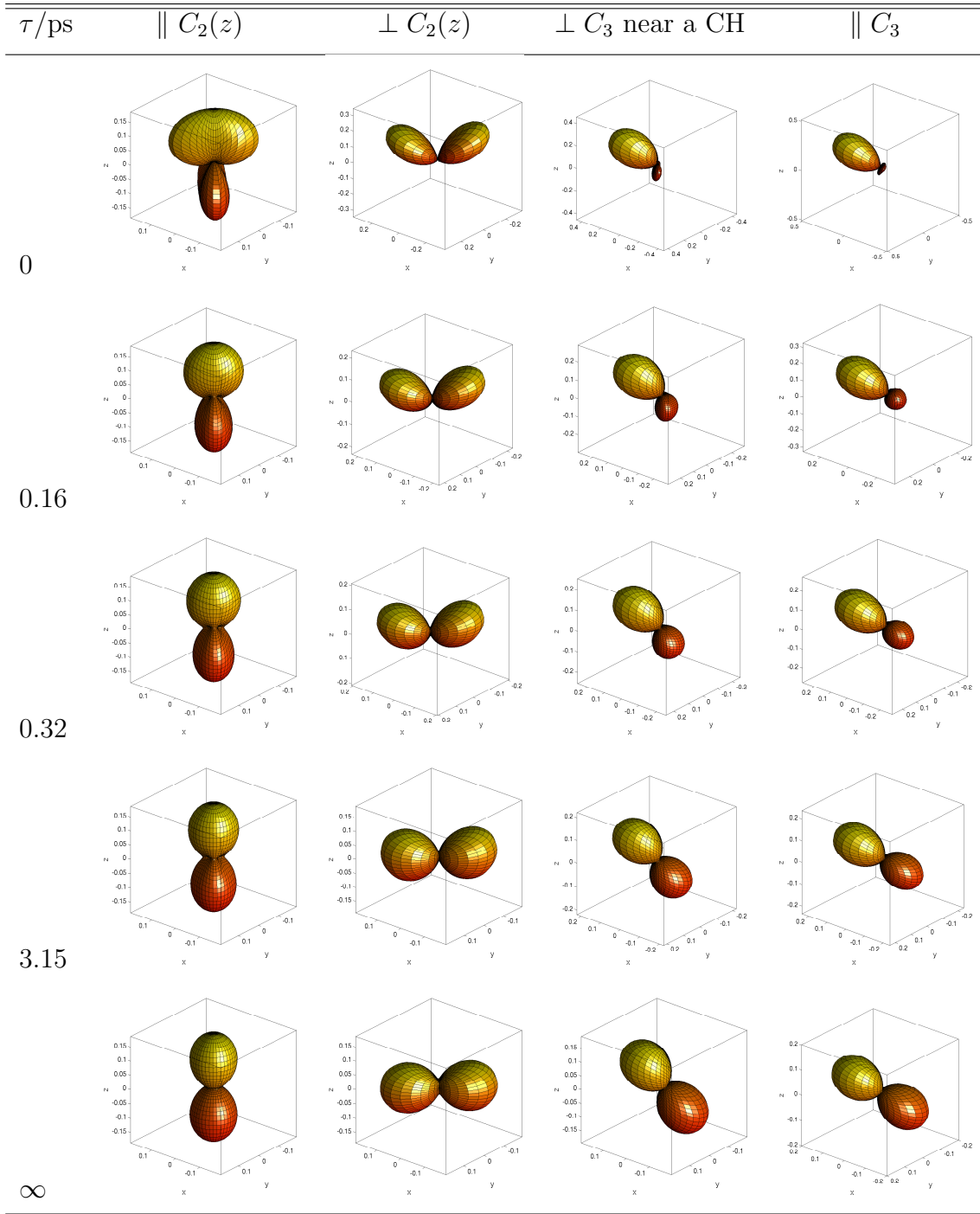
Figure V.2: MFPADs for the photoionization of the C $1s$ orbital of CH_4 molecule. Results computed at $E_k = 1.09$ eV for linearly polarized light (LP). In each column the polarization vectors change: first parallel to the C_2 axis in the z direction; second, perpendicular to the $C_2(z)$ axis and in the plane with two CH bonds; third, perpendicular to a C_3 axis but close to a CH bond, and fourth parallel to a C_3 axis (CH bond). Lifetimes of the pre-dissociative state are indicated for each row.

82

τ/ps	$\parallel C_2(z)$	$\perp C_2(z)$	$\perp C_3$ near a CH	$\parallel C_3$
0				
0.16				
0.32				
3.15				
∞				
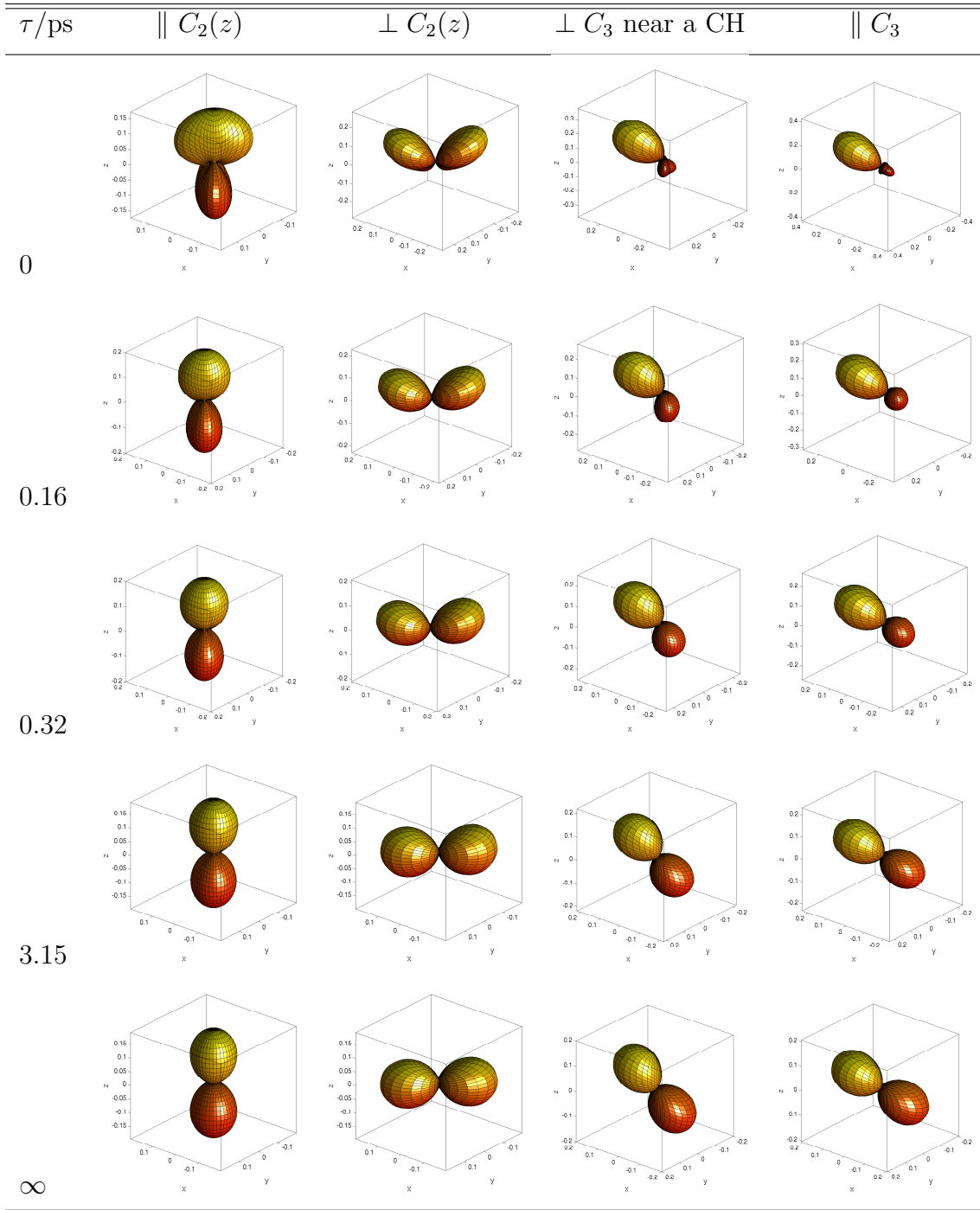
Figure V.3: MFPADs for the photoionization of the C $1s$ orbital of CH_4 molecule. Results computed at $E_k = 4.35$ eV for linearly polarized light (LP). In each column the polarization vectors change: first parallel to the C_2 axis in the z direction; second, perpendicular to the $C_2(z)$ axis and in the plane with two CH bonds; third, perpendicular to a C_3 axis but close to a CH bond, and fourth parallel to a C_3 axis (CH bond). Lifetimes of the pre-dissociative state are indicated for each row.

τ/ps	$\parallel C_2(z)$	$\perp C_2(z)$	$\perp C_3$ near a CH	$\parallel C_3$
0				
0.16				
0.32				
3.15				
∞				
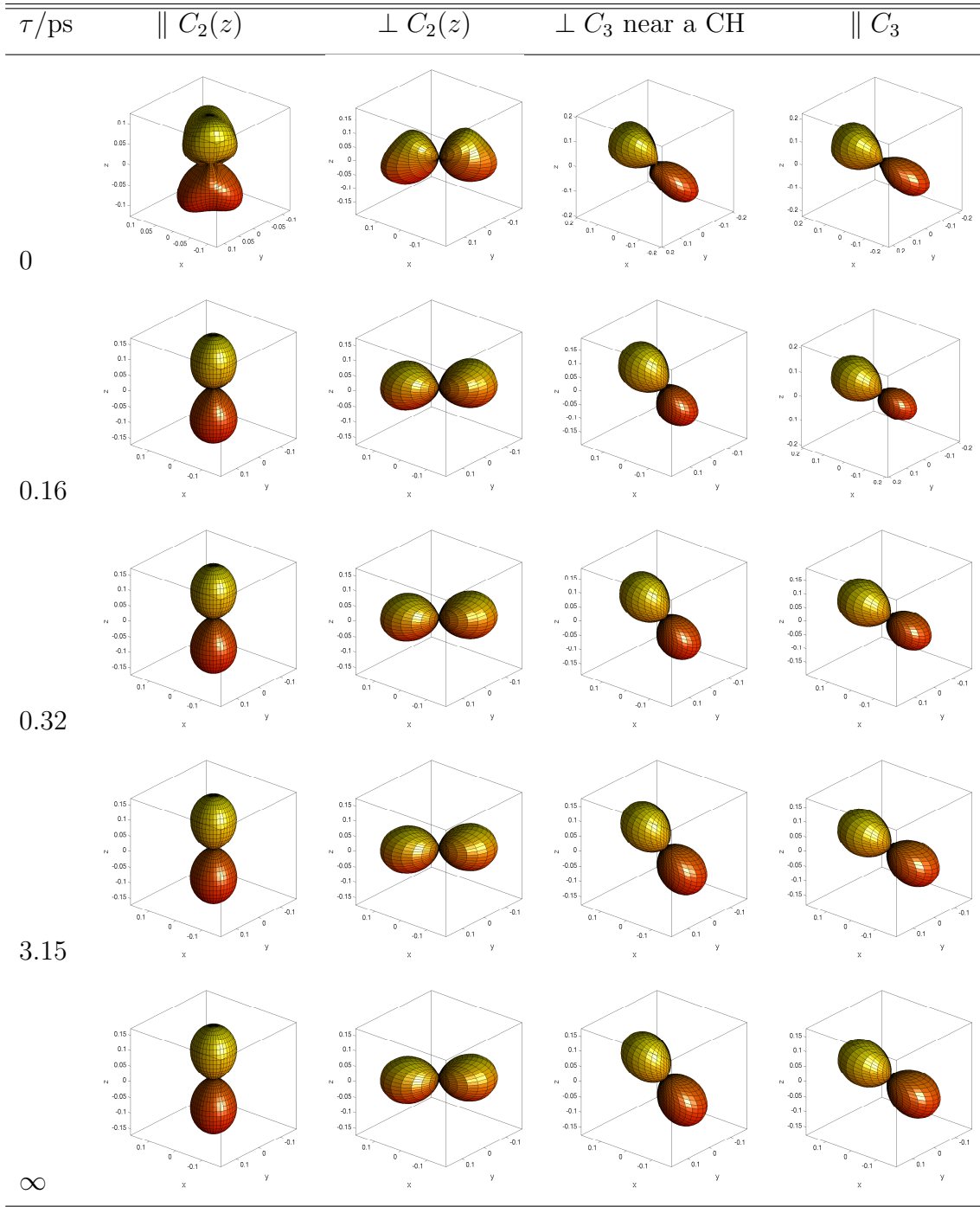
Figure V.4: MFPADs for the photoionization of the C $1s$ orbital of CH_4 molecule. Results computed at $E_k = 15.25$ eV for linearly polarized light (LP). In each column the polarization vectors change: first parallel to the C_2 axis in the z direction; second, perpendicular to the $C_2(z)$ axis and in the plane with two CH bonds; third, perpendicular to a C_3 axis but close to a CH bond, and fourth parallel to a C_3 axis (CH bond). Lifetimes of the pre-dissociative state are indicated for each row.

τ/ps	$\parallel C_2(z)$	$\perp C_2(z)$	$\perp C_3$ near a CH	$\parallel C_3$
0				
0.16				
0.32				
3.15				
∞				
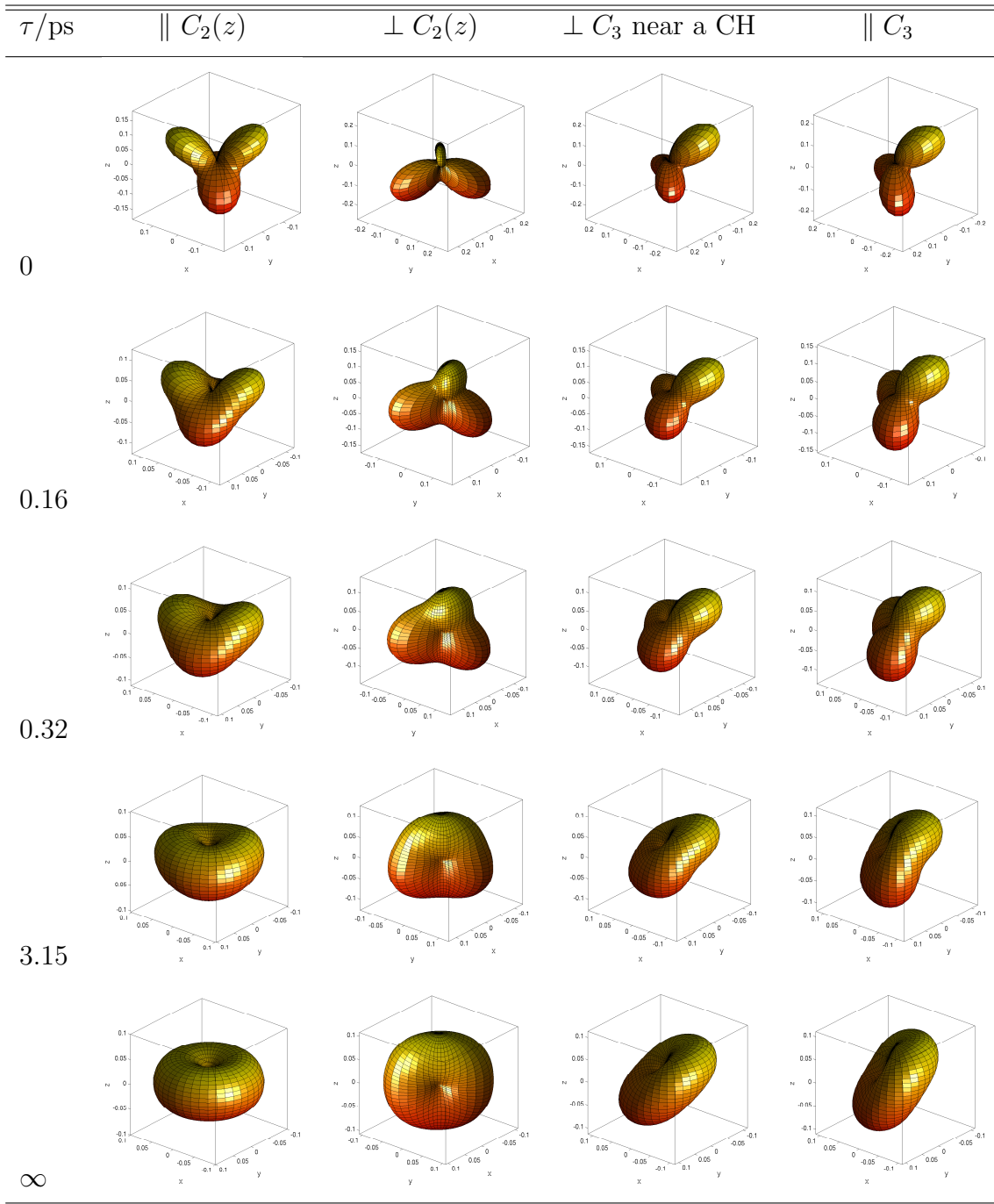
Figure V.5: MFPADs for the photoionization of the C 1s orbital of CH_4 molecule. Results computed at $E_k = 0.1$ eV for right circularly polarized light (RCP). In each column the propagation vectors change: first parallel to the C_2 axis in the z direction; second, perpendicular to the $C_2(z)$ axis and in the plane with two CH bonds; third, perpendicular to a C_3 axis but close to a CH bond, and fourth parallel to a C_3 axis (CH bond). Lifetimes of the pre-dissociative state are indicated for each row.
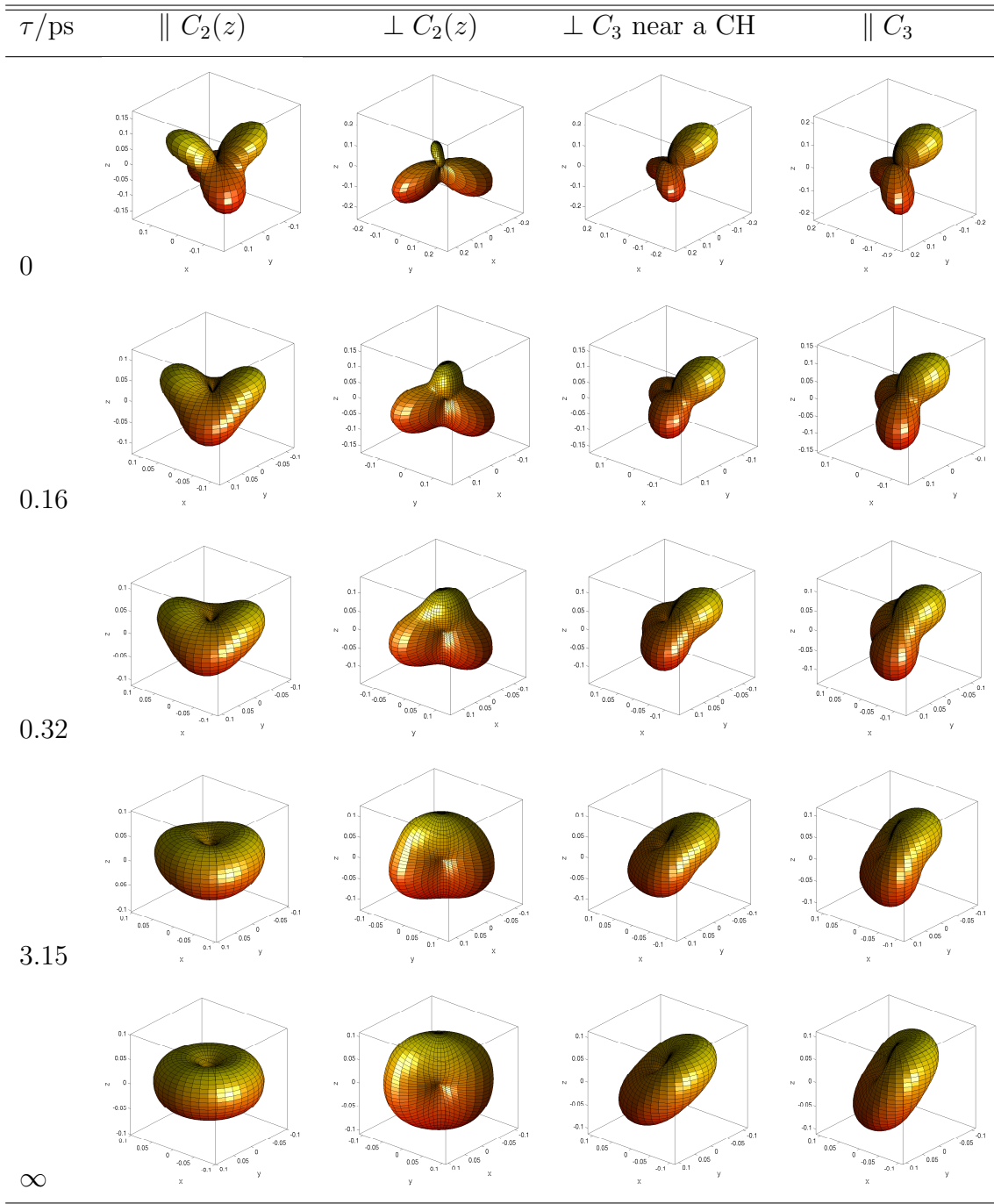
Figure V.6: MFPADs for the photoionization of the C $1s$ orbital of CH_4 molecule. Results computed at $E_k = 1.09$ eV for right circularly polarized light (RCP). In each column the propagation vectors change: first parallel to the C_2 axis in the z direction; second, perpendicular to the $C_2(z)$ axis and in the plane with two CH bonds; third, perpendicular to a C_3 axis but close to a CH bond, and fourth parallel to a C_3 axis (CH bond). Lifetimes of the pre-dissociative state are indicated for each row.

τ/ps	$\parallel C_2(z)$	$\perp C_2(z)$	$\perp C_3$ near a CH	$\parallel C_3$
0				
0.16				
0.32				
3.15				
∞				
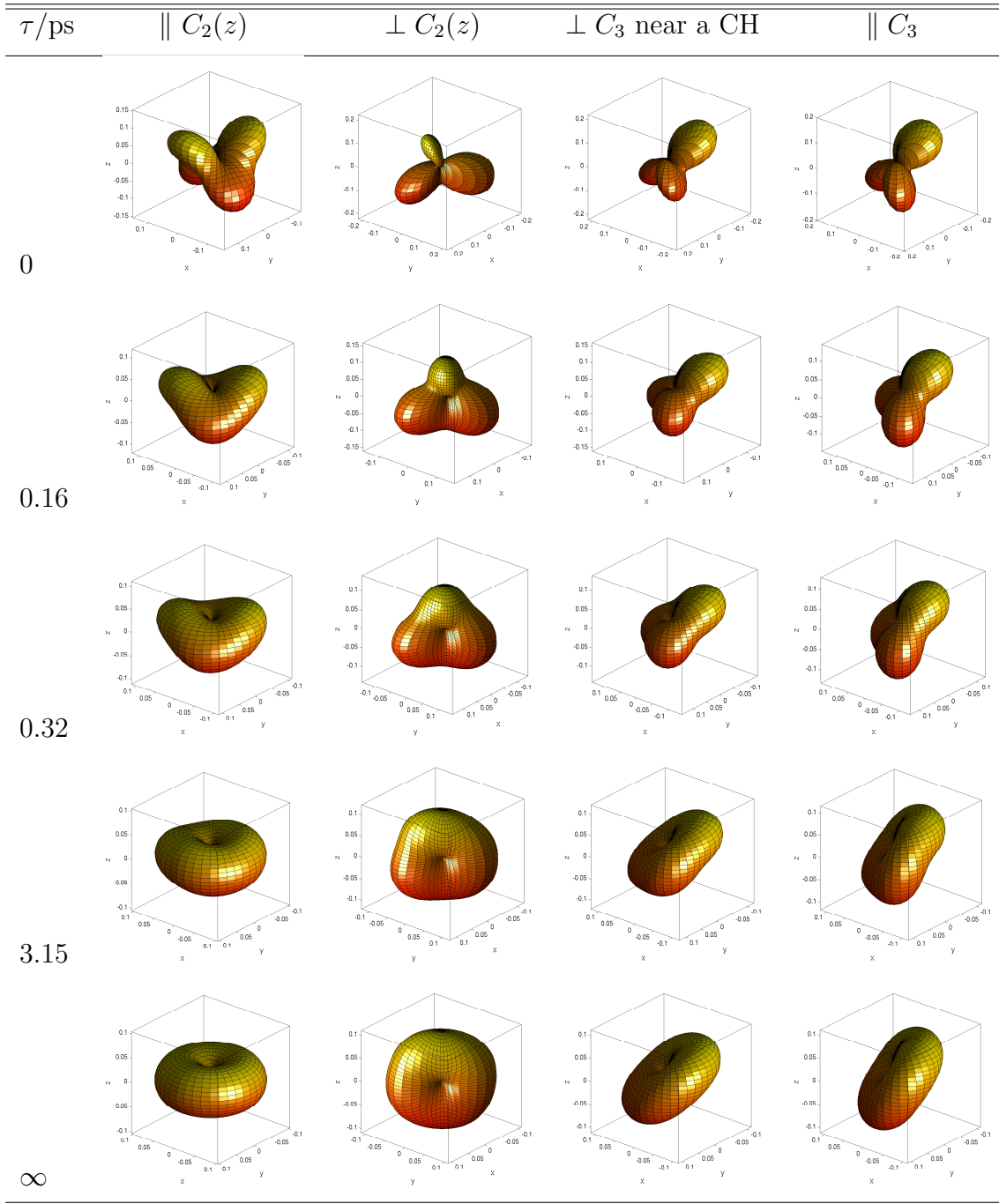
Figure V.7: MFPADs for the photoionization of the C $1s$ orbital of CH_4 molecule. Results computed at $E_k = 4.35$ eV for right circularly polarized light (RCP). In each column the propagation vectors change: first parallel to the C_2 axis in the z direction; second, perpendicular to the $C_2(z)$ axis and in the plane with two CH bonds; third, perpendicular to a C_3 axis but close to a CH bond, and fourth parallel to a C_3 axis (CH bond). Lifetimes of the pre-dissociative state are indicated for each row.

τ/ps	$\parallel C_2(z)$	$\perp C_2(z)$	$\perp C_3$ near a CH	$\parallel C_3$
0				
0.16				
0.32				
3.15				
∞				
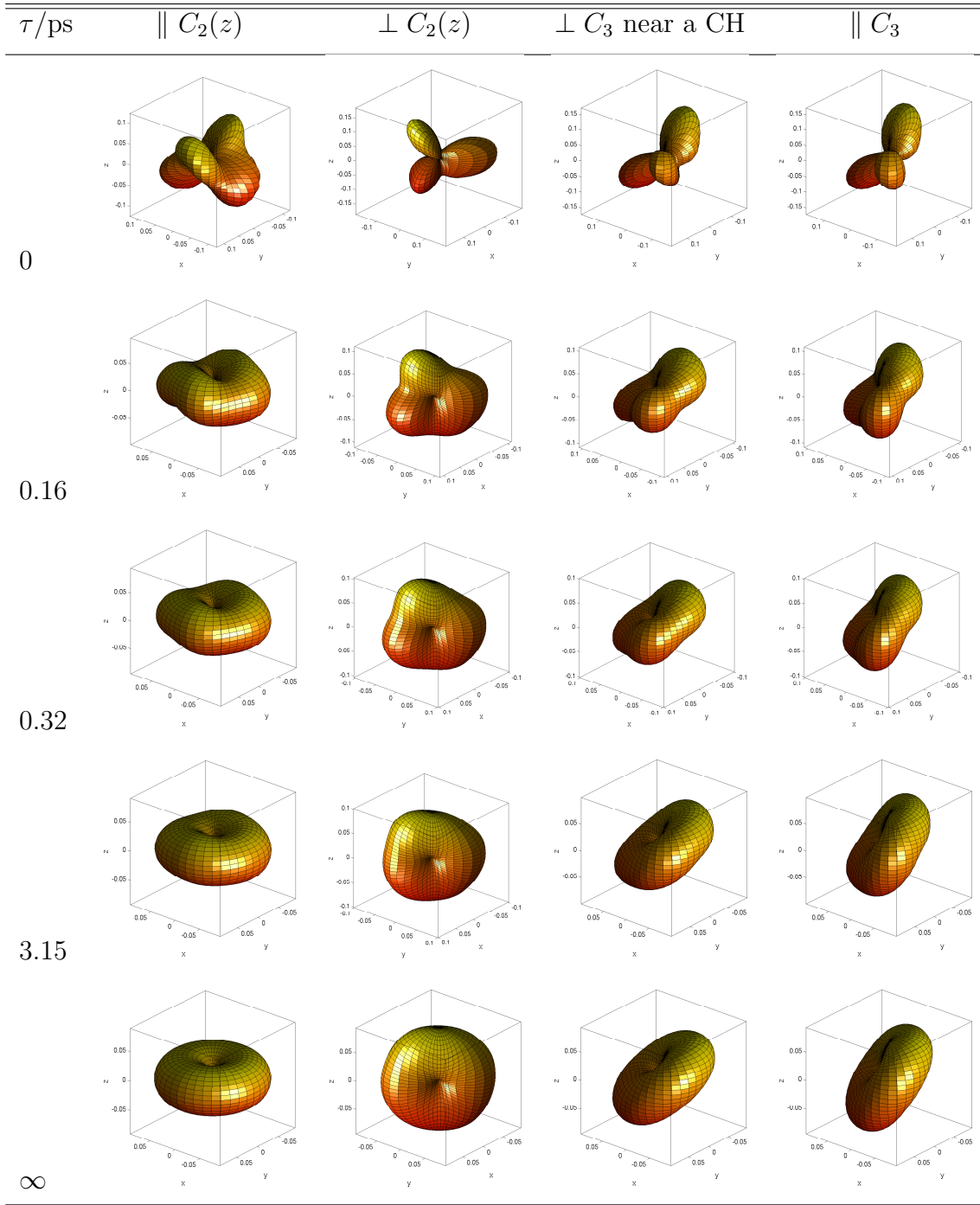
Figure V.8: MFPADs for the photoionization of the C $1s$ orbital of CH_4 molecule. Results computed at $E_k = 15.25$ eV for right circularly polarized light (RCP). In each column the propagation vectors change: first parallel to the C_2 axis in the z direction; second, perpendicular to the $C_2(z)$ axis and in the plane with two CH bonds; third, perpendicular to a C_3 axis but close to a CH bond, and fourth parallel to a C_3 axis (CH bond). Lifetimes of the pre-dissociative state are indicated for each row.

$t = 0$ ps	$t = 0.32$ ps
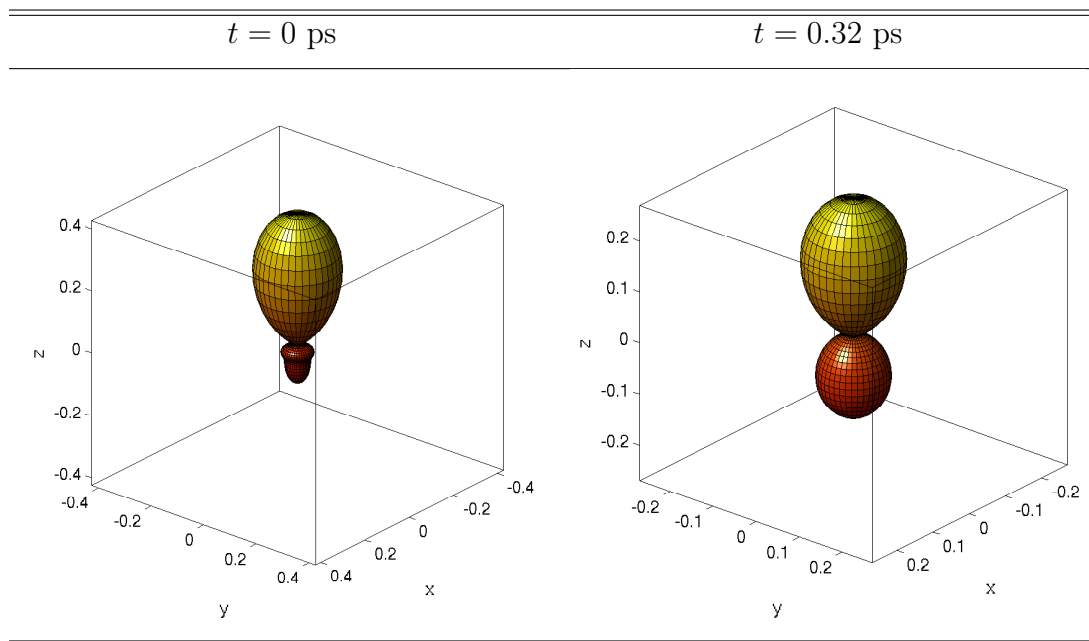
Figure V.9: RFPADs for the photoionization from the C $1s$ orbital of CH_4 molecule. Results computed at $E_k = 4.35$ eV for linearly polarized light (LP). The orientation average was performed around a CH bond, that is a C_3 axis, in this plot pointing in the z direction, and the field of the LP vector is also aligned with the C_3 axis in this figures. The figure at the left assumes a lifetimes of the state of 0 ps, and the figure at the right of 0.32 ps.

C 1s photoionization of methane were in good agreement with previous theoretical predictions [134] when considering the validity of the ARA, and exhibit good agreement with the experiments where the rotational motion is of considerable importance when doing a propagation in time of the rotational states, letting the molecule rotate a fraction of its computed rotational period. The computed RFPADs exhibit how the ARA breaks down for low kinetic energy in the core photoionization of methane, and how important is to consider, for this process, the rotational motion. This model extends the possibilities of studying dynamics of photoionization of states of polyatomic molecules where the ARA is often not a good approximation.

CHAPTER VI

CONCLUSIONS

Throughout this work, we have explored different aspects of molecular photoionization, and developed theoretical tools that proved useful in studies ranging from the study of diverse mechanisms of Franck-Condon breakdown in vibrationally resolved photoionization to the study of photoelectron dynamics of dissociative processes for polyatomic non-linear molecules. We showed how the derived F factor can be related to the deviation of the branching ratios from their Franck-Condon value, allowing the experimental data to be presented as measured F factors. In particular, when $F = 0$, the Franck-Condon approximation is valid. then the deviation from zero indicates the extent of the breakdown on the Franck-Condon approximation. An analysis of the non-Franck-Condon behavior of N_2 and CO showed the effects of the much studied shape resonances at low photon energy. At higher energy, we found that deviations from the Franck Condon value due to molecular Cooper minima and as being due to interference from the ionization from two centers as described by Cohen and Fano [53]. We found that in N_2 and CO, these two descriptions are related by the fact that the partial wave matrix elements obtained from decomposition of the plane-wave matrix elements used in the Cohen-Fano analysis also have energies at which they change sign which is the characteristic of a Cooper minimum.

In the lower symmetry system studied, it was observed that as a molecule becomes more complex with lower symmetry, the resonant states become more delocalized within the molecule, and their position and widths become less sensitive to changes in specific normal modes.

Finally, we presented a theoretical model for computing MFPADs and RFPADs for non-linear molecules that includes the effect of rotational motion between ionization and fragmentation. This model can be used to predict the photoionization dynamics of the photoelectron through the three dimensional MFPADs for systems where the axial-recoil approximation breakdown. The model was tested for the core photoionization of CH_4. The predicted MFPADs for the C $1s$ photoionization of methane were in good agreement with previous theoretical predictions [134] when considering the validity of the ARA, and exhibit good agreement with the experi-

ments where the rotational motion is of considerable importance when doing a propagation in time of the rotational states, letting the molecule rotate a fraction of its computed rotational period. The computed RFPADs exhibit how the ARA breaks down for low fragment kinetic energy in the core photoionization of methane, and how important is to consider, for this process, the rotational motion. This model extends the possibilities of studying dynamics of photoionization of states of polyatomic molecules where the ARA is often not a good approximation.

REFERENCES

[1] J. Clerk Maxwell. A dynamical theory of the electromagnetic field. *Philosophical Transactions of the Royal Society of London*, 155(January):459, 1865.

[2] David J. Griffiths. *Introduction to Electrodynamics.* Addison-Wesley, 4th edition, 2012.

[3] Joseph F. Keithley. *The Story of Electrical and Magnetic Measurements: From 500 B.C. to the 1940's.* Wiley-IEEE Press, 1st edition, 1999.

[4] W. H. Flygare. *Molecular Structure and Dynamics.* Prentice Hall, 1978.

[5] John R. Taylor. *Scattering Theory: The Quantum Theory of Nonrelativistic Collisions.* Dover Publications, Mineola, N.Y., 2006.

[6] Sadhan K. Adhikari. *Variational Principles and the Numerical Solution of Scattering Problems.* Wiley-VCH, 1998.

[7] Jeffrey I. Steinfeld. *Molecules and Radiation: An Introduction to Modern Molecular Spectroscopy.* The MIT Press, 2nd edition, 1985.

[8] Roger G. Newton. *Scattering Theory of Waves and Particles.* Dover Publications, 2nd edition, 2013.

[9] M. S. Child. *Molecular Collision Theory.* Dover Publications, 2010.

[10] Salvador Miret-Artés and Eli Pollak. Classical theory of atomsurface scattering: The rainbow effect. *Surface Science Reports*, 67(7):161, 2012.

[11] Robert R. Lucchese, K. Takatsuka, and V. McKoy. Applications of the Schwinger variational principle to electron-molecule collisions and molecular photoionization. *Physics Reports*, 131(3):147, 1986.

[12] Robert R. Lucchese and Vincent McKoy. Application of the Schwinger variational principle to electron-ion scattering in the static-exchange approximation. *Physical Review A*, 21(1):112, 1980.

[13] Robert R. Lucchese and Vincent McKoy. Application of the Schwinger variational principle to electron-molecular ion scattering. *Physica Scripta*, 21:366, 1980.

[14] Robert R. Lucchese and Vincent McKoy. Application of the Schwinger variational principle to electron scattering. *Journal of Physics B: Atomic, Molecular and Optical Physics*, 12(14):L421, 1979.

[15] Kazuo Takatsuka, Robert R. Lucchese, and Vincent McKoy. Relationship between the Schwinger and Kohn-type variational principles in scattering theory. *Physical Review A*, 24(4):1812, 1981.

[16] Robert R. Lucchese. *Molecular Photoionization*. John Wiley & Sons, Ltd, Chichester, England, March 2005.

[17] L. Spitzer. *Physical Processes in the Interstellar Medium*. Wiley Interscience, New York, 1978.

[18] R. P. Wayne. *Chemistry of Atmospheres*. Oxford, Clarendon, Oxford, 2nd editio edition, 1991.

[19] Norio Taniguchi, Masayuki Ikeda, Iwao Miyamoto, and Toshiuki Miyazaki. *Energy-Beam Processing of Materials: Advanced Manufacturing Using Various Energy Sources*. Oxford, 1989.

[20] M. Born and R. Oppenheimer. Zur Quantentheorie der Molekeln. *Annalen der Physik*, 84:457, 1927.

[21] Philip R. Bunker and Per Jensen. *Molecular Symmetry and Spectroscopy*. NRC Publications, 1998.

[22] David M. Chase. Adiabatic approximation for scattering processes. *Physical Review*, 104(3):838, 1956.

[23] M. N. Piancastelli. The neverending story of shape resonances. *Journal of Electron Spectroscopy and Related Phenomena*, 100(1-3):167, October 1999.

[24] J. L. Dehmer, Dan Dill, and Scott Wallace. Shape-resonance-enhanced nuclear-motion effects in molecular photoionization. *Physical Review Letters*, 43(14):1005, 1979.

[25] Sandeep Kakar, Heung Cheun Choi, and Erwin D. Poliakoff. Franck-Condon breakdown as a probe of continuum coupling in molecular photoionization. *Chemical Physics Letters*, 190(5):489, 1992.

[26] Jaume Rius i Riu, A. Karawajczyk, M. Stankiewicz, K. Yoshiki Franzén, P. Winiarczyk, and L. Veseth. Non Franck-Condon effects in the photoionization of molecular nitrogen to the N_2^+ A $^2\Pi_u$ state in the 19-34 eV photon energy region. *Chemical Physics Letters*, 338(April):285, 2001.

[27] J. Fernández, O. Fojóón, and F. Martín. Double-slit, confinement, and non-Franck-Condon effects in photoionization of H_2 at high photon energy. *Physical Review A*, 79(2):023420, February 2009.

[28] R. M. Rao, E. D. Poliakoff, K. Wang, and V. McKoy. Global Franck-Condon breakdown resulting from Cooper minima. *Physical Review Letters*, 76(15):2666, April 1996.

[29] Anirban Hazra and Marcel Nooijen. Derivation and efficient implementation of a recursion formula to calculate harmonic Franck-Condon factors for polyatomic molecules. *International Journal of Quantum Chemistry*, 95(4-5):643, September 2003.

[30] A. Frank, R. Lemus, and F. Pérez-Bernal. Algebraic derivation of Franck Condon overlap integrals for diatomic molecules. *Journal of Mathematical Chemistry*, 25(4):383, 1999.

[31] J. C. López V., A. L. Rivera, Yu. F. Smirnov, and A. Frank. Simple evaluation of Franck-Condon factors and non-Condon effects in the Morse potential. *International Journal of Quantum Chemistry*, 88(2):280, April 2002.

[32] John H. D. Eland. *Photoelectron Spectroscopy*. Butterworths, London, 2nd edition, 1984.

[33] B. Boudaïffa, Pierre Cloutier, Darel Hunting, Michael A. Huels, and Léon Sanche. Resonant formation of DNA strand breaks by low-energy (3 to 20 eV) electrons. *Science*, 287(5458):1658, March 2000.

[34] Jack Simons. How do low-energy (0.1-2eV) electrons cause DNA-strand breaks? *Accounts of Chemical Research*, 39(10):772, 2006.

[35] M. Lebech, J. C. Houver, A. Lafosse, D. Dowek, C. Alcaraz, L. Nahon, and Robert R. Lucchese. Complete description of linear molecule photoionization achieved by vector correlations using the light of a single circular polarization. *Journal of Chemical Physics*, 118(21):9653, 2003.

[36] George C. Schatz and Mark A. Ratner. *Quantum Mechanics in Chemistry*. Dover Publications, Mineola N.Y., 2002.

[37] G. Herzberg. *Molecular Spectra and Molecular Structure. III. Electronic Spectra and Electronic Structure of Polyatomic Molecules*. Van Nostrand Reinhold Company, New York, 1966.

[38] D. Turner. *Molecular Photoelectron Spectroscopy: A Handbook of He 584 Å Spectra,*. Wiley Interscience, London, England, 1970.

[39] O. Castaños, R. López-Peña, and R. Lemus. A new approach to obtain the non-Condon factors in closed form for two one-dimensional harmonic oscillators. *Journal of Molecular Spectroscopy*, 241(1):51, January 2007.

[40] Ping Lin and Robert R. Lucchese. Theoretical studies of cross sections and photoelectron angular distributions in the valence photoionization of molecular oxygen. *Journal of Chemical Physics*, 116(20):8863, 2002.

[41] Robert R. Lucchese, Georges Raseev, and Vincent McKoy. Studies of differential and total photoionization cross sections of molecular nitrogen. *Physical Review A*, 25(5):2572, 1982.

[42] J. A. López-Domínguez, David Hardy, Aloke Das, E. D. Poliakoff, Alex Aguilar, and Robert R. Lucchese. Mechanisms of FranckCondon breakdown over a broad energy range in the valence photoionization of N_2 and CO. *Journal of Electron Spectroscopy and Related Phenomena*, 185(8-9):211, September 2012.

[43] John W. Cooper. Photoionization from outer atomic subshells. A model study. *Physical Review*, 128(2):681, 1962.

[44] Thomas Young. The Bakerian lecture: Experiments and calculations relative to physical optics. *Philosophical Transactions of the Royal Society of London*, 94(January):1, January 1804.

[45] J. Fernández, O. Fojón, A. Palacios, and F. Martín. Interferences from fast electron emission in molecular photoionization. *Physical Review Letters*, 98(4):043005, January 2007.

[46] J. A. Stephens and V. McKoy. Non-Franck-Condon effects induced by orbital evolution and Cooper minima in excited-state photoionization of OH. *Physical Review Letters*, 62(8):889, 1989.

[47] R. Della Picca, P. D. Fainstein, and A. Dubois. Cooper minima and Young-type interferences in the photoionization of H_2^+. *Physical Review A*, 84(3):033405, September 2011.

[48] D. M. P. Holland, D. Edvardsson, L. Karlsson, R. Maripuu, K. Siegbahn, A. W. Potts, and Wolfgang von Niessen. A systematic investigation of the influence of Cooper minima on the photoionisation dynamics of the monohalobenzenes. *Chemical Physics*, 253:133, 2000.

[49] T. A. Carlson, M. O. Krause, W. A. Svensson, P. Gerard, F. A. Grimm, T. A. Whitley, and B. P. Pullen. Photoelectron dynamics of the Cooper minimum in free molecules. *Zeitschrift für Physik D Atoms, Molecules and Clusters*, 2(4):309, December 1986.

[50] Steven T. Manson. Systematics of zeros in dipole matrix elements for photoionizaing transitions: Nonrelativistic calculations. *Physical Review A*, 31(6):3698, 1985.

[51] G. J. Rathbone, R. M. Rao, E. D. Poliakoff, Kwanghsi Wang, and V. McKoy. Vibrational branching ratios in photoionization of CO and N_2. *Journal of Chemical Physics*, 120(2):778, January 2004.

[52] S. E. Canton, E. Plesiat, J. D. Bozek, B. S. Rude, P. Decleva, and F. Martin. Direct observation of Young's double-slit interferences in vibrationally resolved photoionization of diatomic molecules. *Proceedings of the National Academy of Sciences*, 108(18):7302, April 2011.

[53] Howard D. Cohen and U. Fano. Interference in the photo-ionization of molecules. *Physical Review*, 150(1):30, 1966.

[54] X-J. Liu, N. A. Cherepkov, S. K. Semenov, V. Kimberg, F. Gel'mukhanov, G. Prümper, T. Lischke, T. Tanaka, M. Hoshino, H. Tanaka, and K. Ueda. Young's double-slit experiment using core-level photoemission from N_2 : revisiting CohenFano's two-centre interference phenomenon. *Journal of Physics B: Atomic, Molecular and Optical Physics*, 39(23):4801, December 2006.

[55] R. M. Rao, E. D. Poliakoff, Kwanghsi Wang, and V. McKoy. Molecular photoionization as a probe of vibrationalrotationalelectronic correlations. *Journal of Chemical Physics*, 104(23):9654, 1996.

[56] S. K. Semenov, N. A. Cherepkov, M. Matsumoto, T. Hatamoto, X-J. Liu, G. Prümper, T. Tanaka, M. Hoashino, H. Tanaka, F. Gel'mukhanov, and K. Ueda. Interference modulation in the vibrationally resolved photoionization of the $1\sigma_g$ and $1\sigma_u$ core levels of the N_2 molecule. *Journal of Physics B: Atomic, Molecular and Optical Physics*, 39(12):L261, June 2006.

[57] R. E. Stratmann, G. Bandarage, and Robert R. Lucchese. Electron-correlation effects in the photoionization of N_2. *Physical Review A*, 51(5):3756, 1995.

[58] Bryan Basden and Robert R. Lucchese. Vibrational resolved cross sections and asymmetry parameters for the photoionization of N_2 with coupling between the $(3\ \sigma_g)^{-1}$ and the $(2\ \sigma_u)^{-1}$ channels. *Physical Review A*, 37(1):89, 1988.

[59] O. A. Fojón, J. Fernández, A. Palacios, R. D. Rivarola, and F. Martín. Interference effects in H_2 photoionization at high energies. *Journal of Physics B: Atomic, Molecular and Optical Physics*, 37(15):3035, August 2004.

[60] M. Galassi, R. Rivarola, P. Fainstein, and N. Stolterfoht. Young-type interference patterns in electron emission spectra produced by impact of swift ions on H_2 molecules. *Physical Review A*, 66(5):052705, November 2002.

[61] R. Della Picca, P. D. Fainstein, M. L. Martiarena, and A. Dubois. Zeros in the photoionization partial cross sections of H_2^+. *Physical Review A*, 77(2):022702, February 2008.

[62] R. Della Picca, P. D. Fainstein, M. L. Martiarena, N. Sisourat, and A. Dubois. Cooper minima and Young-type interferences in photoionization of one-electron molecular ions. *Physical Review A*, 79(3):032702, March 2009.

[63] Daniel Rolles, Markus Braune, Slobodan Cvejanović, Oliver Geßner, Rainer Hentges, Sanja Korica, Burkhard Langer, Toralf Lischke, Georg Prümper, Axel Reinköster, Jens Viefhaus, Björn Zimmermann, Vincent McKoy, and Uwe Becker. Isotope-induced partial localization of core electrons in the homonuclear molecule N_2. *Nature*, 437(7059):711, October 2005.

[64] H J Werner, P J Knowles, G Knizia, F R Manby, M Schütz, and Et Al. MOLPRO, 2006.

[65] Alexandra P. P. Natalense and Robert R. Lucchese. Cross section and asymmetry parameter calculation for sulfur $1s$ photoionization of SF_6. *Journal of Chemical Physics*, 111(12):5344, 1999.

[66] F. A. Gianturco, Robert R. Lucchese, and N. Sanna. Calculation of low-energy elastic cross sections for electron-CF_4 scattering. *Journal of Chemical Physics*, 100(9):6464, 1994.

[67] K. Huber and G. Herzberg. *Molecular Spectra and Molecular Structure. IV. Constants of Diatomic Molecules.* Van Nostrand Reinhold Company, New York, 1st edition, 1979.

[68] Scott Wallace, D Dill, and JL Dehmer. Spectral variation of molecular photoelectron angular distributions: valence shells of N2 and CO. *Journal of Physics B: Atomic, Molecular and Optical Physics*, 12:L417, 1979.

[69] Roger Stockbauer, B. E. Cole, D. L. Ederer, John B. West, Albert C. Parr, and J. L. Dehmer. Effects of shape resonances on vibrational intensity distributions in molecular photoionization. *Physical Review Letters*, 43(11):757, 1979.

[70] Zhi-Ping Zhong and Jia-Ming Li. A study of the broad enhancement phenomena in the molecular continuum region: CO spectra in the valence energy region. *Journal of Physics B: Atomic, Molecular and Optical Physics*, 37(4):735, February 2004.

[71] J. A. Sheehy, T. J. Gil, C. L. Winstead, R. E. Farren, and P. W. Langhoff. Correlation of molecular valence- and K-shell photoionization resonances with bond lengths. *Journal of Chemical Physics*, 91(3):1796, 1989.

[72] Jesús A. López-Domínguez, Robert R. Lucchese, K. D. Fulfer, David Hardy, E. D. Poliakoff, and A. A. Aguilar. Vibrationally specific photoionization cross sections of acrolein leading to the $\tilde{X}\ ^2A'$ ionic state. *Journal of Chemical Physics*, 141:094301, 2014.

[73] F. Gianturco and Robert R. Lucchese. Cross sections and asymmetry parameters in gas-phase photoionization of C_{60}. *Physical Review A*, 64(3):032706, August 2001.

[74] E. D. Poliakoff and Robert R. Lucchese. Evolution of photoelectronvibrational coupling with molecular complexity. *Physica Scripta*, 74(5):C71, November 2006.

[75] A. U. Hazi. Behavior of the eigenphase sum near a resonance. *Physical Review A*, 19(2):920, 1979.

[76] Joesph Macek. Behavior of eigenphases near a resonance. *Physical Review A*, 2(3):1101, 1970.

[77] R. Blankenbecler, M. L. Goldberger, S. W. MacDowell, and S. B. Treiman. Singularities of scattering amplitudes on unphysical sheets and their interpretation. *Physical Review*, 123(2):692, 1961.

[78] G. Calucci, L. Fonda, and G. C. Ghirardi. Correspondence between unstable particles and poles in S-matrix theory. *Physical Review*, 166(5):1719, 1968.

[79] G. Calucci and G. C. Ghirardi. Correspondence between unstable particles and poles in S-matrix theory: the exponential decay law. *Physical Review*, 169(5):1339, 1968.

[80] H. Jürgen Korsch, Ruth Möhlenkamp, and H-D. Meyer. On the canonical product expansion of the S matrix. *Journal of Physics B: Atomic, Molecular and Optical Physics*, 17:2955, 1984.

[81] R Lefebvre. Back rotation of complex rotated resonance wave functions: a numerical study. *Physical Review A*, 46(9):6071, 1992.

[82] William P. Reinhardt. Complex coordinaes in the theory of atomic and molecular structure and dynamics. *Annual Reviews of Physical Chemistry*, 33:223, 1982.

[83] Robert R. Lucchese, Henry F. Schaefer III, and Clifford E. Dykstra. Excitation energies of the $n \rightarrow \pi^*$ $^3A''$ and $\pi \rightarrow \pi^*$ $^3A'$ states of acrolein. *Chemical Physics Letters*, 51(3):600, 1977.

[84] Clifford E. Dykstra. Molecular structure of acrolein electronic states. *Journal of the American Chemical Society*, 98(23):7182, 1976.

[85] Wolfgang von Niessen, Gerhard Bieri, and Leif Åsbrink. 30.4 nm He(II) photoelectron spectra of organic molecules. Part III. Oxo-compunds (C, H, O). *Journal of Electron Spectroscopy and Related Phenomena*, 21:175, 1982.

[86] A. Katrib and J. W. Rabalais. Electronic interaction between the vinyl group and its substituents. *Journal of Physical Chemistry*, 77(19):2358, 1973.

[87] A. D. Walsh. The absorption spectra of acrolein, crotonaldehyde and mesityl oxide in the vacuum ultra-violet. *Transactions of the Faraday Society*, 41:498, 1945.

[88] Henry L. McMurry. The long wave-length spectra of aldehydes and ketones part II. conjugated aldehydes and ketones. *Journal of Chemical Physics*, 9(3):241, 1941.

[89] Gaetano Granozzi, David Ajò, and Ignazio Fragalà. Comments on the validity of Koopmans' theorem in photoelectron spectra of α, β-unsaturated carbonyls. *Journal of Electron Spectroscopy and Related Phenomena*, 18:267, 1980.

[90] Li-Hong Xu, Xingjie Jiang, Hongyu Shi, R. M. Lees, A. R. W. McKellar, D. W. Tokaryk, and D. R. T. Appadoo. 10 μm High-resolution spectrum of *trans*-acrolein: Rotational analysis of the v_{11}, v_{16}, v_{14} and $v_{16}+v_{18}v_{18}$ bands. *Journal of Molecular Spectroscopy*, 268(1-2):136, July 2011.

[91] Yoshiaki Hamada, Yoshifumi Nishimura, and Masamichi Tsuboi. Infrared spectrum of trans-acrolein. *Chemical physics*, 100:365, 1985.

[92] G. A. Osborne and D. A. Ramsay. Near ultraviolet absorption spectra of *cis* and *trans* acrolein and acrolein-d_1. *Canadian Journal of Physics*, 51:1170, 1973.

[93] O. S. Bokareva, V. A. Bataev, and I. A. Godunov. A quantum-chemical study of the structure and conformational dynamics of the acrolein molecule in the

ground electronic state. *Russian Journal of Physical Chemistry A*, 83(1):81, January 2009.

[94] A. C. P. Alves, J. Christoffersen, and J. M. Hollas. Near ultra-violet spectra of the *s*-trans and a second rotamer of acrolein vapour. *Molecular Physics*, 20(4):625, January 1971.

[95] Thom H. Dunning. Gaussian basis sets for use in correlated molecular calculations. I. The atoms boron through neon and hydrogen. *Journal of Chemical Physics*, 90(2):1007, 1989.

[96] Rick A. Kendall, Thom H. Dunning, and Robert J. Harrison. Electron affinities of the first-row atoms revisited. Systematic basis sets and wave functions. *Journal of Chemical Physics*, 96(9):6796, 1992.

[97] M. J. Frisch, G. W. Trucks, H. B. Schlegel, and *et al.* GAUSSIAN 09, 2009.

[98] R. E. Stratmann and Robert R. Lucchese. A graphical unitary group approach to study multiplet specific multichannel electron correlation effects in the photoionization of O_2. *Journal of Chemical Physics*, 102(21):8493, 1995.

[99] R. E. Stratmann, Robert W. Zurales, and Robert R. Lucchese. Multiplet-specific multichannel electron-correlation effects in the photoionization of NO. *Journal of Chemical Physics*, 104(22):8989, 1996.

[100] H. Van Dam and A. Oskam. He(I) and He(II) photoelectron spectra of some substituted ethylenes. *Journal of Electron Spectroscopy and Related Phenomena*, 13:273, 1978.

[101] S G Lias. NIST Chemistry WebBook. In P J Lindstrom and W G Mallard, editors, *NIST Chemistry WebBook*, chapter Ionization. National Institute of Standards and Technology, Gaithersburg, 2011.

[102] Alexandra P. P. Natalense, Luiz M. Brescansin, and Robert R. Lucchese. Cross section and asymmetry parameter calculations for the C $1s$ photoionization of CH_4, CF_4, and CCl_4. *Physical Review A*, 68(3):032701, September 2003.

[103] Robert R. Lucchese and F. A. Gianturco. One-electron resonances in electron scattering from polyatomic molecules. *International Reviews in Physical Chemistry*, 15(2):429, 1996.

[104] Richard N. Zare. Photoejection dynamics. *Molecular Photochemistry*, 4(1):1, 1972.

[105] Robert R. Lucchese, R. Carey, C. Elkharrat, J. C. Houver, and D. Dowek. Molecular frame and recoil frame angular distributions in dissociative photoionization of small molecules. *Journal of Physics: Conference Series*, 141:012009, 2008.

[106] Katharine L. Reid. Photoelectron angular distributions. *Annual Review of Physical Chemistry*, 54(19):397, 2003.

[107] Robert R. Lucchese. A simple model for molecular frame photoelectron angular distributions. *Journal of Electron Spectroscopy and Related Phenomena*, 141(May):201, 2004.

[108] A. Lafosse, J. C. Brenot, P. M. Guyon, J. C. Houver, A. V. Golovin, M. Lebech, D. Dowek, P. Lin, and Robert R. Lucchese. Vector correlations in dissociative photoionization of O_2 in the 20-28 eV range. II. Polar and azimuthal dependence of the molecular frame photoelectron angular distribution. *Journal of Chemical Physics*, 117(18):8368, 2002.

[109] Robert R. Lucchese, A. Lafosse, J. Brenot, P. Guyon, J. Houver, M. Lebech, G. Raseev, and D. Dowek. Polar and azimuthal dependence of the molecular frame photoelectron angular distributions of spatially oriented linear molecules. *Physical Review A*, 65:020702, 2002.

[110] Dan Dill. Fixed-molecule angular distributions. *Journal of Chemical Physics*, 65(3):1130, 1976.

[111] Richard N. Zare. Dissociation of H_2^+ by electron impact: calculated angular distribution. *Journal of Chemical Physics*, 47(1):204, 1967.

[112] M. Lebech, J. C. Houver, D. Dowek, and Robert R. Lucchese. Dissociative photoionization of N_2O in the region of the N_2O^+ ($B\ ^2\Pi$) state, studied by ion-electron velocity vector correlation. *Journal of Chemical Physics*, 120(17):8226, 2004.

[113] A. Lafosse, M. Lebech, J. C. Brenot, P. M. Guyon, O. Jagutzki, L. Spielberger, M. Vervloet, J. C. Houver, and D. Dowek. Vector correlations in dissociative

photoionization of diatomic molecules in the VUV range: strong anisotropies in electron emission from spatially oriented NO molecules. *Physical Review Letters*, 84(26):5987, 2000.

[114] John H. D. Eland, Masahiko Takahashi, and Yasumasa Hikosaka. Photoelectron-fragment ion correlations and fixed-molecule photoelectron angular distributions from velocity imaging coincidence experiments. *Faraday Discussions*, 115:119, 2000.

[115] A. Lafosse, J. C. Brenot, A. V. Golovin, P. M. Guyon, K. Hoejrup, J. C. Houver, M. Lebech, and D. Dowek. Vector correlations in dissociative photoionization of O_2 in the 20-28 eV range. I. Electron-ion kinetic energy correlations. *Journal of Chemical Physics*, 114(15):6605, 2001.

[116] A. V. Golovin, N. A. Cherepkov, and V. V. Kuznetsov. Photoionization of oriented molecules in a gas phase. *Zeitschrift für Physik D Atoms, Molecules and Clusters*, 24(4):371, 1992.

[117] T. Jahnke, Th. Weber, A. L. Landers, A. Knapp, S. Schössler, J. Nickles, S. Kammer, O. Jagutzki, L. Schmidt, A. Czasch, T. Osipov, E. Arenholz, A. T. Young, R. Díez Muiño, D. Rolles, F. J. García de Abajo, C. S. Fadley, M. A. Van Hove, S. K. Semenov, N. A. Cherepkov, J. Rösch, M. H. Prior, H. Schmidt-Böcking, C. L. Cocke, and R. Dörner. Circular dichroism in K-shell ionization from fixed-in-space CO and N_2 molecules. *Physical Review Letters*, 88(7):073002, 2002.

[118] H. Fukuzawa, X-J. Liu, R. Montuoro, Robert R. Lucchese, Y. Morishita, N. Saito, M. Kato, I. H. Suzuki, Y. Tamenori, T. Teranishi, T. Lischke, G. Prümper, and K. Ueda. Nitrogen K-shell photoelectron angular distribution from NO molecules in the molecular frame. *Journal of Physics B: Atomic, Molecular and Optical Physics*, 41:045102, 2008.

[119] Ivan Powis. Photoelectron circular dichroism of the randomly oriented chiral molecules glyceraldehyde and lactic acid. *Journal of Chemical Physics*, 112(1):301, 2000.

[120] M. Stener, G. Fronzoni, D. Di Tommaso, and P. Decleva. Density functional study on the circular dichroism of photoelectron angular distribution from chiral derivatives of oxirane. *Journal of Chemical Physics*, 120(7):3284, 2004.

[121] S. Stranges, S. Turchini, M. Alagia, G. Alberti, G. Contini, P. Decleva, G. Fronzoni, M. Stener, N. Zema, and T. Prosperi. Valence photoionization dynamics in circular dichroism of chiral free molecules: The methyl-oxirane. *Journal of Chemical Physics*, 122:244303, 2005.

[122] Paul Hockett, Adrian K. King, Ivan Powis, and Katharine L. Reid. Complete determination of the photoionization dynamics of a polyatomic molecule. I. Experimental photoelectron angular distributions from $\tilde{A}\,^1A_u$ acetylene. *Journal of Chemical Physics*, 127:154307, 2007.

[123] Yasumasa Hikosaka, John H. D. Eland, Tim M. Watson, and Ivan Powis. Molecule frame photoelectron angular distributions from oriented methyl chloride and methyl fluoride molecules. *Journal of Chemical Physics*, 115(10):4593, 2001.

[124] Peter Downie and Ivan Powis. Molecule-frame photoelectron angular distributions from oriented CF_3I molecules. *Physical Review Letters*, 82(14):2864, 1999.

[125] A. Edmonds. *Angular Momentum in Quantum Mechanics*. Princeton University Press, Princeton N.J., 1957.

[126] Richard Zare. *Angular Momentum: Understanding Spatial Aspects in Chemistry and Physics*. Wiley Interscience, New York, 1988.

[127] M. E. Rose. *Elementary Theory of Angular Momentum*. Dover Publications, New York, 1st edition, 1995.

[128] S. Wallace and Dan Dill. Detector integrated angular distribution: Chemisorption-site geometry, axial-recoil photofragmentation, and molecular-beam orientation. *Physical Review B*, 17(4):1692, 1978.

[129] Ira Levine. *Molecular Spectroscopy*. Wiley, New York, 1975.

[130] C. Jonah. Effect of rotation and thermal velocity on the anisotropy in photodissociation spectroscopy. *Journal of Chemical Physics*, 55(4):1915, 1971.

[131] J. K. G. Watson. The asymptotic asymmetric-top rotational partition function. *Molecular Physics*, 65(6):1377, 1988.

[132] J. C. Tully, R. S. Berry, and B. J. Dalton. Angular distribution of molecular photoelectrons. *Physical Review*, 176(1):95, 1968.

[133] V. Myrseth, J. D. Bozek, E. Kukk, L. J. Sæthre, and T. D. Thomas. Adiabatic and vertical carbon 1s ionization energies in representative small molecules. *Journal of Electron Spectroscopy and Related Phenomena*, 122:57, 2002.

[134] J. B. Williams, C. S. Trevisan, M. S. Schöffler, T. Jahnke, I. Bocharova, H. Kim, B. Ulrich, R. Wallauer, F. Sturm, T. N. Rescigno, A. Belkacem, R. Dörner, Th. Weber, C. W. McCurdy, and A. L. Landers. Probing the dynamics of dissociation of methane following core ionization using three-dimensional molecular-frame photoelectron angular distributions. *Journal of Physics B: Atomic, Molecular and Optical Physics*, 45:194003, 2012.

[135] Daniele Toffoli, Robert R. Lucchese, M. Lebech, J. C. Houver, and D. Dowek. Molecular frame and recoil frame photoelectron angular distributions from dissociative photoionization of NO_2. *Journal of Chemical Physics*, 126:054307, 2007.

[136] William H. McMaster. Polarization and the Stokes parameters. *American Journal of Physics*, 22:351, 1954.

[137] Albert Messiah. *Quantum Mechanics*. Dover Publications, Mineola N.Y., 1999.

[138] Jon Mathews and Robert L. Walker. *Mathematical Methods of Physics*. W.A. Benjamin, 2nd edition, 1970.

NOTES ON THE EFFECTS OF ROTATION, BETWEEN IONIZATION AND FRAGMENTATION, FOR NON-LINEAR MOLECULES

A.1   Ionization of non-linear molecules by elliptically polarized light

The present Appendix follows the unpublished notes of Professor Robert R. Lucchese on the same topic for ionization of linear molecules by elliptically polarized light. It is important to note that the final expressions and some intermediate equations have been written for convenience in the way they appear at the FORTRAN codes written for the purpose of doing this type of calculations.

First of all we will start to define the terms and parameters for the light. It follows that the Stokes parameters (s_0, s_1, s_2, s_3) [8, 136] can be parametrized in terms of the angles λ and δ as

$$
\begin{aligned}
s_0 &= a_1^2 + a_2^2 = 1 \\
s_1 &= a_1^2 - a_2^2 = \cos^2 \lambda - \sin^2 \lambda = \cos(2\lambda) \\
s_2 &= 2a_1 a_2 \cos \delta = 2 \cos \lambda \sin \lambda \cos \delta = \sin(2\lambda) \cos \delta \\
s_3 &= 2a_1 a_2 \sin \delta = \sin(2\lambda) \sin \delta
\end{aligned}
\tag{A.1}
$$

so that matrix elements can be written as

$$
\begin{aligned}
T_{\mathrm{fi}}^* &= \exp(i\delta_1) \langle \Psi_{\mathrm{i}} | B | \Psi_{\mathrm{f}} \rangle \\
B &= (\vec{r} \cdot \hat{x}_{FF}) \cos \lambda + (\vec{r} \cdot \hat{y}_{FF}) \sin \lambda \exp(i\delta)
\end{aligned}
\tag{A.2}
$$

where δ_1 is an overall phase in the elliptically polarized light.

Now, let's consider the analysis of the angular distributions with respect to the direction of propagation of light, for elliptically polarized light (EP). In this case we take $\hat{z}_{FF}$ to be the direction of light propagation and define the Euler angles $\hat{R} = (\gamma, \chi, \beta)$ to be the angles that rotate the molecular frame (MF) into the field frame (FF) (see [126], p. 77-81). The direction of the FF axes can then be given in

terms of the MF axes according to

$$
\begin{aligned}
\hat{x}_{FF} =\ & (\cos\gamma\cos\chi\cos\beta - \sin\gamma\sin\beta)\hat{x}_{MF} \\
& + (\sin\gamma\cos\chi\cos\beta + \cos\gamma\sin\beta)\hat{y}_{MF} - (\sin\gamma\cos\beta)\hat{z}_{MF} \\
\hat{y}_{FF} =\ & (-\cos\gamma\cos\chi\sin\beta - \sin\gamma\cos\beta)\hat{x}_{MF} \\
& + (-\sin\gamma\cos\chi\sin\beta + \cos\gamma\cos\beta)\hat{y}_{MF} - (\sin\gamma\sin\beta)\hat{z}_{MF} \\
\hat{z}_{FF} =\ & (\cos\gamma\sin\chi)\hat{x}_{MF} + (\sin\gamma\sin\chi)\hat{y}_{MF} + (\cos\chi)\hat{z}_{MF}
\end{aligned}
\tag{A.3}
$$

Then the field B defined in Equation (A.2) can be written as

$$
B = \frac{1}{\sqrt{2}}\left\{ B_+ \sum_{\mu=-1}^{1} e_\mu D^{(1)}_{\mu,-1}(\hat{R}) - B_- \sum_{\mu=-1}^{1} e_\mu D^{(1)}_{\mu,1}(\hat{R}) \right\}
\tag{A.4}
$$

where

$$
B_\pm = \cos\lambda \pm i\sin\lambda\exp(i\delta)
\tag{A.5}
$$

where the tensor operators e_μ are defined as

$$
e_\mu = rY_{1,\mu}(\theta_e,\phi_e)\sqrt{\frac{4\pi}{3}} =
\begin{cases}
z & \text{for } \mu = 0 \\
-\frac{x+iy}{\sqrt{2}} & \text{for } \mu = 1 \\
\frac{x-iy}{\sqrt{2}} & \text{for } \mu = -1
\end{cases}
\tag{A.6}
$$

Then, expanding the continuum wave function as [41],

$$
\psi_{\vec{k}}^{(-)}(\vec{r}) = \sqrt{\frac{2}{\pi}} \sum_{l,m} i^l \psi_{lm}^{(-)}(\vec{r}) Y_{lm}^*(\Omega_k)
\tag{A.7}
$$

where $\Omega_k = (\theta_k, \phi_k)$. Then the needed matrix elements become (with ζ' and ζ'' indicating the components of a degenerate set of orbitals),

$$
\begin{aligned}
T_{\lambda,\delta}^{(\zeta',\zeta'')}(\Omega_k,\hat{R}) &= \left\langle \Psi_{\zeta'}^{(i)} \middle| B \middle| \Phi_{\zeta''}^{(f)}\psi_{\vec{k}}^{(-)} \right\rangle \\
&= \sum_\mu \frac{1}{\sqrt{2}}\{B_+ D^{(1)}_{\mu,-1}(\hat{R}) - B_- D^{(1)}_{\mu,1}(\hat{R})\} \sum_{l,m} I_{lm\mu}^{(\zeta',\zeta'')} Y_{lm}^*(\Omega_k)
\end{aligned}
\tag{A.8}
$$

where

$$
I_{lm\mu}^{(\zeta',\zeta'')} = \sqrt{\frac{2}{\pi}} i^l \left\langle \Psi_{\zeta'}^{(i)} \middle| e_\mu \middle| \Phi_{\zeta''}^{(f)}\psi_{lm}^{(-)}(\vec{r}) \right\rangle
\tag{A.9}
$$

Now we need to rotate the expression given in Equation (A.8) into the FF where the direction of emission of the photoelectron is defined by the coordinates $\Omega_K = (\theta_K, \phi_K)$, using the inverse of the transformation defined by the angles $\hat{R} = (\gamma, \chi, \beta)$, *i.e.*, we need to apply the Euler angles [137], $\hat{R}^{-1} = (-\beta, -\chi, -\gamma)$ so that we have

$$Y_{l,m}(\Omega_k) = \sum_n Y_{l,n}(\Omega_K) D^l_{n,m}(\hat{R}^{-1}) \tag{A.10}$$

Then Equation (A.8) becomes

$$T^{(\zeta',\zeta'')}_{\lambda,\delta}(\Omega_K, \hat{R}) = \sum_\mu \frac{1}{\sqrt{2}} \{ B_+ D^{(1)}_{\mu,-1}(\hat{R}) - B_- D^{(1)}_{\mu,1}(\hat{R}) \}$$
$$\times \sum_{l,m,n} I^{(\zeta',\zeta'')}_{lm\mu} \left[Y_{l,n}(\Omega_K) D^l_{n,m}(\hat{R}^{-1}) \right]^* \tag{A.11}$$

Then using (see [138], p.464),

$$D^l_{m',m}(R^{-1}) = \left[D^l_{m,m'}(R) \right]^* \tag{A.12}$$

we have

$$T^{(\zeta',\zeta'')}_{\lambda,\delta}(\Omega_K, \hat{R}) = \sum_{l,m,n,\mu} \frac{1}{\sqrt{2}} \{ B_+ D^{(1)}_{\mu,-1}(\hat{R}) - B_- D^{(1)}_{\mu,1}(\hat{R}) \} I^{(\zeta',\zeta'')}_{lm\mu} Y^*_{l,n}(\Omega_K) D^l_{m,n}(\hat{R}) \tag{A.13}$$

A.2   Asymmetric top wave functions and energy levels

The rotational Hamiltonian $\hat{H}_{\text{rot}}$ for an asymmetric top molecule can be written in the principal axis system as ([21], p.240 Equation 11-8),

$$\hat{H}_{\text{rot}} = \hbar^{-2}(A\hat{J}^2_a + B\hat{J}^2_b + C\hat{J}^2_c) \tag{A.14}$$

where the rotational constants A, B and C are defined by

$$D = \frac{\hbar^2}{2hcI^e_{dd}}, \quad D = A, B, C \tag{A.15}$$

and $I^e_{\alpha\beta}$ is the $\alpha\beta$ element of the moment of inertia matrix for the molecule in its equilibrium configuration. Under the convention that the z axis is aligned to the

axis for the smaller moment of inertia ($I_{aa}^e \leq I_{bb}^e \leq I_{cc}^e$), the rotational Hamiltonian becomes ([21], p. 247, Equation 11-54),

$$\hat{H}_{\text{rot}} = \hbar^{-2} \left\{ \frac{(B+C)}{2} \hat{\mathbf{J}}^2 + \frac{A - (B+C)}{2} \hat{J}_z^2 + \frac{B-C}{4} [(\hat{J}_m^+)^2 + (\hat{J}_m^-)^2] \right\} \quad \text{(A.16)}$$

To solve for the energy levels we need the matrix elements of $\hat{\mathbf{J}}^2$, $\hat{J}_z^2$, $(\hat{J}_m^+)^2$, and $(\hat{J}_m^-)^2$ which are given for the $|J, k, m\rangle$ representation as ([21], p. 247),

$$\left\langle J, k, m \middle| \hat{\mathbf{J}}^2 \middle| J, k, m \right\rangle = J(J+1)\hbar^2 \quad \text{(A.17a)}$$

$$\left\langle J, k, m \middle| \hat{J}_z^2 \middle| J, k, m \right\rangle = k^2 \hbar^2 \quad \text{(A.17b)}$$

$$\frac{\left\langle J, k-2, m \middle| (\hat{J}_m^+)^2 \middle| J, k, m \right\rangle}{\hbar^2} = \{[J(J+1) - (k-1)(k-2)][J(J+1) - k(k-1)]\}^{1/2}$$

$$\text{(A.17c)}$$

and

$$\frac{\left\langle J, k+2, m \middle| (\hat{J}_m^-)^2 \middle| J, k, m \right\rangle}{\hbar^2} = \{[J(J+1) - (k+1)(k+2)][J(J+1) - k(k+1)]\}^{1/2}$$

$$\text{(A.17d)}$$

From the matrix elements in (A.17) it follows that the rotational Hamiltonian for an asymmetric top has nonvanishing matrix elements only between states having the same J, m and, same k or with values differing by two units.

In this sense, the expression for the total energy for an asymmetric top can not have a closed analytic form as the symmetric or spherical rotor one's (there are some expressions for low values of J or approximations for higher values up to around $J = 11$) and will be expressed as $E_{J,\kappa}$ from now on, and evaluated numerically from the expression for the asymmetric top Hamiltonian and the matrix elements given before in Equations (A.16) and (A.17) respectively.

The rotational wave function for linear molecules, symmetric tops and spherical

tops $\psi_{\text{rot}} = |J, k, m\rangle$ can be expressed as,

$$\psi_{\text{rot}}(\theta, \phi, \chi) = X_{Jkm} e^{im\phi} e^{ik\chi}$$
$$\times \left\{ \sum_{\sigma} (-1)^{\sigma} \frac{(\cos \frac{\theta}{2})^{2J+k-m-2\sigma} (-\sin \frac{\theta}{2})^{m-k+2\sigma}}{\sigma!(J-m-\sigma)!(m-k+\sigma)!(J+k-\sigma)!} \right\},$$
(A.18)

where,

$$X_{Jkm} = \left[\frac{(J+m)!(J-m)!(J+k)!(J-k)!(2J+1)}{8\pi^2} \right]^{1/2}$$

The index σ runs from 0 or $(k - m)$, whichever is larger, up to $(J - m)$ or $(J + k)$, whichever is smaller. The symmetric top rotational wave function can be rewritten in the form of Equation (A.28) by noticing that the factor $(2J + 1)/(8\pi^2)$ is present in Equation (A.18) within the explicit expression of the X_{Jkm} term, and by noting that the $D^J_{-M_J, -M_{i(f)}}(\hat{R}_M)$ in Equation (A.28) is just,

$$D^J_{-M_J, -M_{i(f)}}(\hat{R}_M) = D^J_{-M_J, -M_{i(f)}}(\theta, \phi, \chi) = e^{iM_J\phi} d^J_{-M_J, -M_{i(f)}}(\theta) e^{iM_{i(f)}\chi} \qquad (A.19)$$

where

$$d^J_{-M_J, -M_{i(f)}}(\theta) = [(J + M_J)!(J - M_J)!(J + M_{i(f)})!(J - M_{i(f)})!]$$
$$\times \sum_{\sigma} (-1)^{\sigma} \frac{(\cos \frac{\theta}{2})^{2J+M_{i(f)}-M_J-2\sigma} (-\sin \frac{\theta}{2})^{M_J-M_{i(f)}+2\sigma}}{\sigma!(J-M_J-\sigma)!(M_J-M_{i(f)}+\sigma)!(J+M_{i(f)}-\sigma)!}$$
(A.20)

And thus, we can write for non-linear or asymmetric tops, the rotational wavefunctions as a linear combination of symmetric top wave functions (now represented by $\phi_{J,M_J,H}$) as,

$$\psi_{J,M_J,\kappa} = \sum_{H} C^J_{H,\kappa} \phi_{J,M_J,H} \qquad (A.21)$$

which is the same equation as Equation (A.27) in the next section (but it has been adopted the letter H to name the angular momentum number (which incorporates the K_o and K_p used in other asymmetric top notations).

A.3   Rotational state specific matrix elements

The normalization of the rotation matrices is determined by considering (see reference [126], Equation 3.125, p. 105 followed by Equation 3.105, p. 99 of the same reference),

$$
\begin{aligned}
(D^J_{MM'})^* D^J_{MM'} &= (-1)^{M-M'} D^J_{-M,-M'} D^J_{M,M'} \\
&= \sum_{J'} (-1)^{M-M'} \langle J \quad -M, J\,M|\,J',0\rangle\, D^{J'}_{0,0} \langle J \quad -M', J\,M'|\,J',0\rangle
\end{aligned}
$$

(A.22)

So that ([126], Equation 3.110, p. 101),

$$
\int \left[D^J_{MM'}(\hat{R}) \right]^* D^J_{MM'}(\hat{R}) d\hat{R} = (-1)^{M-M'} \langle J \quad -M, J\,M|\,0,0\rangle
$$
$$
\times\, 8\pi^2 \langle J \quad -M', J\,M'|\,0,0\rangle
$$

(A.23)

then using ([137], Equation C.13c, p. 1056, followed by [126], Equation 3.111, p. 101),

$$
\langle J \quad -M, J\,M|\,0,0\rangle = (-1)^{J-0+M} \sqrt{\frac{1}{2J+1}} \langle J\,M, 0\,0|\,J,M\rangle
$$
$$
\langle J \quad -M, J\,M|\,0,0\rangle = \frac{(-1)^{J+M}}{\sqrt{2J+1}}
$$

(A.24)

So, finally the normalization is (using the explicit coordinates; see reference [126], Equation 3.113, p. 101),

$$
\int \left[D^{J_1}_{M_1 M'_1}(\gamma,\chi,\beta) \right]^* D^{J_2}_{M_2 M'_2}(\gamma,\chi,\beta) d\gamma \sin\chi\, d\chi\, d\beta = \frac{8\pi^2}{2J_1+1} \delta_{J_1,J_2} \delta_{M_1,M_2} \delta_{M'_1,M'_2}
$$

(A.25)

So that functions

$$
\sqrt{\frac{2J+1}{8\pi^2}} D^J_{MM'}(\hat{R})
$$

(A.26)

are normalized with respect to the integration over the usual three Euler angles. For non-linear molecules, we have rotational wave functions of the form ([126], Equation 6.54, p. 267),

$$
\psi_{J,M_J,\kappa} = \sum_H C^J_{H,\kappa} \phi_{J,M_J,H}
$$

(A.27)

where $\phi_{J,M_J,H}$ is the wave function for a symmetric top, given by

$$\phi_{J,M_J,H} = \left(\frac{2J+1}{8\pi^2}\right)^{\frac{1}{2}} D^J_{-M_J,-H}(\hat{R}_M) \tag{A.28}$$

where $\hat{R}_M$ represents the Euler angles describing the orientation of the recoil frame in the laboratory frame, *i.e.*, in the field frame. The rotation $\hat{R}_M$ then is just the inverse of the rotation that takes the recoil frame into the field frame so that in terms of the angles used in Equation (A.3) we have $\hat{R}_M = \hat{R}^{-1}$. Then using the relationship given in Equation (A.12) we can write the rotational wave function given in Equation (A.27) as

$$\psi_{J,M_J,\kappa(\kappa')} = \sum_{H(H')} C^J_{H(H'),\kappa(\kappa')} \left(\frac{2J+1}{8\pi^2}\right)^{\frac{1}{2}} [D^J_{-H(H'),-M_J}(\hat{R})]^* \tag{A.29}$$

Then the rotation state specific matrix elements for the transitions $(\zeta, J, M_J, \kappa \leftarrow \zeta'', J'', M_{J''}, \kappa'')$, are defined as

$$T^{(\zeta,J,M_J,\kappa \leftarrow \zeta'',J'',M_{J''},\kappa'')}_{\lambda,\delta}(\Omega_K) = \int \left[\psi_{J'',M_{J''},\kappa''}(\hat{R})\right]^* \psi_{J,M_J,\kappa}(\hat{R}) T^{(\zeta'',\zeta)}_{\lambda,\delta}(\Omega_K,\hat{R}) d\hat{R} \tag{A.30}$$

and substituting Equations (A.29) and (A.13) into Equation (A.30) leads to

$$\begin{aligned}
T^{(\zeta,J,M_J,\kappa \leftarrow \zeta'',J'',M_{J''},\kappa'')}_{\lambda,\delta}(\Omega_K) = \int &\sum_{H'} C^{J'}_{H',\kappa'} \left(\frac{2J+1}{8\pi^2}\right)^{\frac{1}{2}} [D^J_{-H',-M_J}(\hat{R})]^* \\
&\times \sum_H C^J_{H,\kappa} \left(\frac{2J''+1}{8\pi^2}\right)^{\frac{1}{2}} D^{J''}_{-H,-M_{J''}}(\hat{R}) \\
&\times \sum_{l,m,n,\mu} \frac{1}{\sqrt{2}} \{B_+ D^{(1)}_{\mu,-1}(\hat{R}) - B_- D^{(1)}_{\mu,1}(\hat{R})\} \\
&\times I^{(\zeta'',\zeta)}_{lm\mu} Y^*_{l,n}(\Omega_K) D^l_{m,n}(\hat{R}) d\hat{R}
\end{aligned} \tag{A.31}$$

A.4 Thermal average

Under thermal equilibrium we assume a Boltzmann distribution of states, which allows us to write the density matrix before the interaction with the light according

to Jonah [130] as

$$\rho = \frac{1}{g_i Q(T)} \left\{ \sum_{\zeta'', J'', M_{J''}, \kappa''} \left| \psi_{J'', M_{J''}, \kappa''} \Psi_{\zeta''}^{(i)} \right\rangle g_{\kappa''} \exp\left(-\frac{E_{J'', \kappa''}}{k_B T} \right) \left\langle \psi_{J'', M_{J''}, \kappa''} \Psi_{\zeta''}^{(i)} \right| \right\}$$

(A.32)

where g_i accounts for the degenerate initial electronic states $\Psi_{\zeta''}^{(i)}$ and $Q(T)$ is the rotational partition function for the initial state for an symmetric-top molecule [131],

$$Q(T) = \sum_{J'', \kappa''} (2J'' + 1) g_{\kappa''} \exp\left(\frac{-E_{J'', \kappa''}}{k_B T} \right)$$

(A.33)

here, $g_{\kappa''}$ is the nuclear-spin statistical weight, and depends on the parities of the quantum numbers K_p and K_o, collectively labeled here as κ, (which are the quantum numbers on the prolate and oblate limits of the asymmetric rotor). After the interaction with the light, with a field operator B as defined in Equation (A.2) we have,

$$\rho' = \frac{4\pi^2 E}{c} B^* \rho B$$

(A.34)

where E is the photon energy and c is the speed of light. This propagates in time to give

$$\rho''(t) = \frac{4\pi^2 E}{c} \exp(-iH_{\rm rot} t/\hbar) B^* \rho B \exp(iH_{\rm rot} t/\hbar).$$

(A.35)

Expanding this in the final states gives,

$$\rho''(t) = \frac{4\pi^2 E}{c} \sum_{\substack{J, M_J, \kappa, \hat{K}, \zeta \\ J', M_{J'}, \kappa', \hat{K}', \zeta'}} \left| \psi_{J', M_{J'}, \kappa'} \Phi_{\zeta'}^{(f)} \psi_{\hat{K}'}^{(-)} \right\rangle$$

$$\times \left\langle \psi_{J', M_{J'}, \kappa'} \Phi_{\zeta'}^{(f)} \psi_{\hat{K}'}^{(-)} \right| \exp(-iH_{\rm rot} t/\hbar) B^* \rho B \exp(iH_{\rm rot} t/\hbar) \left| \psi_{J, M_J, \kappa} \Phi_{\zeta}^{(f)} \psi_{\hat{K}}^{(-)} \right\rangle$$

$$\times \left\langle \psi_{J, M_J, \kappa} \Phi_{\zeta}^{(f)} \psi_{\hat{K}}^{(-)} \right|$$

(A.36)

Since we are expanding in rotational eigenfunctions, we have (from evaluating the Hamiltonian, H_{rot}, over the corresponding functions):

$$
\rho''(t) = \frac{4\pi^2 E}{c} \sum_{\substack{J,M_J,\kappa,\hat{K},\zeta \\ J',M_{J'},\kappa',\hat{K}',\zeta'}} \left| \psi_{J',M_{J'},\kappa'} \Phi_{\zeta'}^{(\text{f})} \psi_{\hat{K}'}^{(-)} \right\rangle
$$
$$
\times \left\langle \psi_{J',M_{J'},\kappa'} \Phi_{\zeta'}^{(\text{f})} \psi_{\hat{K}'}^{(-)} \right| B^* \rho B \left| \psi_{J,M_J,\kappa} \Phi_{\zeta}^{(\text{f})} \psi_{\hat{K}}^{(-)} \right\rangle
$$
$$
\times \left\langle \psi_{J,M_J,\kappa} \Phi_{\zeta}^{(\text{f})} \psi_{\hat{K}}^{(-)} \right| \exp\left\{ -\frac{it}{\hbar}(E_{J',\kappa'} - E_{J,\kappa}) \right\}
$$

(A.37)

where $E_{J',\kappa'}$ and $E_{J,\kappa}$ are the energies of the final states with angular momentum numbers and eigenstate indices J',κ' and J,κ respectively.

Inserting Equation (A.32) for the initial density matrix it gives

$$
\rho''(t) = \frac{4\pi^2 E}{c g_{\text{i}}} \sum_{\substack{J,M_J,\kappa,\hat{K},\zeta \\ J',M_{J'},\kappa',\hat{K}',\zeta' \\ J'',M_{J''},\kappa'',\zeta''}} \left| \psi_{J',M_{J'},\kappa'} \Phi_{\zeta'}^{(\text{f})} \psi_{\hat{K}'}^{(-)} \right\rangle \left\langle \psi_{J',M_{J'},\kappa'} \Phi_{\zeta'}^{(\text{f})} \psi_{\hat{K}'}^{(-)} \right| B^* \left| \psi_{J'',M_{J''},\kappa''} \Psi_{\hat{\zeta}''}^{(\text{i})} \right\rangle
$$
$$
\times \frac{g_{\kappa''}}{Q(T)} \exp\left(-\frac{E_{J'',\kappa''}}{k_B T} \right) \left\langle \psi_{J'',M_{J''},\kappa''} \Psi_{\zeta''}^{(\text{i})} \right| B \left| \psi_{J,M_J,\kappa} \Phi_{\zeta}^{(\text{f})} \psi_{\hat{K}}^{(-)} \right\rangle
$$
$$
\times \left\langle \psi_{J,M_J,\kappa} \Phi_{\zeta}^{(\text{f})} \psi_{\hat{K}}^{(-)} \right| \exp\left\{ -\frac{it}{\hbar}(E_{J',\kappa'} - E_{J,\kappa}) \right\}
$$

(A.38)

Then, for the diagonal elements of the density matrix, for ionization in the coordinate representation at time t after excitation,

$$
\rho''(\Omega_K, \hat{R}, \Omega_K, \hat{R}, t) = \frac{1}{g_{\text{i}} Q(T)} \sum_{\substack{\zeta,\zeta'' \\ J,J',J'' \\ \kappa,\kappa',\kappa''}} g_{\kappa''} \exp\left(-\frac{E_{J'',\kappa''}}{k_B T} \right)
$$
$$
\times \exp\left\{ -\frac{it}{\hbar}(E_{J',\kappa'} - E_{J,\kappa}) \right\} \frac{W_{\lambda,\delta;(\zeta,\zeta'')}^{\binom{J,J',J''}{\kappa,\kappa',\kappa''}}(\Omega_K, \hat{R})}{8\pi^2}
$$

(A.39)

115

where the term that has been summed over the magnetic sub levels is given by

$$
\frac{1}{8\pi^2} W_{\lambda,\delta;(\zeta,\zeta'')}^{\left(\substack{J,J',J'' \\ \kappa,\kappa',\kappa''}\right)}(\Omega_K, \hat{R}) = \frac{4\pi^2 E}{cg_i} \sum_{\substack{M_J,\kappa,M_{J'},\kappa' \\ M_{J''},\kappa''}} \left[T_{\lambda,\delta}^{(\zeta,J',M_{J'},\kappa' \leftarrow \zeta'',J'',M_{J''},\kappa'')}(\Omega_K) \right]^*
$$
$$
\times T_{\lambda,\delta}^{(\zeta,J,M_J,\kappa \leftarrow \zeta'',J'',M_{J''},\kappa'')}(\Omega_K)
$$
$$
\times \left[\psi_{J,M_J,\kappa}(\hat{R}) \right]^* \psi_{J',M_{J'},\kappa'}(\hat{R})
$$

(A.40)

we can note that the density matrix element is also diagonal in the final electronic state, *i.e.*, $\zeta = \zeta'$. Now, the usual molecular frame angular distribution $I(\Omega_K, \hat{R})$ is defined as the differential cross section for the emission of the photoelectron in the direction Ω_K for a fixed orientation of the molecule in the field frame as defined by the Euler angles in $\hat{R}$. Then, the usual integrated target distribution [128] would be obtained by an orientation average of the target [132],

$$
\frac{d\sigma}{d\Omega_K} = \frac{1}{8\pi^2} \int I(\Omega_K, \hat{R}) d\hat{R}
$$

(A.41)

and the final total cross section would be given by

$$
\sigma = \int \frac{d\sigma}{d\Omega_K} d\Omega_K = \frac{1}{8\pi^2} \iint I(\Omega_K, \hat{R}) d\hat{R} d\Omega_K
$$

(A.42)

So, the total cross section at $t = 0$ from the density matrix given in Equation (A.39) would be

$$
\sigma = \iint \rho''(\Omega_K, \hat{R}, \Omega_K, \hat{R}, t = 0) d\Omega_K d\hat{R}
$$

(A.43)

Thus we can see that the RFPAD $I(\Omega_K, \hat{R}, t)$ for fragmentation after time t is related to the diagonal elements of the density

$$
I(\Omega_K, \hat{R}, t) = 8\pi^2 \rho''(\Omega_K, \hat{R}, \Omega_K, \hat{R}, t)
$$

(A.44)

so that

$$I(\Omega_K, \hat{R}, t) = \frac{1}{g_i Q(T)} \sum_{\substack{\zeta,\zeta'' \\ J,J',J'' \\ \kappa,\kappa',\kappa''}} g_{\kappa''} \exp\left(-\frac{E_{J'',\kappa''}}{k_B T}\right) \exp\left\{-\frac{it}{\hbar}(E_{J',\kappa'} - E_{J,\kappa})\right\} W_{\lambda,\delta;(\zeta,\zeta'')}^{\left(J,J',J'' \atop \kappa,\kappa',\kappa''\right)}$$

(A.45)

Assuming a Poisson distribution of decay times $(1/\tau)\exp(-t/\tau)$, the density matrix can be averaged over decay time using

$$\int_0^\infty \frac{1}{\tau}\exp\left(-\frac{t}{\tau}\right)\exp\left(\frac{-i\Delta E t}{\hbar}\right) dt = \frac{1}{\tau}\int_0^\infty \exp\left[-\left(\frac{1}{\tau} + \frac{i\Delta E}{\hbar}\right)t\right] dt$$

$$= \frac{1}{\tau}\left(\frac{1}{\tau} + \frac{i\Delta E}{\hbar}\right)^{-1}$$

(A.46)

$$\int_0^\infty \frac{1}{\tau}\exp\left(-\frac{t}{\tau}\right)\exp\left(\frac{-i\Delta E t}{\hbar}\right) dt = \left(1 + \frac{i\Delta E \tau}{\hbar}\right)^{-1}$$

so that Equation (A.45) becomes

$$I_\tau(\Omega_K, \hat{R}, t) = \frac{1}{g_i Q(T)} \sum_{\substack{\zeta,\zeta'' \\ J,J',J'' \\ \kappa,\kappa',\kappa''}} g_{\kappa''} \exp\left(-\frac{E_{g_s,J'',\kappa''}}{k_B T}\right) \frac{W_{\lambda,\delta;(\zeta,\zeta'')}^{\left(J,J',J'' \atop \kappa,\kappa',\kappa''\right)}}{1 + \frac{i\tau\Delta E^{(J',\kappa',J,\kappa)}}{\hbar}}$$

(A.47)

Expanding the T terms in Equation (A.40) by means of Equation (A.30) leads to

$$W_{\lambda,\delta;(\zeta,\zeta'')}^{\left(J,J',J'' \atop \kappa,\kappa',\kappa''\right)}(\Omega_K, \hat{R}'') = \frac{32\pi^4 E}{c} \sum_{M_J, M_{J'}, M_{J''}} \iint d\hat{R} d\hat{R}' \psi_{J'',M_{J''},\kappa''}(\hat{R}') \left[\psi_{J',M_{J'},\kappa'}(\hat{R}')\right]^*$$

$$\times \left[T_{\lambda,\delta}^{(\zeta'',\zeta)}(\Omega_K, \hat{R}')\right]^* \left[\psi_{J'',M_{J''},\kappa''}(\hat{R})\right]^* \psi_{J,M_J,\kappa}(\hat{R}) T_{\lambda,\delta}^{(\zeta'',\zeta)}(\Omega_K, \hat{R})$$

$$\times \sum_{H_1, H_2'} C_{H_1,\kappa}^{J*} \left(\frac{2J+1}{8\pi^2}\right)^{1/2} D_{-H_1,-M_J}^{J}(\hat{R}'')$$

$$\times C_{H_2',\kappa'}^{J'} \left(\frac{2J'+1}{8\pi^2}\right)^{1/2} \left[D_{-H_2',-M_{J'}}^{J'}(\hat{R}'')\right]^*$$

(A.48)

117

Expanding the additional rotational wave functions leads to

$$
W_{\lambda,\delta;(\zeta,\zeta'')}^{\binom{J,J',J''}{\kappa,\kappa',\kappa''}}(\Omega_K,\hat{R}'') = \frac{32\pi^4 E}{cg_\mathrm{i}} \iint d\hat{R}d\hat{R}' \sum_{M_J,M_{J'},M_{J''}} \left[T_{\lambda,\delta}^{(\zeta'',\zeta)}(\Omega_K,\hat{R}') \right]^* T_{\lambda,\delta}^{(\zeta'',\zeta)}(\Omega_K,\hat{R})
$$

$$
\times \sum_{H_3''} C_{H_3'',\kappa''}^{J''} \left(\frac{2J''+1}{8\pi^2} \right)^{1/2} \left[D_{-H_3'',-M_{J''}}^{J''}(\hat{R}') \right]^*
$$

$$
\times \sum_{H_4'} C_{H_4',\kappa'}^{J'*} \left(\frac{2J'+1}{8\pi^2} \right)^{1/2} D_{-H_4',-M_{J'}}^{J'}(\hat{R}')
$$

$$
\times \sum_{H_5''} C_{H_5'',\kappa''}^{J''*} \left(\frac{2J''+1}{8\pi^2} \right)^{1/2} D_{-H_5'',-M_{J''}}^{J''}(\hat{R})
$$

$$
\times \sum_{H_6} C_{H_6,\kappa}^{J} \left(\frac{2J+1}{8\pi^2} \right)^{1/2} \left[D_{-H_6,-M_J}^{J}(\hat{R}) \right]^*
$$

$$
\times \sum_{H_1} C_{H_1,\kappa}^{J*} \left(\frac{2J+1}{8\pi^2} \right)^{1/2} D_{-H_1,-M_J}^{J}(\hat{R}'')
$$

$$
\times \sum_{H_2'} C_{H_2',\kappa'}^{J'} \left(\frac{2J'+1}{8\pi^2} \right)^{1/2} \left[D_{-H_2',-M_{J'}}^{J'}(\hat{R}'') \right]^*
$$

(A.49)

Then combining terms and rearranging leads to

$$
W_{\lambda,\delta;(\zeta,\zeta'')}^{\binom{J,J',J''}{\kappa,\kappa',\kappa''}}(\Omega_K,\hat{R}'') = \frac{32\pi^4 E}{cg_\mathrm{i}} \iint d\hat{R}d\hat{R}' \sum_{\substack{M_J,M_{J'},M_{J''} \\ \kappa,\kappa',\kappa'' \\ H_1,H_2',H_3'',H_4',H_5'',H_6}} \left[T_{\lambda,\delta}^{(\zeta'',\zeta)}(\Omega_K,\hat{R}') \right]^*
$$

$$
\times T_{\lambda,\delta}^{(\zeta'',\zeta)}(\Omega_K,\hat{R}) \frac{(2J+1)(2J'+1)(2J''+1)}{(8\pi^2)^3}
$$

$$
\times C_{H_3'',\kappa''}^{J''} \cdot C_{H_5'',\kappa''}^{J''*} \times C_{H_2',\kappa'}^{J'} \cdot C_{H_4',\kappa'}^{J'*} \times C_{H_6,\kappa}^{J} \cdot C_{H_1,\kappa}^{J*}
$$

$$
\times \left[D_{-H_3'',-M_{J''}}^{J''}(\hat{R}') \right]^* D_{-H_5'',-M_{J''}}^{J''}(\hat{R})
$$

$$
\times \left[D_{-H_2',-M_{J'}}^{J'}(\hat{R}'') \right]^* D_{-H_4',-M_{J'}}^{J'}(\hat{R}')
$$

$$
\times \left[D_{-H_6,-M_J}^{J}(\hat{R}) \right]^* D_{-H_1,-M_J}^{J}(\hat{R}'')
$$

(A.50)

Now, since there are common terms in the previous equation, we can simplify

by remembering in a geometric picture that since the $D^J_{m_i,m_j}$ *objects* are matrices representing a rotation, then the product of two of them has to be a rotation itself. By applying to Equation (A.50) the following rule ([126] p.88; [125] p.63),

$$
\sum_{m_2} D^J_{m_3,m_2}(\hat{R}_2)\left[D^J_{m_1,m_2}(\hat{R}_1)\right]^* = \sum_{m_2} D^J_{m_3,m_2}(\hat{R}_2)D^J_{m_2,m_1}(\hat{R}_1^{-1})
$$
$$
= D^J_{m_3,m_1}(\hat{R}_1^{-1}\hat{R}_2)
$$

(A.51)

it follows that

$$
W^{\binom{J,J',J''}{\kappa,\kappa',\kappa''}}_{\lambda,\delta;(\zeta,\zeta'')}(\Omega_K,\hat{R}'') = \frac{32\pi^4 E}{cg_i}\iint d\hat{R}d\hat{R}' \sum_{H_1,H_2',H_3'',H_4',H_5'',H_6} \left[T^{(\zeta'',\zeta)}_{\lambda,\delta}(\Omega_K,\hat{R}')\right]^*
$$
$$
\times T^{(\zeta'',\zeta)}_{\lambda,\delta}(\Omega_K,\hat{R})\frac{(2J+1)(2J'+1)(2J''+1)}{(8\pi^2)^3}
$$
$$
\times C^{J''}_{H_3'',\kappa''}\cdot C^{J''*}_{H_5'',\kappa''}\times C^{J'}_{H_2',\kappa'}\cdot C^{J'*}_{H_4',\kappa'}\times C^{J}_{H_6,\kappa}\cdot C^{J*}_{H_1,\kappa}
$$
$$
\times D^{J''}_{-H_5'',-H_3''}(\hat{R}'^{-1}\hat{R})D^{J'}_{-H_4',-H_2'}(\hat{R}''^{-1}\hat{R}')D^{J}_{-H_1,-H_6}(\hat{R}^{-1}\hat{R}'')
$$

(A.52)

Now expanding the $T^{\zeta_i,\zeta_f}_{\lambda,\delta}$ terms we get

$$
W^{\binom{J,J',J''}{\kappa,\kappa',\kappa''}}_{\lambda,\delta;(\zeta,\zeta'')}(\Omega_K,\hat{R}'') = \frac{32\pi^4 E}{cg_i}\iint d\hat{R}d\hat{R}' \sum_{H_1,H_2',H_3'',H_4',H_5'',H_6} \frac{(2J+1)(2J'+1)(2J''+1)}{(8\pi^2)^3}
$$
$$
\times C^{J''}_{H_3'',\kappa''}\cdot C^{J''*}_{H_5'',\kappa''}\times C^{J'}_{H_2',\kappa'}\cdot C^{J'*}_{H_4',\kappa'}\times C^{J}_{H_6,\kappa}\cdot C^{J*}_{H_1,\kappa}
$$
$$
\times D^{J''}_{-H_5'',-H_3''}(\hat{R}'^{-1}\hat{R})D^{J'}_{-H_4',-H_2'}(\hat{R}''^{-1}\hat{R}')D^{J}_{-H_1,-H_6}(\hat{R}^{-1}\hat{R}'')
$$
$$
\times \sum_{\substack{l,m,n,\mu\\l',m',n',\mu'}} \left[\frac{1}{\sqrt{2}}\left\{B_+D^{(1)}_{\mu',-1}(\hat{R}') - B_-D^{(1)}_{\mu',1}(\hat{R}')\right\}\right.
$$
$$
\times \left. I^{(\zeta'',\zeta)}_{l'm'\mu'}Y^*_{l',n'}(\Omega_K)D^{l'}_{m',n'}(\hat{R}')\right]^*
$$
$$
\times \frac{1}{\sqrt{2}}\left\{B_+D^{(1)}_{\mu,-1}(\hat{R}) - B_-D^{(1)}_{\mu,1}(\hat{R})\right\} I^{(\zeta'',\zeta)}_{lm\mu}Y^*_{l,n}(\Omega_K)D^{l}_{m,n}(\hat{R})
$$

(A.53)

Now transforming the photoelectron emission direction into the recoil frame de-

fined by $\hat{R}''$ using the relationship ([126], p. 95, Equation 3.87),

$$Y_{l,n}(\Omega_K) = \sum_p Y_{l,p}(\Omega_k) D_{p,n}^l(\hat{R}'') \tag{A.54}$$

we get

$$
\begin{aligned}
W_{\lambda,\delta;(\zeta,\zeta'')}^{\binom{J,J',J''}{\kappa,\kappa',\kappa''}}(\Omega_K, \hat{R}'') &= \frac{32\pi^4 E}{c g_{\mathrm{i}}} \iint d\hat{R} d\hat{R}' \sum_{H_1,H_2',H_3'',H_4',H_5'',H_6} \frac{(2J+1)(2J'+1)(2J''+1)}{(8\pi^2)^3} \\
&\times C_{H_3'',\kappa''}^{J''} \cdot C_{H_5'',\kappa''}^{J''*} \times C_{H_2',\kappa'}^{J'} \cdot C_{H_4',\kappa'}^{J'*} \times C_{H_6,\kappa}^{J} \cdot C_{H_1,\kappa}^{J*} \\
&\times D_{-H_5'',-H_3''}^{J''}(\hat{R}'^{-1}\hat{R}) D_{-H_4',-H_2'}^{J'}(\hat{R}''^{-1}\hat{R}') D_{-H_1,-H_6}^{J}(\hat{R}^{-1}\hat{R}'') \\
&\times \sum_{\substack{l,m,n,\mu \\ l',m',n',\mu'}} \Bigg[\frac{1}{\sqrt{2}} \left\{ B_+ D_{\mu',-1}^{(1)}(\hat{R}') - B_- D_{\mu',1}^{(1)}(\hat{R}') \right\} I_{l'm'\mu'}^{(\zeta'';\zeta)} \\
&\times \sum_{p'} \left(Y_{l',p'}(\Omega_K) D_{p',n'}^{l'}(\hat{R}'') \right)^* D_{m',n'}^{l'}(\hat{R}') \Bigg]^* \\
&\times \frac{1}{\sqrt{2}} \left\{ B_+ D_{\mu,-1}^{(1)}(\hat{R}) - B_- D_{\mu,1}^{(1)}(\hat{R}) \right\} I_{lm\mu}^{(\zeta'';\zeta)} \\
&\times \sum_p \left(Y_{l,p}(\Omega_K) D_{p,n}^l(\hat{R}'') \right)^* D_{m,n}^l(\hat{R})
\end{aligned}
\tag{A.55}
$$

which can easily be rearranged to

$$
W_{\lambda,\delta;(\zeta,\zeta'')}^{\binom{J,J',J''}{\kappa,\kappa',\kappa''}}(\Omega_K,\hat{R}'') = \frac{32\pi^4 E}{cg_{\mathrm{i}}} \iint d\hat{R}d\hat{R}' \sum_{H_1,H_2',H_3'',H_4',H_5'',H_6} \frac{(2J+1)(2J'+1)(2J''+1)}{(8\pi^2)^3}
$$
$$
\times \, C_{H_3'',\kappa''}^{J''} \cdot C_{H_5'',\kappa''}^{J''*} \times C_{H_2',\kappa'}^{J'} \cdot C_{H_4',\kappa'}^{J'*} \times C_{H_6,\kappa}^{J} \cdot C_{H_1,\kappa}^{J*}
$$
$$
\times \, D_{-H_5'',-H_3''}^{J''}(\hat{R}'^{-1}\hat{R}) D_{-H_4',-H_2'}^{J'}(\hat{R}''^{-1}\hat{R}') D_{-H_1,-H_6}^{J}(\hat{R}^{-1}\hat{R}'')
$$
$$
\times \sum_{\substack{l,m,n,\mu \\ l',m',n',\mu'}} \left[\frac{1}{\sqrt{2}} \left\{ B_+ D_{\mu',-1}^{(1)}(\hat{R}') - B_- D_{\mu',1}^{(1)}(\hat{R}') \right\} I_{l'm'\mu'}^{(\zeta'',\zeta)} \right.
$$
$$
\left. \times \sum_{p'} Y_{l',p'}^*(\Omega_K) D_{n',p'}^{l'}(\hat{R}''^{-1}) D_{m',n'}^{l'}(\hat{R}') \right]^*
$$
$$
\times \frac{1}{\sqrt{2}} \left\{ B_+ D_{\mu,-1}^{(1)}(\hat{R}) - B_- D_{\mu,1}^{(1)}(\hat{R}) \right\} I_{lm\mu}^{(\zeta'',\zeta)}
$$
$$
\times \sum_{p} Y_{l,p}^*(\Omega_K) D_{n,p}^l(\hat{R}''^{-1}) D_{m,n}^l(\hat{R})
$$

$$(A.56)$$

Summing over n and n' using Equation (A.51) we get

$$
W_{\lambda,\delta;(\zeta,\zeta'')}^{\binom{J,J',J''}{\kappa,\kappa',\kappa''}}(\Omega_K,\hat{R}'') = \frac{32\pi^4 E}{c} \iint d\hat{R}d\hat{R}' \sum_{H_1,H_2',H_3'',H_4',H_5'',H_6} \frac{(2J+1)(2J'+1)(2J''+1)}{(8\pi^2)^3}
$$
$$
\times \, C_{H_3'',\kappa''}^{J''} \cdot C_{H_5'',\kappa''}^{J''*} \times C_{H_2',\kappa'}^{J'} \cdot C_{H_4',\kappa'}^{J'*} \times C_{H_6,\kappa}^{J} \cdot C_{H_1,\kappa}^{J*}
$$
$$
\times \, D_{-H_5'',-H_3''}^{J''}(\hat{R}'^{-1}\hat{R}) D_{-H_4',-H_2'}^{J'}(\hat{R}''^{-1}\hat{R}') D_{-H_1,-H_6}^{J}(\hat{R}^{-1}\hat{R}'')
$$
$$
\times \sum_{\substack{l,m,\mu \\ l',m',\mu'}} \left[\frac{1}{\sqrt{2}} \left\{ B_+ D_{\mu',-1}^{(1)}(\hat{R}') - B_- D_{\mu',1}^{(1)}(\hat{R}') \right\} I_{l'm'\mu'}^{(\zeta'',\zeta)} \right.
$$
$$
\left. \times \sum_{p'} Y_{l',p'}^*(\Omega_K) D_{m',p'}^{l'}(\hat{R}''^{-1}\hat{R}') \right]^*
$$
$$
\times \frac{1}{\sqrt{2}} \left\{ B_+ D_{\mu,-1}^{(1)}(\hat{R}) - B_- D_{\mu,1}^{(1)}(\hat{R}) \right\} I_{lm\mu}^{(\zeta'',\zeta)}
$$
$$
\times \sum_{p} Y_{l,p}^*(\Omega_K) D_{m,p}^l(\hat{R}''^{-1}\hat{R})
$$

$$(A.57)$$

121

In order to perform the integrations indicated at Equation (A.57) we need to write the equations in terms of three independent sets of angles, $\hat{R}''$, $\hat{R}''^{-1}\hat{R}$ and $\hat{R}''^{-1}\hat{R}'$. This can be accomplished by rewriting some of the terms in the following manner

$$
\begin{aligned}
D^{J''}_{-H''_i,-H''_j}(\hat{R}'^{-1}\hat{R}) &= D^{J''}_{-H''_i,-H''_j}(\hat{R}'^{-1}\hat{R}''\hat{R}''^{-1}\hat{R}) \\
&= \sum_{q''} D^{J''}_{-H''_i,-q''}(\hat{R}''^{-1}\hat{R})D^{J''}_{-q'',-H''_j}(\hat{R}'^{-1}\hat{R}'') \\
D^{J''}_{-H''_i,-H''_j}(\hat{R}'^{-1}\hat{R}) &= \sum_{q''} D^{J''}_{-H''_i,-q''}(\hat{R}''^{-1}\hat{R})\left[D^{J''}_{-H''_j,-q''}(\hat{R}''^{-1}\hat{R}')\right]^*
\end{aligned}
\tag{A.58}
$$

then the terms involving the field operators can be written as

$$
\begin{aligned}
D^1_{\mu,\pm1}(\hat{R}) &= D^1_{\mu,\pm1}(\hat{R}''\hat{R}''^{-1}\hat{R}) \\
&= \sum_q D^1_{\mu,q}(\hat{R}''^{-1}\hat{R})D^1_{q,\pm1}(\hat{R}'')
\end{aligned}
\tag{A.59}
$$

leading to

$$
\begin{aligned}
W^{\binom{J,J',J''}{\kappa,\kappa',\kappa''}}_{\lambda,\delta;(\zeta,\zeta'')}(\Omega_K,\hat{R}'') = {}&\frac{32\pi^4 E}{cg_{\mathrm{i}}} \sum_{\substack{l,m,\mu,p \\ l',m',\mu',p' \\ q,q',q''}} \iint d\hat{R}d\hat{R}' \sum_{H_1,H'_2,H''_3,H'_4,H''_5,H_6} \\
&\times \frac{(2J+1)(2J'+1)(2J''+1)}{(8\pi^2)^3} \\
&\times C^{J''}_{H''_3,\kappa''}C^{J''*}_{H''_5,\kappa''} \times C^{J'}_{H'_2,\kappa'} \cdot C^{J'*}_{H'_4,\kappa'} \times C^J_{H_6,\kappa} \cdot C^{J*}_{H_1,\kappa} \\
&\times D^{J''}_{H''_5,q''}(\hat{R}''^{-1}\hat{R})\left[D^{J''}_{H''_3,q''}(\hat{R}''^{-1}\hat{R}')\right]^* \\
&\times D^{J'}_{-H'_4,-H'_2}(\hat{R}''^{-1}\hat{R}')\left[D^J_{-H_6,-H_1}(\hat{R}''^{-1}\hat{R})\right]^* \\
&\times \left[\frac{1}{\sqrt{2}}\left\{B_+ D^1_{q',-1}(\hat{R}'') - B_- D^1_{q',1}(\hat{R}'')\right\}\right. \\
&\times \left. D^1_{\mu',q'}(\hat{R}''^{-1}\hat{R}')I^{(\zeta'',\zeta)}_{l'm'\mu'}Y^*_{l',p'}(\Omega_K)D^{l'}_{m',p'}(\hat{R}''^{-1}\hat{R}')\right]^* \\
&\times \frac{1}{\sqrt{2}}\left\{B_+ D^1_{q,-1}(\hat{R}'') - B_- D^1_{q,1}(\hat{R}'')\right\} \\
&\times D^1_{\mu,q}(\hat{R}''^{-1}\hat{R})I^{(\zeta'',\zeta)}_{lm\mu}Y^*_{l,p}(\Omega_K)D^l_{m,p}(\hat{R}''^{-1}\hat{R})
\end{aligned}
\tag{A.60}
$$

122

Making a change in the integration variables from $\hat{R}$ and $\hat{R}'$ to $\hat{R}''^{-1}\hat{R}$ and $\hat{R}''^{-1}\hat{R}'$ respectively and re-labeling the variables of integration back to $\hat{R}$ and $\hat{R}'$ one can then rewrite Equation (A.60) as

$$
W_{\lambda,\delta;(\zeta,\zeta'')}^{\binom{J,J',J''}{\kappa,\kappa',\kappa''}}(\Omega_K, \hat{R}'') = \frac{32\pi^4 E}{cg_{\mathrm{i}}} \sum_{\substack{l,m,\mu,p \\ l',m',\mu',p' \\ q,q',q''}} \sum_{H_1,H_2',H_3'',H_4',H_5'',H_6} \frac{(2J+1)(2J'+1)(2J''+1)}{(8\pi^2)^3}
$$
$$
\times C_{H_3'',\kappa''}^{J''} \cdot C_{H_5'',\kappa''}^{J''*} \times C_{H_2',\kappa'}^{J'} \cdot C_{H_4',\kappa'}^{J'*} \times C_{H_6,\kappa}^{J} \cdot C_{H_1,\kappa}^{J*}
$$
$$
\times \left[\frac{1}{\sqrt{2}} \left\{ B_+ D_{q',-1}^1(\hat{R}'') - B_- D_{q',1}^1(\hat{R}'') \right\} I_{l'm'\mu'}^{(\zeta'',\zeta)} Y_{l',p'}^*(\Omega_K) \right]^*
$$
$$
\times \frac{1}{\sqrt{2}} \left\{ B_+ D_{q,-1}^1(\hat{R}'') - B_- D_{q,1}^1(\hat{R}'') \right\} I_{lm\mu}^{(\zeta'',\zeta)} Y_{l,p}^*(\Omega_K)
$$
$$
\times \int d\hat{R} \left[D_{-H_6,-H_1}^J(\hat{R}) \right]^* D_{-H_5'',q''}^{J''}(\hat{R}) D_{\mu,q}^1(\hat{R}) D_{m,p}^l(\hat{R})
$$
$$
\times \left\{ \int d\hat{R}' \left[D_{-H_4',-H_2'}^{J'}(\hat{R}') \right]^* D_{-H_3'',q''}^{J''}(\hat{R}') D_{\mu',q'}^1(\hat{R}') D_{m',p'}^{l'}(\hat{R}') \right\}^*
$$
$$
\tag{A.61}
$$

The two integrals have the same functional form and can be evaluated to give,

$$
X_{\mu,m,q'',p,q}^{(J,J'',l,H_6,H_1,H_5'')}(-1)^{-H_5''-q''} = \frac{1}{8\pi^2} \int d\hat{R} \left[D_{-H_6,-H_1}^J(\hat{R}) \right]^* D_{-H_5'',q''}^{J''}(\hat{R}) D_{\mu,q}^1(\hat{R}) D_{m,p}^l(\hat{R})
$$
$$
\tag{A.62}
$$

Then, by using first, Equation 3.125 on p. 105 and then Equation 3.105 on p. 99, of

Zare's book [126] we get,

$$
\begin{aligned}
X^{(J,J'',l,H_6,H_1,H_5'')}_{\mu,m,q'',p,q}(-1)^{-H_5''-q''} &= \frac{1}{8\pi^2}\int d\hat{R}\left[D^J_{-H_6,-H_1}(\hat{R})\right]^*\left[D^{J''}_{H_5'',-q''}(\hat{R})\right]^* \\
&\quad \times (-1)^{-H_5''-q''}D^1_{\mu,q}(\hat{R})D^l_{m,p}(\hat{R}) \\
&= \frac{1}{8\pi^2}\int d\hat{R}\sum_{K,K'}[\langle J-H_6,J''\,H_5''|\,K,H_5''-H_6\rangle \\
&\quad \times D^K_{H_5''-H_6,-H_1-q''}(\hat{R}) \\
&\quad \times \langle J-H_1,J''-q''|\,K,-H_1-q''\rangle]^* \\
&\quad \times (-1)^{-H_5''-q''}\langle 1\,\mu,l\,m|\,K',\mu+m\rangle \\
&\quad \times D^{K'}_{\mu+m,q+p}(\hat{R})\langle 1\,q,l\,p|\,K',q+p\rangle
\end{aligned}
$$

(A.63)

Using the integral of a product of rotational matrices ([126], Equation 3.113, p. 101),

$$
\int d\Omega\left[D^{J_1}_{M_1'M_1}(R)\right]^*D^{J_2}_{M_2'M_2}(R) = \frac{8\pi^2}{2J_1+1}\delta_{J_1J_2}\delta_{M_1'M_2'}\delta_{M_1M_2}
$$

(A.64)

the function $X^{(J,J'',l,H_6,H_1,H_5'')}_{\mu,m,q'',p,q}(-1)^{-H_5''-q''}$ can be expressed as

$$
\begin{aligned}
X^{(J,J'',l,H_6,H_1,H_5'')}_{\mu,m,q'',p,q}(-1)^{-H_5''-q''} &= (-1)^{-H_5''-q''}\sum_K\frac{1}{2K+1} \\
&\quad \times \langle J\quad-H_6,J''\,H_5''|\,K,H_5''-H_6\rangle \\
&\quad \times \langle J\quad-H_1,J''\quad-q''|\,K,-H_1-q''\rangle \\
&\quad \times \langle 1\,\mu,l\,m|\,K,H_5''-H_6\rangle\langle 1\,q,l\,p|\,K,-H_1-q''\rangle
\end{aligned}
$$

(A.65)

by noting that $\mu+m = H_5''-H_6$ and that $q+p = -H_1-q''$ it follows that the dependence of this X functions on H_6 and H_1 is dropped since they themselves are not independent from the other variables related to X. So it can be rearranged for convenience to,

$$
\begin{aligned}
X^{(J,J'',l,H_6,H_1,H_5'')}_{\mu,m,q'',p,q} &= \sum_K\frac{1}{2K+1}\langle J\quad-H_6,J''\,H_5''|\,K,H_5''-H_6\rangle \\
&\quad \times \langle J\quad-H_1,J''\quad-q''|\,K,-H_1-q''\rangle \\
&\quad \times \langle 1\,\mu,l\,m|\,K,H_5''-H_6\rangle\langle 1\,q,l\,p|\,K,-H_1-q''\rangle
\end{aligned}
$$

(A.66)

124

to eliminate the direct dependence on H_6 and H_1, Equation (A.66) is rewritten as

$$
\begin{aligned}
X_{\mu,m,q'',p,q}^{(J,J'',l,H_5'';H_6)} = \sum_K \frac{1}{2K+1} &\langle J \quad \mu+m-H_5'', J'' \ H_5'' |\ K, \mu+m \rangle \\
&\times \langle J \quad q+p+q'', J'' \quad -q'' |\ K, q+p \rangle \\
&\times \langle 1\,\mu, l\,m |\ K, \mu+m \rangle \langle 1\,q, l\,p |\ K, q+p \rangle
\end{aligned}
\tag{A.67}
$$

To compute (A.67) some Clebsch-Gordan (CG) coefficients most be evaluated, and must be re-written in such a way that they conform to the order that the used subroutine, CLEBG(J2, J3, M1, M2, F, J1MIN), requires. To do this, lets look at each CG coefficient separately, first

$$
\langle J \quad \mu+m-H_5'', J'' \ H_5'' |\ K, \mu+m \rangle
$$

note that in the program the variables Mum $= \mu+m$ is defined. Using Equation C.13b of Messiah's book [137] it can be expressed as

$$
(-1)^{J-K+H_5''} \left(\frac{2K+1}{2J+1} \right)^{1/2} \langle K \quad \mu+m, J'' - H_5'' |\ J, \mu+m-H_5'' \rangle
$$

which is the form to be used in the program. In a similar way, in the program we defined qp $= q+p$, and

$$
\begin{aligned}
\langle J \quad q+p+q'', J'' \quad -q'' |\ K, q+p \rangle = (-1)^{J-K-q''} &\left(\frac{2K+1}{2J+1} \right)^{1/2} \\
&\times \langle K \quad q+p, J'' \quad q'' |\ J, q+p+q'' \rangle
\end{aligned}
\tag{A.68}
$$

For the other two CG coefficients involved in evaluating Equation (A.66) we have,

$$
\begin{aligned}
\langle 1\,\mu, l\,m |\ K, \mu+m \rangle &= (-1)^{1-K+m} \left(\frac{2K+1}{2(1)+1} \right)^{1/2} \langle K\,\mu+m, l \ -m |\ 1, \mu \rangle \\
\langle 1\,q, l\,p |\ K, q+p \rangle &= (-1)^{1-K+p} \left(\frac{2K+1}{2(1)+1} \right)^{1/2} \langle K\,q+p, l \ -p |\ 1, q \rangle
\end{aligned}
\tag{A.69}
$$

When substituting these previously rearranged terms into Equation (A.67) we end

up with,

$$X_{\mu,m,q'',p,q}^{(J,J'',l,H_5'';H_6)} = \sum_K (-1)^{H_5''-q''+m+p} \left(\frac{2K+1}{3(2J+1)} \right)$$

$$\times \langle K \quad \mu+m, J'' \ -H_5''|\ J, \mu+m-H_5''\rangle \qquad (A.70)$$

$$\times \langle K \quad q+p, J'' \quad q''|\ J, q+p+q''\rangle$$

$$\times \langle K\ \mu+m, l\ -m|\ 1, \mu\rangle \langle K\ q+p, l\ -p|\ 1, q\rangle$$

and in a very similar way for $\left[X_{\mu',m',q'',p',q'}^{(J',J'',l',H_4',H_2',H_3'')} \right]^*$ the dependence on H_4' and H_2' can be removed leading to

$$\left[X_{\mu',m',q'',p',q'}^{(J',J'',l',H_3'';H_4')} \right]^* = \left[\sum_K (-1)^{H_3''-q''+m'+p'} \left(\frac{2K+1}{3(2J'+1)} \right) \right.$$

$$\times \langle K \quad \mu'+m', J'' \ -H_3''|\ J', \mu'+m'-H_3''\rangle \qquad (A.71)$$

$$\times \langle K \quad p'+q', J'' \quad q''|\ J', p'+q'+q''\rangle$$

$$\left. \times \langle K\ \mu'+m', l'\ -m'|\ 1, \mu\rangle \langle K\ p'+q', l'\ -p'|\ 1, q'\rangle \right]^*$$

where, in the program notation, the variables MuPmP $= \mu'+m'$ and pPqP $= pP+qP$ have been used. It should be noted that in Equation (A.71) the value of X is real, and the complex conjugate notation is employed only to make more easy to follow where this quantity fits into the rest of the equations. So that Equation (A.61) can be rewritten as

$$W_{\lambda,\delta;(\zeta,\zeta'')}^{\left(\begin{smallmatrix} J,J',J'' \\ \kappa,\kappa',\kappa'' \end{smallmatrix} \right)}(\Omega_K, \hat{R}'') = \frac{4\pi^2 E}{cg_i} \sum_{\substack{l,m,\mu,p \\ l',m',\mu',p' \\ q,q',q''}} \sum_{H_1,H_2',H_3'',H_4',H_5'',H_6} (2J+1)(2J'+1)(2J''+1)$$

$$\times C_{H_3'',\kappa''}^{J''} \cdot C_{H_5'',\kappa''}^{J''*} \times C_{H_2',\kappa'}^{J'} \cdot C_{H_4',\kappa'}^{J'*} \times C_{H_6,\kappa}^{J} \cdot C_{H_1,\kappa}^{J*}$$

$$\times \left[\frac{1}{\sqrt{2}} \left\{ B_+ D_{q',-1}^1(\hat{R}'') - B_- D_{q',1}^1(\hat{R}'') \right\} I_{l'm'\mu'}^{(\zeta'';\zeta)} Y_{l',p'}^*(\Omega_K) \right]^*$$

$$\times \frac{1}{\sqrt{2}} \left\{ B_+ D_{q,-1}^1(\hat{R}'') - B_- D_{q,1}^1(\hat{R}'') \right\} I_{lm\mu}^{(\zeta'';\zeta)} Y_{l,p}^*(\Omega_K)$$

$$\times X_{\mu,m,q'',p,q}^{(J,J'',l,H_5'';H_6)} \left[X_{\mu',m',q'',p',q'}^{(J',J'',l',H_3'';H_4')} \right]^*$$

$$(A.72)$$

126

Let's define a function $Z_{\lambda,\delta}^{(q,N)}$ as

$$Z_{\lambda,\delta}^{(q,N)}(\hat{R}'') = \frac{1}{2}\left\{B_+ D_{q',-1}^1(\hat{R}'') - B_- D_{q',1}^1(\hat{R}'')\right\}^* \left\{B_+ D_{q,-1}^1(\hat{R}'') - B_- D_{q,1}^1(\hat{R}'')\right\}$$
(A.73)

From the definition of $B_\pm = \cos\lambda \pm i\sin\lambda e^{i\delta}$ and Equation (A.1) it follows that

$$
\begin{aligned}
B_+^* B_- &= (\cos\lambda - i\sin\lambda e^{-i\lambda})(\cos\lambda - i\sin\lambda e^{i\delta}) \\
&= \cos^2\lambda - i\cos\lambda\sin\lambda e^{i\delta} - i\sin\lambda\cos\lambda e^{-i\delta} - \sin^2\lambda \\
&= \cos 2\lambda - i\cos\lambda\sin\lambda(\cos\delta + i\sin\delta + \cos\delta - i\sin\delta) \\
&= \cos 2\lambda - i2\cos\lambda\sin\lambda\cos\delta \\
&= s_1 - is_2
\end{aligned}
$$
(A.74)

in a similar way

$$
\begin{aligned}
B_+^* B_+ &= 1 - s_3 \\
B_-^* B_+ &= s_1 + is_2 \\
B_-^* B_- &= 1 + s_3
\end{aligned}
$$
(A.75)

So that the $Z_{\lambda,\delta}^{(q,N)}(\hat{R}'')$ can be written in terms of the Stokes parameters (see Equation (A.1) as

$$
\begin{aligned}
Z_{\lambda,\delta}^{(q,N)}(\hat{R}'') = \frac{1}{2}\Big\{ &(1 - s_3)\left[D_{q',-1}^1(\hat{R}'')\right]^* D_{q,-1}^1(\hat{R}'') \\
&- (s_1 - is_2)\left[D_{q',-1}^1(\hat{R}'')\right]^* D_{q,1}^1(\hat{R}'') \\
&- (s_1 + is_2)\left[D_{q',1}^1(\hat{R}'')\right]^* D_{q,-1}^1(\hat{R}'') \\
&+ (1 + s_3)\left[D_{q',1}^1(\hat{R}'')\right]^* D_{q,1}^1(\hat{R}'')\Big\}
\end{aligned}
$$
(A.76)

By using the next property of rotation matrices ([126], Equation 3.125 p. 105),

$$\left[D_{MK}^J(R)\right]^* = (-1)^{M-K} D_{-M\,-K}^J(R)$$
(A.77)

we can rewrite Equation (A.76) as

$$
\begin{aligned}
Z_{\lambda,\delta}^{(q,N)}(\hat{R}'') = \frac{1}{2}\Big\{ & (-1)^{q'+1}(1-s_3)D_{-q',1}^1(\hat{R}'')D_{q,-1}^1(\hat{R}'') \\
& - (-1)^{q'+1}(s_1-is_2)D_{-q',1}^1(\hat{R}'')D_{q,1}^1(\hat{R}'') \\
& - (-1)^{q'-1}(s_1+is_2)D_{-q',-1}^1(\hat{R}'')D_{q,-1}^1(\hat{R}'') \\
& + (-1)^{q'-1}(1+s_3)D_{-q',-1}^1(\hat{R}'')D_{q,1}^1(\hat{R}'') \Big\}
\end{aligned}
\tag{A.78}
$$

Expanding now the matrix products into Clebsch-Gordan coefficients we have

$$
\begin{aligned}
Z_{\lambda,\delta}^{(q,N)}(\hat{R}'') = \frac{1}{2}\Big\{ & (-1)^{q'+1}(1-s_3)\sum_L \langle 1\ -q',1\ q|\ L,q-q'\rangle \langle 1\ 1,1\ -1|\ L,0\rangle D_{q-q',0}^L(\hat{R}'') \\
& - (-1)^{q'+1}(s_1-is_2)\sum_L \langle 1\ -q',1\ q|\ L,q-q'\rangle \langle 1\ 1,1\ 1|\ L,2\rangle D_{q-q',2}^L(\hat{R}'') \\
& - (-1)^{q'-1}(s_1+is_2)\sum_L \langle 1\ -q',1\ q|\ L,q-q'\rangle \\
& \times \langle 1\ -1,1\ -1|\ L,-2\rangle D_{q-q',-2}^L(\hat{R}'') \\
& + (-1)^{q'-1}(1+s_3)\sum_L \langle 1\ -q',1\ q|\ L,q-q'\rangle \langle 1\ -1,1\ 1|\ L,0\rangle D_{q-q',0}^L(\hat{R}'') \Big\}
\end{aligned}
\tag{A.79}
$$

Rearranging terms and defining $N = q - q'$ we have,

$$
\begin{aligned}
Z_{\lambda,\delta}^{(q,N)}(\hat{R}'') = \frac{1}{2}(-1)^{q-N+1}\sum_L & \langle 1\ -q',1\ q|\ L,N\rangle \\
\times \Big\{ & (1-s_3)\langle 1\ 1,1\ -1|\ L,0\rangle D_{N,0}^L(\hat{R}'') \\
& - (s_1-is_2)\langle 1\ 1,1\ 1|\ L,2\rangle D_{N,2}^L(\hat{R}'') \\
& - (s_1+is_2)\langle 1\ -1,1\ -1|\ L,-2\rangle D_{N,-2}^L(\hat{R}'') \\
& + (1+s_3)\langle 1\ -1,1\ 1|\ L,0\rangle D_{N,0}^L(\hat{R}'') \Big\}
\end{aligned}
\tag{A.80}
$$

Note that Equations (A.65) and (A.66) have the following constraints on some of the

indices in the sums

$$q + p = -H_1 - q''$$
$$q' + p' = -H_2' - q''$$

(A.81)

so that by equating previous definitions on q'' and using the definition of N we get,

$$q + p + H_1 = q' + p' + H_2'$$
$$q - q' = p' - p + H_2' - H_1$$
$$N = p' - p + H_2' - H_1$$

(A.82)

so, primed indices q'', q' and p' can be written as

$$q'' = -H_1 - q - p$$
$$q' = q - N$$
$$p' = N + p - H_2' + H_1$$

(A.83)

also for convenience we will define the quantity N_H as,

$$N_H = -N + H_2' - H_1$$

(A.84)

and it immediately follows that,

$$p' = p - N_H$$

(A.85)

Then Equation (A.72) can be rewritten as

$$W_{\lambda,\delta;(\zeta,\zeta'')}^{\binom{J,J',J''}{\kappa,\kappa',\kappa''}}(\Omega_K, \hat{R}'') = \frac{4\pi^2 E}{c g_i} \sum_{\substack{l,m,\mu,p,q \\ l',m',\mu',N}} \sum_{H_1,H_2',H_3'',H_4',H_5'',H_6} (2J+1)(2J'+1)(2J''+1)$$
$$\times C_{H_3'',\kappa''}^{J''} \cdot C_{H_5'',\kappa''}^{J''*} \times C_{H_2',\kappa'}^{J'} \cdot C_{H_4',\kappa'}^{J'*} \times C_{H_6,\kappa}^{J} \cdot C_{H_1,\kappa}^{J*}$$
$$\times \left[I_{l'm'\mu'}^{(\zeta'',\zeta)} \right]^* I_{lm\mu}^{(\zeta'',\zeta)} Y_{l',N+p-H_2'+H_1}(\Omega_K) Y_{l,-p}(\Omega_K)(-1)^p$$
$$\times X_{\mu,m,q'',p,q}^{(J,J'',l,H_5'';H_6)} \left[X_{\mu',m',q'',p',q'}^{(J',J'',l',H_3'';H_4')} \right]^* Z_{\lambda,\delta}^{(q,N)}(\hat{R}'')$$

(A.86)

129

And by using the relation $Y_{LM}(\theta, \phi) = \left(\frac{2L+1}{4\pi}\right)^{1/2} \left[D_{M0}^L(\phi, \theta, \chi)\right]^*$ (see [126], Equation 3.94, p. 97), it can be expressed as

$$
W_{\lambda,\delta;(\zeta,\zeta'')}^{\binom{J,J',J''}{\kappa,\kappa',\kappa''}}(\Omega_K, \hat{R}'') = \frac{4\pi^2 E}{cg_i} \sum_{\substack{l,m,\mu,p,q \\ l',m',\mu',N}} \sum_{H_1,H_2',H_3'',H_4',H_5'',H_6} (2J+1)(2J'+1)(2J''+1)
$$

$$
\times C_{H_3'',\kappa''}^{J''} \cdot C_{H_5'',\kappa''}^{J''*} \times C_{H_2',\kappa'}^{J'} \cdot C_{H_4',\kappa'}^{J'*} \times C_{H_6,\kappa}^{J} \cdot C_{H_1,\kappa}^{J*}
$$

$$
\times \left[I_{l'm'\mu'}^{(\zeta'',\zeta)}\right]^* I_{lm\mu}^{(\zeta'',\zeta)} \left(\frac{2l'+1}{4\pi}\right)^{1/2} \left[D_{N+p-H_2'+H_1,0}^{l'}(\Omega_K)\right]^*
$$

$$
\times \left(\frac{2l+1}{4\pi}\right)^{1/2} \left[D_{-p,0}^l(\Omega_K)\right]^* (-1)^p
$$

$$
\times X_{\mu,m,q'',p,q}^{(J,J'',l,H_5'';H_6)} \left[X_{\mu',m',q'',p',q'}^{(J',J'',l',H_3'';H_4')}\right]^* Z_{\lambda,\delta}^{(q,N)}(\hat{R}'')
$$

$$(\text{A.87})$$

Considering Equations (A.77), and then taking the products of the 'paired' rotation matrices and expressing them as Clebsch-Gordan coefficients (which is equivalent to use Equation (A.22)), it follows that

$$
W_{\lambda,\delta;(\zeta,\zeta'')}^{\binom{J,J',J''}{\kappa,\kappa',\kappa''}}(\Omega_K, \hat{R}'') = \frac{4\pi^2 E}{cg_i} \sum_{\substack{l,m,\mu,p,q \\ l',m',\mu',N}} \sum_{H_1,H_2',H_3'',H_4',H_5'',H_6} (2J+1)(2J'+1)(2J''+1)
$$

$$
\times C_{H_3'',\kappa''}^{J''} \cdot C_{H_5'',\kappa''}^{J''*} \times C_{H_2',\kappa'}^{J'} \cdot C_{H_4',\kappa'}^{J'*} \times C_{H_6,\kappa}^{J} \cdot C_{H_1,\kappa}^{J*}
$$

$$
\times \left[I_{l'm'\mu'}^{(\zeta'',\zeta)}\right]^* I_{lm\mu}^{(\zeta'',\zeta)} (-1)^{N+p-H_2'+H_1} \left(\frac{2l'+1}{4\pi}\right)^{1/2} \left(\frac{2l+1}{4\pi}\right)^{1/2}
$$

$$
\times \sum_{L'} \langle l' - N - p + H_2' - H_1, l\, p|\, L', -N + H_2' - H_1 \rangle
$$

$$
\times \langle l'\, 0, l\, 0|\, L', 0\rangle\, D_{-N+H_2'-H_1,0}^{L'}(\Omega_K)
$$

$$
\times X_{\mu,m,q'',p,q}^{(J,J'',l,H_5'';H_6)} \left[X_{\mu',m',q'',p',q'}^{(J',J'',l',H_3'';H_4')}\right]^* Z_{\lambda,\delta}^{(q,N)}(\hat{R}'')
$$

$$(\text{A.88})$$

Finally this expression can be rearranged and the rotation matrix left expressed as a spherical harmonic function ([126], Equation 3.93, p.97 and Equation 3.98, p97)

to have

$$
W_{\lambda,\delta;(\zeta,\zeta'')}^{\binom{J,J',J''}{\kappa,\kappa',\kappa''}}(\Omega_K,\hat{R}'') = \frac{4\pi^2 E}{c g_{\mathrm{i}}} \sum_{\substack{l,m,\mu,p,q \\ l',m',\mu',N}} \sum_{H_1,H_2',H_3'',H_4',H_5'',H_6} (2J+1)(2J'+1)(2J''+1)
$$

$$
\times\, C_{H_3'',\kappa''}^{J''} \cdot C_{H_5'',\kappa''}^{J''*} \times C_{H_2',\kappa'}^{J'} \cdot C_{H_4',\kappa'}^{J'*} \times C_{H_6,\kappa}^{J} \cdot C_{H_1,\kappa}^{J*}
$$

$$
\times\, \left[I_{l'm'\mu'}^{(\zeta'',\zeta)}\right]^* I_{lm\mu}^{(\zeta'',\zeta)}(-1)^{N+p-H_2'+H_1}\left(\frac{2l'+1}{4\pi}\right)^{1/2}\left(\frac{2l+1}{4\pi}\right)^{1/2}
$$

$$
\times\, \sum_{L'} \langle l' -N-p+H_2'-H_1, l\, p|\, L',-N+H_2'-H_1\rangle
$$

$$
\times\, \langle l'\, 0, l\, 0|\, L',0\rangle \left(\frac{4\pi}{2L'+1}\right)^{1/2} Y_{L',-N+H_2'-H_1}^*(\Omega_K)
$$

$$
\times\, X_{\mu,m,q'',p,q}^{(J,J'',l,H_5'';H_6)}\left[X_{\mu',m',q'',p',q'}^{(J',J'',l',H_3'';H_4')}\right]^* Z_{\lambda,\delta}^{(q,N)}(\hat{R}'')
$$

$$\tag{A.89}$$

leading to

$$
W_{\lambda,\delta;(\zeta,\zeta'')}^{\binom{J,J',J''}{\kappa,\kappa',\kappa''}}(\Omega_K,\hat{R}'') = \frac{4\pi^2 E}{c g_{\mathrm{i}}} \sum_{\substack{l,m,\mu,p,q \\ l',m',\mu',N}} \sum_{H_1,H_2',H_3'',H_4',H_5'',H_6} (2J+1)(2J'+1)(2J''+1)
$$

$$
\times\, C_{H_3'',\kappa''}^{J''} \cdot C_{H_5'',\kappa''}^{J''*} \times C_{H_2',\kappa'}^{J'} \cdot C_{H_4',\kappa'}^{J'*} \times C_{H_6,\kappa}^{J} \cdot C_{H_1,\kappa}^{J*}
$$

$$
\times\, \left[I_{l'm'\mu'}^{(\zeta'',\zeta)}\right]^* I_{lm\mu}^{(\zeta'',\zeta)}(-1)^{p} \sum_{L'}\left[\frac{(2l'+1)(2l+1)}{4\pi(2L'+1)}\right]^{1/2}
$$

$$
\times\, \langle l' -N-p+H_2'-H_1, l\, p|\, L',-N+H_2'-H_1\rangle
$$

$$
\times\, \langle l'\, 0, l\, 0|\, L',0\rangle\, Y_{L',N-H_2'+H_1}(\Omega_K)
$$

$$
\times\, X_{\mu,m,q'',p,q}^{(J,J'',l,H_5'';H_6)}\left[X_{\mu',m',q'',p',q'}^{(J',J'',l',H_3'';H_4')}\right]^* Z_{\lambda,\delta}^{(q,N)}(\hat{R}'')
$$

$$\tag{A.90}$$

Now define the terms

$$
M_{q'',p,q}^{(J,J'',l,H_5'',H_6,\zeta'',\zeta)} = \sum_{\mu} I_{lm\mu}^{(\zeta'',\zeta)} X_{\mu,m,q'',p,q}^{(J,J'',l,H_5'';H_6)}
$$

$$
\left[M_{q'',p',q'}^{(J',J'',l',H_3'',H_4',\zeta'',\zeta)}\right]^* = \sum_{\mu'} \left[I_{l'm'\mu'}^{(\zeta'',\zeta)}\right]^* X_{\mu',m',q'',p',q'}^{(J',J'',l',H_3'';H_4')}
$$

$$\tag{A.91}$$

131

and

$$E_{L,N}^{(\lambda,\delta)}(\hat{R}'') = \frac{1}{2}\sqrt{\frac{2L+1}{4\pi}}\Bigg\{(1-s_3)\langle 1\,1, 1\,-1|\,L, 0\rangle\,D_{N,0}^{L}(\hat{R}'')$$
$$-(s_1 - is_2)\langle 1\,1, 1\,1|\,L, 2\rangle\,D_{N,2}^{L}(\hat{R}'')$$
$$-(s_1 + is_2)\langle 1\,-1, 1\,-1|\,L, -2\rangle\,D_{N,-2}^{L}(\hat{R}'')$$
$$+(1+s_3)\langle 1\,-1, 1\,1|\,L, 0\rangle\,D_{N,0}^{L}(\hat{R}'')\Bigg\} \tag{A.92}$$

with this definition Equation (A.80) can be rewritten as

$$Z_{\lambda,\delta}^{(q,N)}(\hat{R}'') = (-1)^{q-N+1}\sum_{L}\langle 1\,-q', 1\,q|\,L, N\rangle\,\sqrt{\frac{4\pi}{2L+1}}\,E_{L,N}^{(\lambda,\delta)}(\hat{R}'') \tag{A.93}$$

For specific values of L, explicit formulas for the $E_{L,N}^{(\lambda,\delta)}$ (algebraic expressions for some specific values of the Clebsch-Gordan coefficients can be found elsewhere (for example [126], p.57-61) can be written as:

$$E_{0,0}^{\lambda,\delta}(\hat{R}'') = \frac{1}{\sqrt{3}}\frac{1}{\sqrt{4\pi}} \tag{A.94a}$$

$$E_{1,N}^{(\lambda,\delta)}(\hat{R}'') = \frac{1}{\sqrt{2}}\sqrt{\frac{3}{4\pi}}s_3 D_{N,0}^{(1)}(\hat{R}'') \tag{A.94b}$$

$$E_{2,N}^{(\lambda,\delta)}(\hat{R}'') = \sqrt{\frac{5}{4\pi}}\Bigg\{\frac{1}{\sqrt{6}}D_{N,0}^{(2)}(\hat{R}'') - \frac{s_1}{2}\left[D_{N,2}^{(2)}(\hat{R}'') + D_{N,-2}^{(2)}(\hat{R}'')\right]$$
$$+\frac{is_2}{2}\left[D_{N,2}^{(2)}(\hat{R}'') - D_{N,-2}^{(2)}(\hat{R}'')\right]\Bigg\} \tag{A.94c}$$

The $W_{\lambda,\delta;(\zeta,\zeta'')}^{\binom{J,J',J''}{\kappa,\kappa',\kappa''}}$ can now be written as

$$
W_{\lambda,\delta;(\zeta,\zeta'')}^{\left(\substack{J,J',J'' \\ \kappa,\kappa',\kappa''}\right)}(\Omega_K,\hat{R}'') = \frac{4\pi^2 E}{c g_{\mathrm{i}}} \sum_{L',L,N} Y_{L',N-H_2'+H_1}(\Omega_K) E_{L,N}^{(\lambda,\delta)}(\hat{R}'')
$$

$$
\times \sum_{l,p,q,l'} \sum_{H_1,H_2',H_3'',H_4',H_5'',H_6} (2J+1)(2J'+1)(2J''+1)
$$

$$
\times \left[\frac{(2l'+1)(2l+1)}{(2L+1)(2L'+1)} \right]^{1/2}
$$

$$
\times C_{H_3'',\kappa''}^{J''} \cdot C_{H_5'',\kappa''}^{J''*} \times C_{H_2',\kappa'}^{J'} \cdot C_{H_4',\kappa'}^{J'*} \times C_{H_6,\kappa}^{J} \cdot C_{H_1,\kappa}^{J*}
$$

$$
\times (-1)^{p+q-N+1} \langle l' - N - p + H_2' - H_1, l\,p|\, L', -N + H_2' - H_1 \rangle
$$

$$
\times \langle l'\,0, l\,0|\, L',0 \rangle \langle 1 - q', 1\,q|\, L, N \rangle
$$

$$
\times M_{q'',p,q}^{(J,J'',l,H_5'',H_6,\zeta'',\zeta)} \left[M_{q'',p',q'}^{(J',J'',l',H_3'',H_4',\zeta'',\zeta)} \right]^*
$$

$$
(\text{A.95})
$$

This definition of $W_{\lambda,\delta;(\zeta,\zeta'')}^{\left(\substack{J,J',J'' \\ \kappa,\kappa',\kappa''}\right)}(\Omega_K,\hat{R}'')$ can be rearranged in such a way that the only terms containing H_3'', H_4', H_5'' and H_6 are placed together, as it is done in the program.

$$
W_{\lambda,\delta;(\zeta,\zeta'')}^{\left(\substack{J,J',J'' \\ \kappa,\kappa',\kappa''}\right)}(\Omega_K,\hat{R}'') = \frac{4\pi^2 E}{c g_{\mathrm{i}}} \sum_{L',L,N} Y_{L',N-H_2'+H_1}(\Omega_K) E_{L,N}^{(\lambda,\delta)}(\hat{R}'')
$$

$$
\times \sum_{l,p,q,l'} \sum_{H_1,H_2'} (2J+1)(2J'+1)(2J''+1)
$$

$$
\times \left[\frac{(2l'+1)(2l+1)}{(2L+1)(2L'+1)} \right]^{1/2} C_{H_2',\kappa'}^{J'} \times C_{H_1,\kappa}^{J*} \cdot (-1)^{p+q-N+1}
$$

$$
\times \langle l' - N - p + H_2' - H_1, l\,p|\, L', -N + H_2' - H_1 \rangle
$$

$$
\times \langle l'\,0, l\,0|\, L',0 \rangle \langle 1 - q', 1\,q|\, L, N \rangle
$$

$$
\times \sum_{H_5'',H_6} C_{H_5'',\kappa''}^{J''*} \cdot C_{H_6,\kappa}^{J} \cdot M_{q'',p,q}^{(J,J'',l,H_5'',H_6,\zeta'',\zeta)}
$$

$$
\times \sum_{H_3'',H_4'} C_{H_3'',\kappa''}^{J''} \cdot C_{H_4',\kappa'}^{J'*} \cdot \left[M_{q'',p',q'}^{(J',J'',l',H_3'',H_4',\zeta'',\zeta)} \right]^*
$$

$$
(\text{A.96})
$$

By performing the indicated products on M and M^*, and the corresponding sums over H_3'', H_4', H_5'' and H_6 a transformation is carried taking $M_{q'',p,q}^{(J,J'',l,H_5'',H_6,\zeta'',\zeta)}$ and

133

$$\left[M_{q'',p',q'}^{(J',J'',l',H_3'',H_4',\zeta'',\zeta)}\right]^* \text{ to } M_{q'',p,q}^{(J,J'',l,\kappa'',\kappa,\zeta'',\zeta)} \text{ and } \left[M_{q'',p',q'}^{(J',J'',l',\kappa'',\kappa',\zeta'',\zeta)}\right]^* \text{ respectively.}$$

Now defining $H_{L'LN;(\zeta,\zeta'')}^{\binom{J,J',J''}{\kappa,\kappa',\kappa''}}$ as

$$
\begin{aligned}
H_{L'LN;(\zeta,\zeta'')}^{\binom{J,J',J''}{\kappa,\kappa',\kappa''}} = {} & \frac{4\pi^2 E}{c g_\mathrm{i}} \sum_{l,p,q,l'} \sum_{H_1,H_2'} (2J+1)(2J'+1)(2J''+1) \\
& \times \left[\frac{(2l'+1)(2l+1)}{(2L+1)(2L'+1)}\right]^{1/2} \times C_{H_2',\kappa'}^{J'} \cdot C_{H_1,\kappa}^{J*} \\
& \times (-1)^{p+q-N+1} \left\langle l' \; -N - p + H_2' - H_1, l\, p\right| L', -N + H_2' - H_1 \rangle \\
& \times \left\langle l'\, 0, l\, 0 \middle| L', 0\right\rangle \left\langle 1 - q', 1\, q \middle| L, N\right\rangle \\
& \times M_{q'',p,q}^{(J,J'',l,\kappa'',\kappa,\zeta'',\zeta)} \left[M_{q'',p',q'}^{(J',J'',l',\kappa'',\kappa',\zeta'',\zeta)}\right]^*
\end{aligned}
$$

$$(A.97)$$

Looking at Equation (A.97) for $H_{L'LN;(\zeta,\zeta'')}^{\binom{J,J',J''}{\kappa,\kappa',\kappa''}}$ we have some CG coefficients that need to be re-expressed for convenience by using Equation C.13b of Messiah's book [137] (or Equation 2.26 of [126]), in order to use the CLEBG(J2,J3, M1, M2, F, J1MIN) subroutine. Let's define $N_H = -N + H_2' - H_1$ so that,

$$\left\langle l' \; -N - p + H_2' - H_1, l\, p \middle| L', -N + H_2' - H_1\right\rangle = \left\langle l'\, N_H - p, l\, p \middle| L', N_H\right\rangle \quad (A.98)$$

and re-expressing it, leads to,

$$\left\langle l'\, N_H - p, l\, p \middle| L', N_H\right\rangle = (-1)^{l'-L'+p} \left(\frac{2L'+1}{2l'+1}\right)^{1/2} \left\langle L'\, N_H, l \; -p \middle| l', N_H - p\right\rangle$$

$$(A.99)$$

and in a similar way

$$\left\langle l'\, 0, l\, 0 \middle| L', 0\right\rangle = (-1)^{l'-L'} \left(\frac{2L'+1}{2l'+1}\right)^{1/2} \left\langle L'\, 0, l\, 0 \middle| l', 0\right\rangle \quad (A.100)$$

by introducing this equivalent expressions for the CG coefficients appearing in Equation (A.97) we get (note that the summation over H_1 and H_2' can be dropped for a

summation over q'' since $H_1 = -(q'' + q + p)$ and $H'_2 = N_H + N + H_1$),

$$
\begin{aligned}
H_{L'N_H LN;(\zeta,\zeta'')}^{\binom{J,J',J''}{\kappa,\kappa',\kappa''}} = {} & \frac{4\pi^2 E}{cg_i} \sum_{l,p,q,l'} \sum_{q''} (2J+1)(2J'+1)(2J''+1) \\
& \times \left[\frac{(2L'+1)(2l+1)}{(2l'+1)(2L+1)} \right]^{1/2} \times C_{H'_2,\kappa'}^{J'} \cdot C_{H_1,\kappa}^{J*} \\
& \times (-1)^{q-N+1} \langle L' \, N_H, l \, -p | \, l', N_H - p \rangle \\
& \times \langle L' \, 0, l \, 0 | \, l', 0 \rangle \langle 1 \, -q', 1 \, q | \, L, N \rangle \\
& \times M_{q'',p,q}^{(J,J'',l,\kappa'',\kappa,\zeta'',\zeta)} \left[M_{q'',p',q'}^{(J',J'',l',\kappa'',\kappa',\zeta'',\zeta)} \right]^*
\end{aligned}
\tag{A.101}
$$

So that the intensity from Equation (A.47) can be written as,

$$
\begin{aligned}
I_\tau(\Omega_K, \hat{R}, t) = {} & \frac{1}{g_i Q(T)} \sum_{L',L,N,N_H} Y_{L',N-H'_2+H_1=-N_H}(\Omega_K) E_{L,N}^{(\lambda,\delta)}(\hat{R}'') \\
& \times \sum_{\substack{\zeta,\zeta'' \\ J,J',J'' \\ \kappa,\kappa',\kappa''}} g_{\kappa''} \exp\left(-\frac{E_{g_s,J'',\kappa''}}{k_B T} \right) \times \frac{H_{L',N_H,L,N;(\zeta,\zeta'')}^{\binom{J,J',J''}{\kappa,\kappa',\kappa''}}}{1 + \frac{i\tau \Delta E^{(J,\kappa,J',\kappa')}}{\hbar}}
\end{aligned}
\tag{A.102}
$$

or defining $H_{L',N_H,L,N}^{(\tau,T)}$ as

$$
H_{L',N_H,L,N}^{(\tau,T)} = \frac{1}{g_i Q(T)} \sum_{\substack{\zeta,\zeta'' \\ J,J',J'' \\ \kappa,\kappa',\kappa''}} g_{\kappa''} \exp\left(-\frac{E_{g_s,J'',\kappa''}}{k_B T} \right) \frac{H_{L',N_H,L,N;(\zeta,\zeta'')}^{\binom{J,J',J''}{\kappa,\kappa',\kappa''}}}{1 + \frac{i\tau \Delta E^{(J,\kappa,J',\kappa')}}{\hbar}}
\tag{A.103}
$$

we can write the intensity as

$$
I_\tau^{(\lambda,\delta)}(\Omega_K, \hat{R}) = \sum_{L',L,N,N_H} Y_{L',-N_H}(\Omega_K) E_{L,N}^{(\lambda,\delta)}(\hat{R}'') H_{L',N_H,L,N}^{(\tau,T)}
\tag{A.104}
$$

suming over L' and N_H we can define $G_{L,N}^{(\tau,T)}(\Omega_K)$,

$$
G_{L,N}^{(\tau,T)}(\Omega_K) = \sum_{L',N_H} Y_{L',-N_H}(\Omega_K) H_{L',N_H,L,N}^{(\tau,T)}
\tag{A.105}
$$

135

then the final expression for the intensity becomes,

$$I_\tau^{(\lambda,\delta)}(\Omega_K, \hat{R}) = \sum_{L,N} G_{L,N}^{(\tau,T)}(\Omega_K) E_{L,N}^{(\lambda,\delta)}(\hat{R}'')$$

(A.106)

A.5 Symmetry test for $H_{L'N_HLN;(\zeta,\zeta'')}^{\binom{J,J',J''}{\kappa,\kappa',\kappa''}}$

In this section we explore the relation that changing the signs on variables N_H and N and complex conjugation of the quantity $H_{L'N_HLN;(\zeta,\zeta'')}^{\binom{J,J',J''}{\kappa,\kappa',\kappa''}}$ has on the origin expression of itself. This symmetry test will be useful for the program as it can be taken as a simple test of the "correctness" of its computation, to certain extent. Let's start with the original expression, that was outlined before on Equation (A.101)

$$
\begin{aligned}
H_{L'N_HLN;(\zeta,\zeta'')}^{\binom{J,J',J''}{\kappa,\kappa',\kappa''}} = {} & \frac{4\pi^2 E}{c} \sum_{l,p,q,l'} \sum_{H_1,H_2'} (2J+1)(2J'+1)(2J''+1) \\
& \times \left[\frac{(2L'+1)(2l+1)}{(2l'+1)(2L+1)} \right]^{1/2} \times C_{H_2',\kappa'}^{J'} \cdot C_{H_1,\kappa}^{J*} \\
& \times (-1)^{q-N+1} \langle L'\, N_H, l\, -p|\, l', N_H - p \rangle \langle L'\, 0, l\, 0|\, l', 0 \rangle \\
& \times \langle 1\, -q', 1\, q|\, L, N \rangle \\
& \times M_{q'',p,q}^{(J,J'',l,\kappa'',\kappa,\zeta'',\zeta)} \left[M_{q'',p',q'}^{(J',J'',l',\kappa'',\kappa',\zeta'',\zeta)} \right]^*
\end{aligned}
$$

(A.107)

Some useful relations from the previous section are:

$$
\begin{aligned}
N_H &= -N + H_2' - H_1 \\
p' &= N + p - H_2' + H_1
\end{aligned}
$$

(A.108)

Taking the complex conjugate on both sides and changing N to $-N$ and N_H to $-N_H$ we get (notice that $N_H - p = -p'$, too),

$$
\left[H_{L',-N_H,L,-N;(\zeta,\zeta'')}^{\binom{J,J',J''}{\kappa,\kappa',\kappa''}} \right]^* = \frac{4\pi^2 E}{c} \sum_{l,p,q,l'} \sum_{H_1,H_2'} (2J+1)(2J'+1)(2J''+1)
$$
$$
\times \left[\frac{(2L'+1)(2l+1)}{(2l'+1)(2L+1)} \right]^{1/2} \times C_{H_2',\kappa'}^{J'} \cdot C_{H_1,\kappa}^{J*}
$$
$$
\times (-1)^{q+N+1} \langle L' - N_H, l - p | l', -p' \rangle \langle L' 0, l 0 | l', 0 \rangle
$$
$$
\times \langle 1 - q', 1 q | L, -N \rangle
$$
$$
\times \left[M_{q'',p,q}^{(J,J'',l,\kappa'',\kappa,\zeta'',\zeta)} \right]^* M_{q'',p',q'}^{(J',J'',l',\kappa'',\kappa',\zeta'',\zeta)}
$$

$$(A.109)$$

Now by means of equation C.13d of Messiah [137], we can bring back the CG coefficients to the original form,

$$
\left[H_{L',-N_H,L,-N;(\zeta,\zeta'')}^{\binom{J,J',J''}{\kappa,\kappa',\kappa''}} \right]^* = \frac{4\pi^2 E}{c} \sum_{l,p,q,l'} \sum_{H_1,H_2'} (2J+1)(2J'+1)(2J''+1)
$$
$$
\times \left[\frac{(2L'+1)(2l+1)}{(2l'+1)(2L+1)} \right]^{1/2} \times C_{H_2',\kappa'}^{J'} \cdot C_{H_1,\kappa}^{J*}
$$
$$
\times (-1)^{q+N+1}(-1)^{L'+l-l'} \langle L' N_H, l p | l', p' \rangle
$$
$$
\langle L' 0, l 0 | l', 0 \rangle (-1)^{2-L} \langle 1 q', 1 - q | L, N \rangle
$$
$$
\times \left[M_{q'',p,q}^{(J,J'',l,\kappa'',\kappa,\zeta'',\zeta)} \right]^* M_{q'',p',q'}^{(J',J'',l',\kappa'',\kappa',\zeta'',\zeta)}
$$

$$(A.110)$$

Now, swapping J and J', κ and κ', q and q', p and p', l and l', H_2' and H_1 on (A.110) we get

$$
\left[H^{\binom{J,J',J''}{\kappa,\kappa',\kappa''}}_{L',-N_H,L,-N;(\zeta,\zeta'')} \right]^* = \frac{4\pi^2 E}{c} \sum_{l,p,q,l'} \sum_{H_1,H_2'} (2J+1)(2J'+1)(2J''+1)
$$
$$
\times \left[\frac{(2L'+1)(2l'+1)}{(2l+1)(2L+1)} \right]^{1/2} \times C^{J'}_{H_2',\kappa'} \cdot C^{J*}_{H_1,\kappa} \qquad \text{(A.111)}
$$
$$
\times (-1)^{q'+N+1}(-1)^{L'+l'-l} \langle L'\, N_H, l'\, p' |\, l,p \rangle
$$
$$
\langle L'\, 0, l'\, 0 |\, l, 0 \rangle (-1)^{2-L} \langle 1\, q, 1\, -q' |\, L, N \rangle
$$
$$
\times \left[M^{(J',J'',l',\kappa'',\kappa',\zeta'',\zeta)}_{q'',p',q'} \right]^* M^{(J,J'',l,\kappa'',\kappa,\zeta'',\zeta)}_{q'',p,q}
$$

By applying C.13c and C.13a from [137] we get

$$
\left[H^{\binom{J,J',J''}{\kappa,\kappa',\kappa''}}_{L',-N_H,L,-N;(\zeta,\zeta'')} \right]^* = \frac{4\pi^2 E}{c} \sum_{l,p,q,l'} \sum_{H_1,H_2'} (2J+1)(2J'+1)(2J''+1)
$$
$$
\times \left[\frac{(2L'+1)(2l'+1)}{(2l+1)(2L+1)} \right]^{1/2} \times C^{J'}_{H_2',\kappa'} \cdot C^{J*}_{H_1,\kappa}
$$
$$
\times (-1)^{q'+N+1}(-1)^{L'+l'-l}(-1)^{l'-l-N_H}
$$
$$
\times \left(\frac{2l+1}{2l'+1} \right)^{1/2} \langle L'\, -N_H, l\, p |\, l', p' \rangle \qquad \text{(A.112)}
$$
$$
\times (-1)^{l'-l} \left(\frac{2l+1}{2l'+1} \right)^{1/2} \langle L'\, 0, l\, 0 |\, l', 0 \rangle
$$
$$
\times (-1)^{2-L}(-1)^{2-L} \langle 1\, -q', 1\, q |\, L, N \rangle
$$
$$
\times \left[M^{(J',J'',l',\kappa'',\kappa',\zeta'',\zeta)}_{q'',p',q'} \right]^* M^{(J,J'',l,\kappa'',\kappa,\zeta'',\zeta)}_{q'',p,q}
$$

Grouping phases and common terms in Equation (A.112) can be rearranged to

$$
\left[H^{\binom{J,J',J''}{\kappa,\kappa',\kappa''}}_{L',-N_H,L,-N;(\zeta,\zeta'')} \right]^* = \frac{4\pi^2 E}{c} \sum_{l,p,q,l'} \sum_{H_1,H_2'} (2J+1)(2J'+1)(2J''+1)
$$
$$
\times \left[\frac{(2L'+1)(2l+1)}{(2l'+1)(2L+1)} \right]^{1/2} \times C^{J'}_{H_2',\kappa'} \cdot C^{J*}_{H_1,\kappa}
$$
$$
\times (-1)^{q'+N+1} (-1)^{L'+l'-l-N_H} \langle L' \; -N_H, l \; p | \; l', p' \rangle
$$
$$
\times \langle L' \, 0, l \, 0 | \, l', 0 \rangle \, \langle 1 \; -q', 1 \, q | \, L, N \rangle
$$
$$
\times \left[M^{(J',J'',l',\kappa'',\kappa',\zeta'',\zeta)}_{q'',p',q'} \right]^* M^{(J,J'',l,\kappa'',\kappa,\zeta'',\zeta)}_{q'',p,q}
$$

(A.113)

Applying C.13d from [137] we get,

$$
\left[H^{\binom{J,J',J''}{\kappa,\kappa',\kappa''}}_{L',-N_H,L,-N;(\zeta,\zeta'')} \right]^* = \frac{4\pi^2 E}{c} \sum_{l,p,q,l'} \sum_{H_1,H_2'} (2J+1)(2J'+1)(2J''+1)
$$
$$
\times \left[\frac{(2L'+1)(2l+1)}{(2l'+1)(2L+1)} \right]^{1/2} \times C^{J'}_{H_2',\kappa'} \cdot C^{J*}_{H_1,\kappa}
$$
$$
\times (-1)^{q'+N+1} (-1)^{L'+l'-l-N_H} (-1)^{L'+l-l'}
$$
$$
\times \langle L' \, N_H, l \; -p | \; l', -p' \rangle \, \langle L' \, 0, l \, 0 | \, l', 0 \rangle \, \langle 1 \; -q', 1 \, q | \, L, N \rangle
$$
$$
\times \left[M^{(J',J'',l',\kappa'',\kappa',\zeta'',\zeta)}_{q'',p',q'} \right]^* M^{(J,J'',l,\kappa'',\kappa,\zeta'',\zeta)}_{q'',p,q}
$$

(A.114)

since $-p' = N_H - p$ and $q' = q - N$, it leads to

$$
\left[H^{\binom{J,J',J''}{\kappa,\kappa',\kappa''}}_{L',-N_H,L,-N;(\zeta,\zeta'')} \right]^* = \frac{4\pi^2 E}{c} \sum_{l,p,q,l'} \sum_{H_1,H_2'} (2J+1)(2J'+1)(2J''+1)
$$
$$
\times \left[\frac{(2L'+1)(2l+1)}{(2l'+1)(2L+1)} \right]^{1/2} \times C^{J'}_{H_2',\kappa'} \cdot C^{J*}_{H_1,\kappa}
$$
$$
\times (-1)^{q-N_H+1} \langle L' \, N_H, l \; -p | \; l', N_H - p \rangle
$$
$$
\langle L' \, 0, l \, 0 | \, l', 0 \rangle \, \langle 1 \; -q', 1 \, q | \, L, N \rangle
$$
$$
\times \left[M^{(J',J'',l',\kappa'',\kappa',\zeta'',\zeta)}_{q'',p',q'} \right]^* M^{(J,J'',l,\kappa'',\kappa,\zeta'',\zeta)}_{q'',p,q}
$$

(A.115)

So, multiplying both sides by $(-1)^{N_H - N}$ will return the original expression for $H_{L',N_H,L,N;(\zeta,\zeta'')}^{\binom{J,J',J''}{\kappa,\kappa',\kappa''}}$ on the right, thus,

$$(-1)^{N_H-N}\left[H_{L',-N_H,L,-N;(\zeta,\zeta'')}^{\binom{J,J',J''}{\kappa,\kappa',\kappa''}}\right]^* = H_{L',N_H,L,N;(\zeta,\zeta'')}^{\binom{J,J',J''}{\kappa,\kappa',\kappa''}} \tag{A.116}$$

A.6 Polarization special cases

The field dependent term given in Equation (A.92) can be simplified in the case of linear or circularly polarized light. With linearly polarized light, $\lambda = 0$ so that $s_1 = 1$ and $s_2 = s_3 = 0$. Giving for $E_{L,N}^{\lambda,\delta}$ (see Equation (A.94)):

$$E_{0,0}^{(LP)}(\hat{R}'') = \frac{1}{\sqrt{3}}\frac{1}{\sqrt{4\pi}} = \sqrt{\frac{1}{3}}Y_{00}(\chi_{LP},\gamma_{LP})$$

$$E_{0,0}^{(LP)}\left(\gamma_{LP}-\frac{\pi}{2},\frac{\pi}{2},\pi-\chi_{LP}\right) = \frac{1}{\sqrt{3}}\frac{1}{\sqrt{4\pi}}$$

$$E_{1,N}^{(LP)}(\hat{R}'') = 0$$

$$E_{2,N}^{(LP)}(\hat{R}'') = \sqrt{\frac{5}{4\pi}}\left\{\frac{1}{\sqrt{6}}D_{N,0}^{(2)}(\hat{R}'') - \frac{1}{2}\left[D_{N,2}^{(2)}(\hat{R}'') + D_{N,-2}^{(2)}(\hat{R}'')\right]\right\} \tag{A.117}$$

Then from NotesMPI.doc we have

$$\chi = \frac{\pi}{2}, \quad \gamma = \gamma_{LP}, \quad \beta = \pi - \chi_{LP} \tag{A.118}$$

and $\hat{R}'' = (\gamma,\chi,\beta)$ we have,

$$E_{0,0}^{(LP)}\left(\gamma_{LP}-\frac{\pi}{2},\frac{\pi}{2},\pi-\chi_{LP}\right) = \frac{1}{\sqrt{3}}\frac{1}{\sqrt{4\pi}} \tag{A.119}$$

$$E_{2,0}^{(LP)}\left(\gamma_{LP} - \frac{\pi}{2}, \frac{\pi}{2}, \pi - \chi_{LP}\right) = \sqrt{\frac{5}{4\pi}} \left\{ \sqrt{\frac{1}{6}} D_{0,0}^{(2)}\left(\gamma_{LP} - \frac{\pi}{2}, \frac{\pi}{2}, \pi - \chi_{LP}\right) \right.$$

$$- \frac{1}{2} \left[D_{0,2}^{(2)}\left(\gamma_{LP} - \frac{\pi}{2}, \frac{\pi}{2}, \pi - \chi_{LP}\right) \right. \tag{A.120}$$

$$\left. \left. + D_{0,-2}^{(2)}\left(\gamma_{LP} - \frac{\pi}{2}, \frac{\pi}{2}, \pi - \chi_{LP}\right) \right] \right\}$$

In summary, writing the angular funcitons in terms of the two angles that characterize the direction of the polarization of light (χ_{LP}, γ_{LP})

$$E_{0,0}^{(LP)}(\chi_{LP}, \gamma_{LP}) = \sqrt{\frac{1}{3}} Y_{00}(\chi_{LP}, \gamma_{LP}) \tag{A.121a}$$

$$E_{2,N}^{(LP)}(\chi_{LP}, \gamma_{LP}) = (-1)^{N+1} \sqrt{\frac{2}{3}} Y_{2,-N}(\chi_{LP}, \gamma_{LP})$$

$$= -\sqrt{\frac{2}{3}} [Y_{2,N}(\chi_{LP}, \gamma_{LP})]^* \tag{A.121b}$$

Or using the Clebsch-Gordan coefficients we can write a single formula

$$E_{L,N}^{(LP)}(\chi_{LP}, \gamma_{lp}) = - \langle 1\,0, 1\,0 | L, 0 \rangle [Y_{L,N}(\chi_{LP}, \gamma_{LP})]^* \tag{A.122}$$

For circularly polarized light we have $s_3 = \mp 1$ and $s_1 = s_2 = 0$, where the top sign is for left hand circularly polarized light (LCP) and the bottom sign is for right hand circularly polarized light (RCP). Alternatively we can write $s_3 = -\mu_0$ where $\mu_0 = 1$ for LCP (positive helicity) and $\mu_0 = -1$ for RCP (negative helicity). Then, the $E_{L,N}^{(\lambda,\delta)}$ can be written as:

$$E_{0,0}^{(CP)}(\hat{R}'') = \frac{1}{2} \sqrt{\frac{2L+1}{4\pi}} \left\{ (1 - s_3) \langle 1\,1, 1\quad -1| 0, 0 \rangle (1) \right.$$

$$\left. + (1 + s_3) \langle 1\quad -1, 1\,1| 0, 0 \rangle (1) \right\}$$

$$= \frac{1}{2} \sqrt{\frac{1}{4\pi}} \left\{ (1 - s_3) \left(\frac{1}{3}\right)^{\frac{1}{2}} + (1 + s_3) \left(\frac{1}{3}\right)^{\frac{1}{2}} \right\} \tag{A.123}$$

$$= \frac{1}{\sqrt{3}} \frac{1}{\sqrt{4\pi}}$$

$$E_{1,N}^{(CP)}(\hat{R}'') = \frac{1}{2}\sqrt{\frac{2+1}{4\pi}} \left\{ (i-s_3)\,\langle 1\,1, 1 \quad -1|\,1, 0\rangle\, D_{N,0}^{(1)}(\hat{R}'') \right.$$
$$\left. +(1+s_3)\,\langle 1 \quad -1, 1\,1|\,1, 0\rangle\, D_{N,0}^{(1)} \right\} \tag{A.124}$$
$$= -\mu_0 \frac{1}{\sqrt{2}}\sqrt{\frac{3}{4\pi}} D_{N,0}^{(1)}(\hat{R}'')$$

$$E_{2,N}^{(CP)}(\hat{R}'') = \frac{1}{2}\sqrt{\frac{2(2)+1}{4\pi}} \left\{ (i-s_3)\,\langle 1\,1, 1 \quad -1|\,2, 0\rangle\, D_{N,0}^{(2)}(\hat{R}'') \right.$$
$$\left. +(1+s_3)\,\langle 1 \quad -1, 1\,1|\,2, 0\rangle\, D_{N,0}^{(2)} \right\} \tag{A.125}$$
$$= \frac{1}{\sqrt{6}}\sqrt{\frac{5}{4\pi}} D_{N,0}^{(2)}(\hat{R}'')$$

Or using the Clebsch-Gordan coefficients we have,

$$E_{L,N}^{(CP)}(\gamma, \chi, \beta) = \frac{1}{2}\sqrt{\frac{2L+1}{4\pi}} \left\{ (1-s_3)\,\langle 1\,1, 1 \quad -1|\,L, 0\rangle\, D_{N,0}^{(L)}(\hat{R}'') \right.$$
$$\left. +(1+s_3)\,\langle 1 \quad -1, 1\,1|\,L, 0\rangle\, D_{N,0}^{(L)}(\hat{R}'') \right\} \tag{A.126}$$

Analizing each case ($s_3 = 1$ or $s_3 = -1$) it follows only one of the terms in the rhs will remain (that is the one with either $(1-s_3)$ or $(1+s_3)$ in front) giving thus the simplified expresion in terms of μ_0

$$E_{L,N}^{(CP)}(\gamma, \chi, \beta) = \langle 1 \quad -\mu_0, 1\,\mu_0|\,L, 0\rangle\, \sqrt{\frac{2L+1}{4\pi}} D_{N,0}^{(L)}(\gamma, \chi, \beta) \tag{A.127}$$
$$= \langle 1 \quad -\mu_0, 1\,\mu_0|\,L, 0\rangle\, [Y_{LN}(\chi, \gamma)]^*$$

So, taking $\mu_0 = 0$ for the linearly polarized case, we can combine Equations (A.126) and (A.127) into a single formula,

$$E_{L,N}^{(\mu_0)}(\chi, \gamma) = (-1)^{\mu_0+1}\,\langle 1 \quad -\mu_0, 1\,\mu_0|\,L, 0\rangle\, [Y_{LN}(\chi, \gamma)]^* \tag{A.128}$$

where for LP light we use (χ_{LP}, γ_{LP}) in place of (χ, γ). Now Equation (A.106) can

be written as

$$I_\tau^{(\mu_0)}(\Omega_K, \chi, \gamma) = \sum_{L,N} G_{LN}^{(\tau)}(\Omega_k)[Y_{LN}(\chi, \gamma)]^*(-1)^{\mu_0+1} \langle 1 - \mu_0, 1 \, \mu_0 | \, L, 0 \rangle \quad \text{(A.129)}$$

A.7 Rotational effects with elliptically polarized light

In the general elliptically polarized case, it is also possible to rewrite the angular functions into a simpler form. Firs, in analogy to the $Q_N^\pm(\chi)$ functions defined in earlier publications [35] for $N \geq 0$

$$Q_N^\pm(\chi) = 3(-1)^N \sqrt{\frac{(2+N)!}{4!(2-N)!}} \left[d_{N,2}^{(2)}(\chi) \pm d_{N,-2}^{(2)}(\chi) \right] \quad \text{(A.130)}$$

We now define the functions $U_N^{(\pm)}(\chi, \gamma)$ as

$$\left[U_N^{(\pm)}(\chi, \gamma) \right]^* = \sqrt{\frac{15}{32\pi}} \left[d_{N,2}^{(2)}(\chi) \pm d_{N,-2}^{(2)}(\chi) \right] e^{(-i\gamma N)} \quad \text{(A.131)}$$

So that
$$d_{N,\pm 2}^{(2)}(\chi) = \sqrt{\frac{8\pi}{15}} \left[U_N^{(+)}(\chi, \gamma) \pm U_N^{(-)}(\chi, \gamma) \right]^* e^{(i\gamma N)} \quad \text{(A.132)}$$

Note that again, for $N \geq 0$ we have,

$$\begin{aligned}
U_N^{(\pm)}(\chi, \gamma) &= (-1)^N \sqrt{\frac{4!(2-N)!15}{9(2+N)!32\pi}} Q_N^\pm(\chi) e^{(i\gamma N)} \\
&= (-1)^N \sqrt{\frac{5(2-N)!}{4(2+N)!\pi}} Q_N^\pm(\chi) e^{(i\gamma N)}
\end{aligned} \quad \text{(A.133)}$$

Then Equation (A.94) becomes (see references [127], p. 60 Equation 4.30 or [125],

143

p. 59 Equation 4.1.25),

$$
\begin{aligned}
E_{2,N}^{(\lambda,\delta)}(\gamma,\chi,\beta) &= \sqrt{\frac{5}{4\pi}}\frac{1}{\sqrt{6}}D_{N,0}^{(2)}(\hat{R}'') \\
&\quad -\sqrt{\frac{5}{4\pi}}\frac{s_1}{2}\left[e^{(-i\gamma N)}d_{N,2}^{(2)}(\chi)e^{(-2i\beta)}+e^{(-i\gamma N)}d_{N,-2}^{(2)}(\chi)e^{(2i\beta)}\right] \\
&\quad +\sqrt{\frac{5}{4\pi}}\frac{is_2}{2}\left[e^{(-i\gamma N)}d_{N,2}^{(2)}(\chi)e^{(-2i\beta)}-e^{(-i\gamma N)}d_{N,-2}^{(2)}(\chi)e^{(2i\beta)}\right] \\
&= \frac{1}{\sqrt{6}}[Y_{2,N}(\chi,\gamma)]^{*}-e^{(-i\gamma N)}\sqrt{\frac{5}{4\pi}}\frac{s_1}{2}\left[d_{N,2}^{(2)}(\chi)e^{(-2i\beta)}+d_{N,-2}^{(2)}(\chi)e^{(2i\beta)}\right] \\
&\quad +e^{(-i\gamma N)}\sqrt{\frac{5}{4\pi}}\frac{is_2}{2}\left[d_{N,2}^{(2)}(\chi)e^{(-2i\beta)}-d_{N,-2}^{(2)}(\chi)e^{(2i\beta)}\right]
\end{aligned}
$$

$$\tag{A.134}$$

From the equation of $d_{N,\pm2}^{(2)}(\chi)$ in terms of $U_N^{(\pm)}(\chi,\gamma)$ we can substitute to obtain,

$$
E_{2,N}^{(\lambda,\delta)}(\gamma,\chi,\beta) = \frac{1}{\sqrt{6}}[Y_{2,N}(\chi,\gamma)]^{*}-\frac{s_1}{2}
\tag{A.135}
$$